Ivan Halimski | Spectroscopic Signatures of Intermolecular Interactions: from Dimers to Crystallites and van der Waals Complexes

Vilnius University

Spectroscopic Signatures of Intermolecular Interactions: from Dimers to Crystallites and van der Waals Complexes

Ivan Halimski

DOCTORAL DISSERTATION
2026



Natural Sciences
Physics **N 002**

https://doi.org/10.15388/vu.thesis.1015
https://orcid.org/0000-0002-4966-4655

VILNIUS UNIVERSITY
CENTER FOR PHYSICAL SCIENCES AND TECHNOLOGY

Ivan Halimski

Spectroscopic Signatures of Intermolecular Interactions: from Dimers to Crystallites and van der Waals Complexes

DOCTORAL DISSERTATION

Natural Sciences,
Physics (N 002)

VILNIUS 2026

The dissertation was prepared between 2022 and 2026 at the Center for Physical Sciences and Technology. The research was supported by the Research Council of Lithuania with scholarship that was granted for academic accomplishment for the 2026 year (reg. Nr. P-DAP-26-191).

Academic Supervisor – Dr. Jevgenij Chmeliov **(**Center for Physical Sciences and Technology, Natural Sciences, Physics, N 002).

This doctoral dissertation will be defended in a public meeting of the Dissertation Defence Panel:

Chairman – Prof. Dr. Justinas Čeponkus (Vilnius University, Natural Sciences, Physics, N 002).
Members:
Dr. Alytis Gruodis (Vilnius University, Natural Sciences, Physics, N 002),
Dr. Ernestas Kasparavičius (Kaunas University of Technology, Natural Sciences, Chemistry, N 003),
Prof. Habil. Dr. Gediminas Niaura (Center for Physical Sciences and Technology, Natural Sciences, Physics, N 002),
Prof. Dr. Olivia Pulci (University of Rome "Tor Vergata" and National Institute of Nuclear Physics, Natural Sciences, Physics, N 002).

The dissertation shall be defended at a public meeting of the Dissertation Defence Panel at 4 p.m. on December 7, 2026 in conference hall A101 of the Center for Physical Sciences and Technology.

Address: Saulėtekio ave. 3, A101, Vilnius, Lithuania
Tel. +37064515550; e-mail: office@ftmc.lt

https://doi.org/10.15388/vu.thesis.1015
https://orcid.org/0000-0002-4966-4655

VILNIAUS UNIVERSITETAS
FIZINIŲ IR TECHNOLOGIJOS MOKSLŲ CENTRAS

Ivan Halimski

Tarpmolekulinių sąveikų spektroskopiniai požymiai: nuo dimerų iki kristalitų ir van der Waalso kompleksų

DAKTARO DISERTACIJA

Gamtos mokslai,
Fizika (N 002)

VILNIUS 2026

Disertacija rengta 2022–2026 metais Fizinių ir technologijos mokslų centre. Tyrimą finansavo Lietuvos mokslo taryba, skyrusi stipendiją už akademinius pasiekimus 2026 metams (reg. Nr. P-DAP-26-191).

Mokslinis vadovas – dr. Jevgenij Chmeliov (Fizinių ir technologijos mokslų centras, gamtos mokslai, fizika, N 002).

Gynimo taryba:

Pirmininkas – prof. dr. Justinas Čeponkus (Vilniaus universitetas, gamtos mokslai, fizika, N 002).

Nariai:
dr. Alytis Gruodis (Vilniaus universitetas, gamtos mokslai, fizika, N 002),
dr. Ernestas Kasparavičius (Kauno technologijos universitetas, gamtos mokslai, chemija, N 003),
prof. habil. dr. Gediminas Niaura (Fizinių ir technologijos mokslų centras, gamtos mokslai, fizika, N 002),
prof. dr. Olivia Pulci (Romos Tor Vergata universitetas ir Nacionalinis branduolinės fizikos institutas, gamtos mokslai, fizika, N 002).

Disertacija ginama viešame Gynimo tarybos posėdyje 2026 m. gruodžio 7 d. 16:00 val. Fizinių ir technologijos mokslų centro A101 posėdžių salėje.
Adresas: Saulėtekio al. 3, A101, Vilnius, Lietuva
Tel. +37064515550; el. paštas: office@ftmc.lt

*…**We** have to change from*
doubters to believers. Now…
Jürgen Klopp
Liverpool, October 2015

ACKNOWLEDGMENTS

It would be very hard to mention all the people to whom I owe infinite gratitude.

This thesis would not have been completed without my scientific supervisor – Dr. Jevgenij Chmeliov – who generously shared his knowledge and inspired me with his enthusiasm throughout these four years. As a theoretician, Jevgenij encouraged my interest in the interplay between experiments and theoretical modelling, making this time particularly fascinating. This thesis would not have been completed without Dr. Renata Karpicz, who introduced me to the exciting world of electronic spectroscopy and generously mentored me throughout these four years. A special role during these four years was played by Dr. Maksim Shundalau, who shared his knowledge of molecular spectroscopy with me and was an example of what a scientist should be.

I would like to acknowledge all the members of the Department of Molecular Compound Physics, especially Prof. Dr. Leonas Valkūnas and Dr. Andrius Gelžinis, for their help and support, and Dr. Simona Streckaitė for her help with sample preparation and experimental techniques, as well as for her infinite patience throughout this process. I would also like to thank Dr. Lena Golubewa and Dr. Yaraslau Padrez for their help, both in life and in science, during my first months at FTMC. It would be remiss not to mention some of the Bachelor, Master and Doctoral students with whom I shared the lab, especially Vilius Čirgelis, Paulius Rindzevičius and Martynas Zalieckas, who made the working atmosphere so positive.

It was my pleasure to collaborate with Prof. Dr. Darius Abramavičius from Vilnius University, Prof. Dr. Patrizia Lamberti from the University of Salerno, as well as with Dr. Nikita Belko and Dr. Hanna Maltanava from the University of Eastern Finland.

Some of my acknowledgements must also reach my Motherland, Belarus. I would like to thank my undergraduate thesis supervisor, Prof. Dr. Nikolai Poklonski, and his close colleague, Dr. Anatoli Vlassov, under whose

supervision I conducted my first scientific research. I would also like to thank Dr. Alexey Ivanov, who encouraged my love of physics.

I would like to thank my friends Dr. Darya Meisak and Uladzislau Pirtan for the joy and happiness we shared during my four years in Vilnius.

Also, I want to thank Liverpool FC – fans, players and managers – for being an example of never giving up and constantly reminding me that *I will never walk alone*.

It is impossible to overestimate the role played by Paula. She was not only an example of what a young researcher should be and how one should approach scientific work, always showing genuine enthusiasm and fire in her eyes when working in the lab and talking about science. Her thoughtful and deep questions during poster sessions helped me deepen my understanding. Above all, she always gave me endless care and support whenever I faced difficulties along the way and, at critical moments, she believed in me more than I believed in myself.

Of course, I owe infinite gratitude to my family, which consists mainly of scientists. One of my motivations for studying physics was simply to understand the conversations during family gatherings! I want to acknowledge my parents – Polina and Andrey – who have been my guides and role models for as long as I can remember. They have provided me with endless support throughout my life, especially during these four years. I want to thank my uncle Pavel, who was the first person with whom I pretended to do science when I was eight years old. I want to thank my grandad Pavel, who was the first person with whom I seriously talked about science and who helped deepen my knowledge in optics. I want to thank the only *Dr. Sci.* in our family – my granny Tat'yana – who is an example of what hard work and late nights in the lab can lead to. I also want to thank my grandparents Petr and Halina for the love they gave me from the very first moments of my life.

Ivan Halimski
Vilnius, October 2026

ABBREVIATIONS AND NOTATIONS

- BO – Born-Oppenheimer (approximation)
- μ_{ij} – electronic transition dipole moment from the electronic state i to the electronic state j
- FC – Franck-Condon (principle, factor)
- S_0 – electronic ground state
- S_i – ith electronic excited state ($i \geq 1$)
- VR – vibrational relaxation
- IC – internal conversion
- ISC – intersystem crossing
- FL – fluorescence
- k – rate constant
- τ – lifetime
- QY – quantum yield
- vdW – van der Waals (interaction, force)
- R – separation distance between two species
- ACQ – aggregation-caused quenching
- AIE – aggregation-induced emission
- EET – excitation energy transfer
- D – donor
- A – acceptor
- DA – single donor, surrounded by infinite number of acceptors (model)
- FRET – Förster resonance energy transfer
- R_F – Förster radius
- CQ – concentration quenching
- TTBPc – 2,9,16,23-tetra-tert-butyl-29H,31H-phthalocyanine ($C_{48}H_{50}N_8$)
- ZnTTBPc – zinc 2,9,16,23-tetra-tert-butyl-29H,31H-phthalocyanine ($C_{48}H_{48}N_8Zn$)
- TS – *trans*-stilbene ($C_{14}H_{12}$)
- PS – polystyrene
- hBN – hexagonal boron nitride
- AFM – atomic force microscopy
- CARS – coherent anti-Stokes Raman scattering
- OD – optical density

- IRF – instrument response function
- NNMF – non-negative matrix factorization
- DFT – density functional theory
- TD-DFT – time-dependent density functional theory
- UV – ultraviolet
- UV/vis – ultraviolet/visible
- 2D – two-dimensional
- 3D – three-dimensional
- 0D – zero-dimensional
- TA – transient absorption
- TRFL – time-resolved fluorescence

TABLE OF CONTENTS

1. INTRODUCTION 13
1.1. Aim of the dissertation 14
1.2. Research objectives 14
1.3. Research tasks 14
1.4. Statements for the defense 15
1.5. Scientific novelty 16
1.6. List of peer-reviewed papers 17
1.7. List of conference presentations 17
1.8. Author's contribution 20
2. LITERATURE OVERVIEW 22
2.1. Basics of electronic spectroscopy 22
2.1.1. Electronic absorption 22
2.1.2. Excited-state relaxation processes and fluorescence 24
2.1.3. Excited-state relaxation dynamics and fluorescence decay kinetics 26
2.2. Interactions in molecular systems 27
2.2.1. Van der Waals interactions 27
2.2.2. Molecular aggregates 29
2.2.3. Excitonically-coupled aggregates: H- and J-aggregates 30
2.3. Excitation energy transfer 32
2.3.1. Introduction to excitation energy transfer 32
2.3.2. Mechanisms of excitation energy transfer 33
2.3.3. Förster resonance energy transfer 35
2.3.4. Concentration quenching of fluorescence 37
3. MATERIALS AND METHODS 39
3.1. Materials 39
3.2. Sample preparation 39
3.2.1. TTBPc and ZnTTBPc solutions 39

3.2.2. TS spin-coated films 39
3.2.3. TS + hBN van der Waals complex 40
3.3. Electronic absorption measurements 40
3.4. Steady-state fluorescence measurements 41
3.4.1. Insights into minimizing the influence of reabsorption effect on ZnTTBPc and TTBPc fluorescence spectra 41
3.5. Fluorescence decay kinetics measurements 44
3.6. Data processing and analysis 45
3.6.1. Data processing of steady-state spectroscopy 45
3.6.2. Target analysis of FL decay kinetics 45
3.6.3. Global analysis of FL spectra and FL decay kinetics 45
3.7. Supporting experimental and theoretical methods 46
3.7.1. TTBPc and ZnTTBPc chloroform solutions 46
3.7.2. TS spin-coated thin films 46
3.7.3. TS + hBN van der Waals complex 47
4. RESULTS AND DISCUSSION 49
4.1. Concentration quenching of fluorescence in phthalocyanine chloroform solutions 49
4.1.1. Initial remarks 49
4.1.2. Short overview of phthalocyanine compounds applications and properties 49
4.1.3. Steady-state absorption and fluorescence of TTBPc and ZnTTBPc 50
4.1.4. Concentration-dependent FL decay kinetics of TTBPc and ZnTTBPc 53
4.1.5. CQ in ZnTTBPc and TTBPc due to excitation energy migration to trap species 55
4.1.6. Current limitations and unresolved questions 58
4.1.7. Summarizing remarks 60
4.2. Morphology-induced changes in FL properties of *trans*-stilbene thin films 60

4.2.1. Initial remarks 60
4.2.2. Short overview of stilbene compounds applications and properties 61
4.2.3. Structural transitions in TS thin films observed via CARS and AFM 62
4.2.4. Steady-state electronic spectroscopy of TS thin films 65
4.2.5. FL decay kinetics of TS thin films 67
4.2.6. Observation of structural transitions via global analysis of FL spectra and kinetics 70
4.2.7. Current limitations and unresolved questions 72
4.2.8. Summarizing remarks 73
4.3. Manifestation of van der Waals interaction between *trans*-stilbene and hexagonal boron nitride 73
4.3.1. Initial remarks 73
4.3.2. Short overview of hexagonal boron nitride applications and properties 75
4.3.3. Observation of vdW interaction between TS and hBN via vibrational spectroscopy 76
4.3.4. Electronic manifestation of vdW interaction between TS and hBN 82
4.3.5. Current limitations and unresolved questions 85
4.3.6. Summarizing remarks 85
5. CONCLUSIONS AND OUTLOOK 86
5.1. Conclusions 86
5.2. Outlook 87
6. AI STATEMENT 90
7. SANTRAUKA 91
7.1. Įvadas 91
7.1.1. Disertacijos tikslas 92
7.1.2. Tyrimo uždaviniai 92
7.1.3. Tyrimo užduotys 92

7.1.4. Ginamieji teiginiai 93
7.1.5. Mokslinis naujumas 94
7.2. Metodologija 95
7.2.1. Mėginiai 95
7.2.2. Elektroninė spektroskopija 95
7.2.3. Duomenų analizė 96
7.3. Rezultatai ir aptarimas 97
7.3.1. Ftalocianinų chloroformo tirpalų fluorescencijos koncentracinis gesinimas 97
7.3.2. Morfologijos sukelti *trans*-stilbeno plonųjų plėvelių fluorescencinių savybių pokyčiai 101
7.3.3. Van der Waals sąveikos tarp *trans*-stilbeno ir heksagoninio boro nitrido pasireiškimas 106
7.4. Išvados 110
7.5. Publikacijos 111
7.5.1. Straipsniai 111
7.5.2. Pranešimai konferencijose 112
7.6. Autoriaus indėlis 115
7.7. Pareiškimas apie dirbtinio intelekto naudojimą 115
8. BIBLIOGRAPHY 116
About Author (In English) 130
Apie autorių (lietuvių kalba) 131

1. INTRODUCTION

Light-matter interaction plays a fundamental role in many natural and technological processes. For example, it governs photosynthesis – the natural set of chemical reactions occurring within plants, algae or moss, where the sunlight is absorbed and converted into chemical energy [1]. It plays an important role in the development of sustainable energy technologies, such as artificial photosynthesis [2] and photovoltaics [3]. The knowledge gained from the light-matter interaction studies has inspired scientists to develop new branches of chemical physics, for example quantum biology [4] or polaritonic chemistry [5]. Additionally, light-matter interaction plays a central role in disease theranostics, including such currently developing fields as biosensing [6], bioimaging [7], and photodynamic cancer therapy [8].

Usually, light interacts not with isolated molecules, but rather with some kind of a *molecular system* – the most common of them are *molecular aggregates*, *crystallites* or *molecules adsorbed on a surface* – stabilized by different *intermolecular interactions*. Usually, such interactions lead to significant differences in the photophysical properties of such a compound compared with an isolated molecule [9–12].

Optical spectroscopy is an effective tool for analyzing such intermolecular interactions. Both steady-state electronic absorption and fluorescence spectra can exhibit features attributed to the spectroscopic signatures of aggregates or adsorption-related phenomena. Time-resolved fluorescence decay kinetics is an additional useful tool for analyzing such phenomena. In addition to exhibiting decay components which can be possibly attributed to different fluorescent species, thus confirming presence of them, it can reveal such intermolecular processes as excitation energy migration between different species.

Understanding the intermolecular interactions in various molecular systems is an essential task for a wide range of applications. On the one hand, the manifestation of such interactions can be useful for applications: for example sometimes they result in notable structural transitions [13] – thus being promising for sensing applications [14] – or in the enhanced light emission, being promising for applications whose efficiency is determined by the efficient light emission or light-to-energy conversion. On the other hand, sometimes they lead to the reduced emission efficiency, and, consequently, losses in energy, which is detrimental for photovoltaics [15,16] and optoelectronics [17].

Despite being crucial for practical applications, such molecular interactions, as the formation of aggregates, including excitonically-coupled

ones, and crystallites, as well as manifestation of van der Waals interaction, and their photophysical responses under various conditions remain underexplored to date.

1.1. Aim of the dissertation

This dissertation aims to reveal and analyze the spectroscopic changes associated with different types of intermolecular interactions, namely H-aggregate formation, morphology-dependent molecular organization, and van der Waals interaction between two non-polar compounds.

1.2. Research objectives

To fulfill the formulated aim of the dissertation, the following objectives were set:

1. To investigate concentration-induced fluorescence quenching in phthalocyanine chloroform solutions and to relate the observed quenching dynamics to a specific quenching mechanism.
2. To investigate the spectroscopic manifestations of the morphology-induced changes in the optical spectra of *trans*-stilbene thin films.
3. To investigate the spectroscopic manifestations of van der Waals interaction between bulk *trans*-stilbene and hexagonal boron nitride.

1.3. Research tasks

The first part of the study focused on concentration quenching of fluorescence in free-base and zinc-phthalocyanine solutions in chloroform. Steady-state absorption and fluorescence spectra were measured over a two-order-of-magnitude concentration range to identify concentration-dependent spectral changes, while fluorescence decay kinetics were recorded to characterize the corresponding excited-state dynamics. The decay profiles were analyzed using mono-exponential, bi-exponential, and stretched-exponential models. By combining the steady-state and time-resolved data, the observed fluorescence quenching behavior was related to a specific quenching mechanism.

The second part addressed morphology-dependent optical properties of *trans*-stilbene thin films. Steady-state absorption and fluorescence spectra, together with time-resolved fluorescence decay kinetics, were measured for films with different *trans*-stilbene concentrations and thicknesses. Target analysis of the decay kinetics was used to determine characteristic fluorescence lifetimes, while global analysis of the complete sets of steady-state fluorescence spectra and decay kinetics was employed to separate the

contributions of different structural forms of *trans*-stilbene. These spectroscopic results were interpreted together with coherent anti-Stokes Raman scattering microspectroscopy and atomic force microscopy data in order to establish the relationship between film morphology and optical properties.

The third part investigated the spectroscopic manifestations of van der Waals interaction between *trans*-stilbene and hexagonal boron nitride. Steady-state and time-resolved fluorescence measurements were performed for bulk *trans*-stilbene, hBN, and their van der Waals complex, and the fluorescence decay kinetics were analyzed using bi-exponential models to determine average lifetimes. The interaction-induced changes in fluorescence were considered together with quantum-chemical calculations, Raman spectroscopy, and THz spectroscopy. This combined analysis was used to assess how van der Waals interaction between two non-polar materials manifests itself across the THz, infrared, and visible spectral regions.

1.4. Statements for the defense

I) *Phthalocyanine solutions in chloroform exhibit concentration quenching of fluorescence, governed by Förster-type excitation energy migration from monomeric species to H-dimers. It manifests only in the time-resolved fluorescence decay kinetics through their monotonic acceleration and a smooth transition from mono-exponential to non-exponential decay with increasing concentration, making this technique the most efficient way to observe and study such type of the phenomenon.*

II) *Trans-stilbene in spin-coated films exhibit monomer → disordered aggregates → highly ordered single crystallites structural transitions with an increase in molecular concentration. Both the steady-state fluorescence spectra and fluorescence decay kinetics undergo smooth and monotonic changes governed by these transitions, therefore fluorescent properties of trans-stilbene in thin films can be fine-tuned by sample preparation conditions.*

III) *Van der Waals interaction between non-polar hexagonal boron nitride and trans-stilbene results in an increased intensity of one fluorescence band and a slight acceleration of fluorescence decay. The combination of steady-state and time-resolved fluorescence*

might serve as a useful supporting technique for exploring extremely weak intermolecular interactions.

1.5. Scientific novelty

The main novelty of this dissertation lies in the field of *chemical physics*, namely it provides insights into the following questions that remained unresolved:

1. Even though concentration quenching of fluorescence is observed in various molecular systems, its molecular origin and the physical processes governing this quenching are not completely understood. Phthalocyanine compounds serve as a good model system for studying such a phenomenon [18,19], however precise experimental characterization of this phenomenon is rare due to significant reabsorption effects at high molecular concentrations [20]. This dissertation utilizes the thinnest possible commercially available glasses to avoid/minimize reabsorption effects, which allows correct interpretation of the concentration quenching behavior in highly concentrated (up to 10 mmol/L) free-base and zinc phthalocyanine solutions. Concentration quenching in highly concentrated solutions is attributed to the trap-mediated mechanism originating from the formation of H-dimers at high concentrations.
2. Changes in the optical properties of *trans*-stilbene thin films with an increase in molecular concentration were observed previously by *Karpicz, et.al.* [13]. This work provides deeper insights into this topic, varying both molecular concentration of the films and their thicknesses. The application of global analysis in combination with microscopy techniques allows precise determination of the steady-state and time-resolved fluorescence properties of different structural forms of *trans*-stilbene. Additionally, this work shows that fluorescence properties of *trans*-stilbene thin films can be controlled by controlling sample preparation conditions (molecular concentration and thickness of the film).
3. The spectroscopic manifestation of the van der Waals interaction is studied rarely experimentally to date. In most cases, adsorption-related phenomena and the corresponding spectral changes attract more attention [10,21–23]. In contrast, this dissertation concentrates on spectroscopic features of the van der Waals interaction itself between non-polar compounds using *trans*-stilbene (TS) and two-dimensional (2D) hexagonal boron nitride (hBN) complex as a model

system. It is shown that the van-der-Waals-induced changes can be observed in THz, infra-red and visible regions of the spectrum. Additionally, it is stated that Raman spectroscopy is the most effective tool for analyzing such a complex, while THz spectroscopy as well as combination of the steady-state and time-resolved fluorescence can provide complementary information. This complex serves as a suitable model system for studying features of van der Waals interactions between organic compounds and 2D materials.

1.6. List of peer-reviewed papers

The dissertation is based on three published peer-reviewed papers:

[A1] **I. Halimski**, S. Streckaite, D. Likandrovas, A. Gelzinis, L. Valkunas, J. Chmeliov, Fluorescence concentration quenching in phthalocyanine solutions: experimental observation and theoretical insights, J. Chem. Phys. 164 (2026) 184304. https://doi.org/10.1063/5.0323795

[A2] **I. Halimski**, R. Karpicz, A. Dementjev, M. Jankunec, J. Chmeliov, M. Macernis, D. Abramavicius, L. Valkunas, *trans*-Stilbene aggregates and crystallites in polystyrene films: microscopy and spectroscopy studies, Phys. Chem. Chem. Phys. 26 (2024) 23692–23702. https://doi.org/10.1039/D4CP02291B

[A3] **I. Halimski**, D. Pashnev, M. Talaikis, A. Dementjev, R. Karpicz, J. Chmeliov, I. Kašalynas, A. Urbanovič, P. Lamberti, M. Shundalau, Spectroscopic manifestation of a weak van der Waals interaction between *trans*-stilbene and hexagonal boron nitride surface, Langmuir 41 (2025) 7364–7375. https://doi.org/10.1021/acs.langmuir.4c04717

1.7. List of conference presentations

1. The results included in this thesis were presented at the following conferences:

- **Oral presentations:**

[C1] **I. Halimski**, S. Streckaitė, J. Chmeliov, A. Gelzinis, L. Valkunas. Fluoerescence concentration quenching in solutions of Zinc- and Free Base phthalocyanines. FizTeCh conference, October 2024, Vilnius, Lithuania.

[C2] **I. Halimski**, S. Streckaitė, R. Karpicz, J. Chmeliov, A. Gelzinis, D. Abramavicius, L. Valkunas. Concentration quenching of fluorescence in different molecular systems: similarities and differences. 68th International Open Readings conference for students of Physics and Natural Science, May 2025, Vilnius, Lithuania.

[C3] **I. Halimski**, M. Talaikis, A. Dementjev, R. Karpicz, J. Chmeliov, I. Kasalynas, P. Lamberti, M. Shundalau. Spectroscopic and theoretical insights into van der Waals interaction between organic compounds and hexagonal boron nitride. 19th Nanotechnology based innovation

for the environment, energy and health, September 2025, Salerno, Italy.

[C4] **I. Halimski**, P. Rindzevičius, J. Fedotova, S. Streckaitė, M. Talaikis, A. Dementjev, A. Gelzinis, B. Robert, P. Lamberti, D. Abramavičius, L. Valkunas, M. Shundalau, R. Karpicz, J. Chmeliov. Is fluorescence decay kinetics an effective tool to analyze the origin of fluorescence quecnhing and the manifestation of van der Waals interaction? 46th Lithuanian National Physical Conference (LNFK), October 2025, Kaunas, Lithuania.

[C5] **I. Halimski**, A. Dementjev, J. Chmeliov, M. Mačernis, D. Abramavicius, L. Valkūnas, R. Karpicz. Optical properties of trans-stilbene in different phases: monomers, aggregates and crystallites. FizTeCh conference, October 2025, Vilnius, Lithuania.

[C6] **I. Halimski**, P. Rindzevičius, D. Pashnev, A. Dementjev, M. Talaikis, I. Kašalynas, P. Lamberti, D. Abramavicius, L. Valkunas, M. Macernis, M. Shundalau, R. Karpicz, J. Chmeliov. Optical properties of trans-stilbene under various conditions. 6th EuroCC Vilnius Workshop on using HPC, January 2026, Vilnius, Lithuania.

- **Poster presentations:**

[C7] **I. Halimski**, S. Streckaitė, J. Chmeliov, A. Gelzinis. Fluoerescence concentration quenching in (Zinc)-Phthalocyanine solutions. FizTeCh conference, September 2023, Vilnius, Lithuania.

[C8] **I. Halimski**, G. Kareivaitė, R. Karpicz, A. Dementjev, M. Mačernis, D. Abramavičius, L. Valkunas. Trans-stilbene spectral properties changes induced by aggregates formation in a polystyrene matrix. Lithuanian National Physical Conference (LNFK), October 2023, Vilnius, Lithuania.

[C9] **I. Halimski**, R. Karpicz, A. Dementjev, M. Jankunec, J. Chmeliov, M. Macernis, D. Abramavicius, L. Valkunas. Characterization of trans-stilbene nanocrystals in polystyrene films by CARS and AFM microscopy and optical spectroscopy. 67th International Open Readings conference for students of Physics and Natural Science, April 2024, Vilnius, Lithuania.

[C10] **I. Halimski**, R. Karpicz, A. Dementjev, M. Jankunec, J. Chmeliov, M. Macernis, D. Abramavicius, L. Valkunas. Trans-stilbene aggregates and crystallites in polystyrene films: microscopy and spectroscopy. 8th International Workshop on Advanced Spectroscopy and Optical Materials. July 2024, Gdansk, Poland.

[C11] **I. Halimski**, S. Streckaitė, J. Chmeliov, A. Gelzinis, L. Valkunas. Fluoerescence concentration quenching in Zinc-containing as well as non-containing phthalocyanines. 9th International Workshop Nanocarbon Photonics and Optoelectronics. August 2024, Kuopio, Finland.

[C12] **I. Halimski**, D. Pashnev, M. Talaikis, A. Dementjev, R. Karpicz, J.

Chmeliov, I. Kašalynas, A. Urbanovič, Y. Padrez, M. Tutkus, P. Lamberti, M. Shundalau. Interaction of organic molecules and nanomaterials: Spectroscopic and theoretical insights into a weak-bound complex of hexagonal boron nitride and trans-stilbene. Advanced Properties and Processes in Optoelectronic Materials and Systems 'APROPOS 19', October 2024, Vilnius, Lithuania.

[C13] **I. Halimski**, S. Streckaitė, J. Chmeliov, A. Gelzinis, L. Valkunas. Fluorescence concentration quenching in solutions of Zinc-containing and non-containing phthalocyanines. Advanced Properties and Processes in Optoelectronic Materials and Systems 'APROPOS 19', October 2024, Vilnius, Lithuania.

[C14] **I. Halimski**, S. Streckaitė, M. Talaikis, A. Dementjev, A. Gelzinis, B. Robert, P. Lamberti, D. Abramavicius, L. Valkunas, R. Karpicz, M. Shundalau, J. Chmeliov. Probing spectroscopic manifestation of van der Waals interaction and fluorescence quenching with time-resolved fluorescence spectroscopy. Thematic School MECAREACT 2025: Vibrational and electronic spectroscopies applied to the study of reaction mechanisms, June 2025, Paris, France.

[C15] **I. Halimski**, R. Karpicz, A. Dementjev, M. Jankunec, J. Chmeliov, M. Macernis, D. Abramavicius, L. Valkunas. Spectroscopic characterization of different phases of trans-stilbene: monomers, aggregates, mono- and polycrystals. 19th Nanotechnology based innovation for the environment, energy and health, September 2025, Salerno, Italy.

- **Conference presentations by co-workers:**

[C16] **I. Halimski**, D. Pashnev, M. Talaikis, A. Dementjev, R. Karpicz, I. Kašalynas, A. Urbanovič, P. Lamberti, **M. Shundalau**. THz, Raman, and fluorescence characterization of a weak-bound complex of hBN and trans-stilbene. 9th International Workshop Nanocarbon Photonics and Optoelectronics. August 2024, Kuopio, Finland.

[C17] **I. Halimski**, D. Pashnev, M. Talaikis, A. Dementjev, R. Karpicz, J. Chmeliov, I. Kašalynas, A. Urbanovič, B. Robert, P. Lamberti, **M. Shundalau**. Spectroscopy of van der Waals interaction between organic molecules and hexagonal boron nitride. International Conference Celebrating the 220th Anniversary of the First Theory of Electrolysis by Theodor von Grotthuss, June 2025, Vilnius, Lithuania.

2. Conference presentations, which are not directly related to the scientific basis of the thesis:

[C18] **I. Halimski**, V. Jašinskas, A. Aukauloo, R. Karpicz, J. Chmeliov. V. Gulbinas. Time-resolved spectroscopic characterization of the porphyrin-containing molecular dimers. 66th International Open Readings conference for students of Physics and Natural Science, April 2023, Vilnius, Lithuania.

[C19] **I. Halimski**, J. Fedotova, D. Pashnev, M. Talaikis, A. Dementjev, R. Karpicz, J. Chmeliov, I. Kašalynas, A. Urbanovič, B. Robert, P. Lamberti, M. Shundalau. Spectroscopic study of Tetraphenylporphyrin and 2D hexagonal boron nitride van der Waals complex. International Conference Celebrating the 220th Anniversary of the First Theory of Electrolysis by Theodor von Grotthuss, June 2025, Vilnius, Lithuania.

[C20] **J. Fedotova**, **I. Halimski**, M. Talaikis, R. Karpicz, J. Chmeliov, P. Lamberti, M. Shundalau. Spectroscopic study of free-base meso-tetraphenylporphyrin and hexagonal boron nitride van der Waals complex. 68th International Open Readings conference for students of Physics and Natural Science, May 2025, Vilnius, Lithuania.

[C21] **P. Rindzevičius**, **I. Halimski**. Spectroscopic insights into van der Waals interaction between resveratrol and hexagonal boron nitride. LMT 2025 student's summer practice conference, August 2025, Vilnius r, Lithuania.

[C22] A. Dementjev, **I. Halimski**, P. Rindzevičius, S. Malykhin, L. Valkunas, **R. Karpicz**. Application of CARS microscopy to chemical structural imaging of micro- and nanocrystals. 19th Nanotechnology based innovation for the environment, energy and health, September 2025, Salerno, Italy.

[C23] **P. Rindzevičius**, M. Talaikis, A. Dementjev, P. Lamberti, J. Chmeliov, M. Shundalau, **I. Halimski**, R. Karpicz. Spectroscopic investigation of van der Waals interaction between resveratrol and hexagonal boron nitride. 46th Lithuanian National Physical Conference (LNFK), October 2025, Kaunas, Lithuania.

[C24] **J. Fedotova**, M. Talaikis, P. Lamberti, J. Chmeliov, M. Shundalau. R. Karpicz, **I. Halimski**. Investigation of spectroscopic properties of free-base tetraphenylporphyrin and hexagonal boron nitride van der Waals complex. FizTeCh conference, October 2025, Vilnius, Lithuania

1.8. Author's contribution

The author of the thesis prepared all the samples for all the measurements. He performed all the steady-state absorption measurements, as well as steady-state fluorescence, fluorescence excitation and fluorescence decay kinetics measurements. He processed, analyzed and interpreted the obtained data, participated in the analysis of the complementary experiments results, contributed to the preparation of all the articles, including both original draft creation and review & editing stages, as well as to response on referees' comments.

The co-authors' contributions used in this thesis are specified below:

Paper A1: Darius Likandrovas and Dr. Andrius Gelzinis performed quantum chemical calculations which support the conclusions of the thesis.

Paper A2: Dr. Marija Jankunec performed AFM microscopy, while Dr. Andrej Dementjev carried out CARS microspectroscopy experiments. Dr. Mindaugas Mačernis performed quantum chemical calculations. The global analysis of the steady-state fluorescence spectra and decay kinetics applying non-negative matrix factorization technique was performed by author of the thesis together with his scientific supervisor Dr. Jevgenij Chmeliov. All the mentioned insights are necessary to make conclusions based on this paper.

***Paper A3*:** Dr. Martynas Talaikis carried out Raman scattering measurements. Dr. Daniil Pashnev together with Dr. Maksim Shundalau, Dr. Andžej Urbanovič and Dr. Irmantas Kašalynas performed THz spectroscopy measurements. Additionally, Dr. Maksim Shundalau carried out quantum chemical calculations. All these results are used in formulating the conclusions of the thesis.

2. LITERATURE OVERVIEW

2.1. Basics of electronic spectroscopy

2.1.1. Electronic absorption

The total energy of a molecule is a sum of electronic, vibrational, and rotational contributions. The Born-Oppenheimer (BO) approximation is based on the fact, that the mass of an atomic nucleus is much bigger compared with those of electrons, therefore their motion can be considered to be separated. According to the BO approximation, each electronic state has corresponding set of vibrational energy levels, whereas each vibrational level has a corresponding rotational subsystem.

Electronic absorption of light occurs when the energy $E = \mathrm{h}\nu$ of the incident light corresponds to the energy difference between a vibrational level of a ground electronic state and a vibrational level of an electronic excited state:

$$E = h\nu = E_{f,v'} - E_{i,v''}, \tag{2.1}$$

where E is the energy of the incident light, h is the Planck constant, ν is the frequency of the incident light, $E_{f,v'}$ is the energy of v'-th vibrational level of the f-th electronically excited state and $E_{i,v''}$ is the energy of v''-th vibrational energy level of a ground electronic state. *Electronic absorption usually corresponds to the ultraviolet (UV) or visible spectral regions.*

However, the Eq. 2.1 is not the only requirement for the electronic absorption event to occur. The *dipole approximation* is based on the fact that the wavelength of the incident light is much larger than the size of a molecule, therefore the electric field of the light is considered to be spatially uniform within the molecule. Within this approximation, light interaction with the molecule is described by the interaction of molecular dipole moment μ with the electric field of the light. The transition probability P_{if} from the state i to the state f is proportional to the squared magnitude of the corresponding transition dipole moment μ_{if}, which can be expressed as follows [24]:

$$\mu_{if} = \langle \Psi_f | \hat{\mu} | \Psi_i \rangle = \left(\int \psi_f^{e*} \mu \, \psi_i^e \, dA^e \right) \left(\int \chi_{v_f}^* \, \chi_{v_i} dA^v \right) \left(\int \sigma_f^* \, \sigma_i dA^s \right), \tag{2.2}$$

μ_{if} denotes the transition dipole moment from the state i to the state f, Ψ_i and Ψ_f denote the wave functions of the initial and finite states, respectively, $\int \sigma_f^* \, \sigma_i dA^s$ denote the overlap integral between spin contributions, $\int \chi_{v_f}^* \, \chi_{v_i} dA^v$ the vibrational overlap integral, $\int \psi_f^{e*} \mu \, \psi_i^e \, dA^e$ is the electronic transition integral, asterisk '*' indicates the complex conjugate operation.

For an electronic transition to be allowed in terms of dipole approximation, the electronic transition dipole moment μ_{if} must exhibit non-zero value, i.e., all the parts in Eq. 2.2 must have non-zero values. Therefore, the following ***selection rules*** are applied:

1. *The electronic transition event must preserve the spin multiplicity*, because spin wave functions corresponding to different spin multiplicities are orthogonal, resulting in zero spin overlap integral value [24]. Usually, molecules have a singlet ground state, therefore spin-allowed transitions are usually singlet-singlet ones.
2. The *spatial symmetries* of the initial and finite states must result in non-zero electronic dipole transition integral [25].

In addition to the mentioned rules, *The Franck-Condon (FC) principle* states, that the electronic transition happens without changes in nuclear coordinates. Therefore, the FC factor denoted as the squared vibrational overlap integral plays an important role in the intensities of *vibronic transitions*, i.e., transitions between different vibrational levels of different electronic levels:

$$\mathrm{FC} = \left(\int \chi^*_{v_f} \chi_{v_i} dA^v \right)^2 \tag{2.3}$$

Figure 2.1 represents the intensities of different vibronic transitions in terms of Franck-Condon principle, i.e., the band's intensity is determined by the overlap between wave functions of the corresponding vibrational levels.

Experimentally electronic absorption is characterized in terms of the ***Beer-Lambert law*** [26]:

$$\mathrm{A}(\lambda) = \log \frac{I_0^\lambda}{I^\lambda} = \varepsilon(\lambda) l c, \tag{2.4}$$

where $\mathrm{A}(\lambda)$ denotes the absorbance at the specific wavelength λ, I_0^λ and I^λ are the intensities of the incident and transmitted light at a wavelength λ, respectively, $\varepsilon(\lambda)$ is the molar absorption coefficient, c is the molar concentration and l is an absorption path length.

Usually, the electronic absorption spectrum is a starting point in studies of different intermolecular processes and interactions [13,18,27–30], because it provides information on the electronic structure of the studied system.

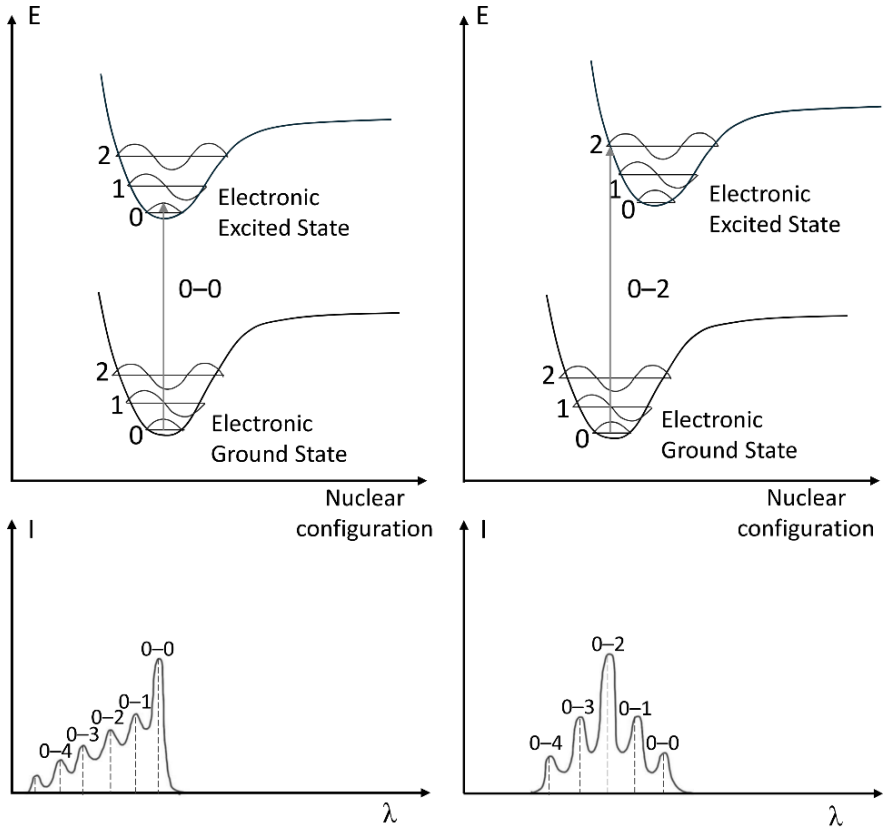
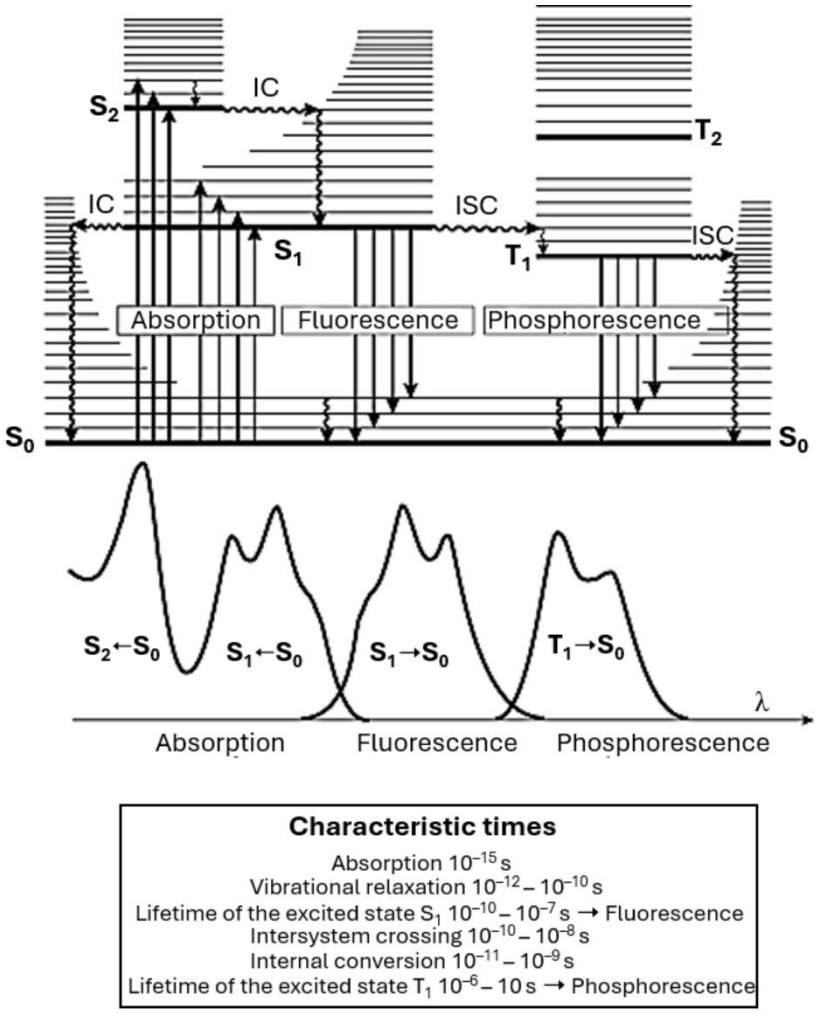


Figure 2.1. *The schematic illustration of the Franck-Condon principle. The upper panel indicates potential energy surfaces of the electronic ground and excited states, as well as the wave functions of the corresponding vibrational states. The lower panel indicates the schematic electronic absorption spectra corresponding to the overlap in the wave functions presented in the upper panel. Adapted from Ref. [26] with the permission from Wiley-VCH. Copyright © 2012 Wiley-VCH Verlag GmbH & Co. KGaA.*

2.1.2. Excited-state relaxation processes and fluorescence

After absorption of light takes place, the following processes can occur. Being excited to some vibrational level of some electronically excited state, the two sets of events can take place: radiative and non-radiative relaxation. Figure 2.2 represents Jablonski diagram showing both radiative and non-radiative processes occurring within a molecular system after light absorption; the middle and lower panels indicate schematic absorption, fluorescence and phosphorescence spectra, as well as characteristic time scales of the radiative and non-radiative relaxation processes, respectively.



Characteristic times

Absorption 10^{-15} s
Vibrational relaxation $10^{-12} - 10^{-10}$ s
Lifetime of the excited state S_1 $10^{-10} - 10^{-7}$ s → Fluorescence
Intersystem crossing $10^{-10} - 10^{-8}$ s
Internal conversion $10^{-11} - 10^{-9}$ s
Lifetime of the excited state T_1 $10^{-6} - 10$ s → Phosphorescence

Figure. 2.2. *The upper panel represents the Jablonski diagram illustrating processes occurring within a molecular system after light absorption. Straight upward arrows indicate absorption of light, straight downward arrows indicate radiative relaxation processes (fluorescence and phosphorescence), wavy arrows indicate non-radiative relaxation processes. The middle panel represents schematic spectra of absorption, fluorescence and phosphorescence. The lower panel shows the characteristic timescales of the processes indicated in the Jablonski diagram. Adapted from Ref.* [26] *with the permission from Wiley-VCH. Copyright © 2012 Wiley-VCH Verlag GmbH & Co. KGaA.*

Usually, absorption to the high excited state (S_2 and further) is followed by the fast (10^{-12} s – 10^{-9} s) non-radiative relaxation processes (vibrational

relaxation (VR) and/or internal conversion (IC)) to the lowest vibrational level of the first excited singlet state (S_1). Fluorescence usually occurs from the lowest vibrational state of the first singlet excited state. This empirical principle is called *Kasha's rule* [31]. However, it should be noted that some molecules, such as metal-porphyrins or polyenes, exhibit fluorescence from higher excited states [32]. Such type of fluorescence is called *anti-Kasha emission* [33]. Fluorescence competes with non-radiative relaxation process, such as intersystem crossing (ISC). ISC sometimes exhibits the timescales comparable with those of fluorescence. ISC is a non-radiative transition between electronic states of different spin multiplicities, typically from singlet one to triplet one. Usually, excitation relaxes from the triplet state either with the emission – phosphorescence – or non-radiatively by dissipating excitation energy to the environment.

The Jablonski diagram presented in Figure 2.2 suggests the difference in absorption and fluorescence band positions of a fluorophore. This difference is usually called the *Stokes shift* [34]. The probability of absorption is determined, among other factors, by the FC factor (see *Section 2.1.1*), whereas fluorescence usually occurs from the lowest vibrational level of the first electronically excited singlet state. This fact, as well as relaxation processes prior to emission, explains the occurrence of the Stokes shifts. However, some molecules, for example free-base porphyrins [35], exhibit ideally overlapping absorption and fluorescence spectra.

Fluorescence (FL) spectroscopy is a useful tool for studying different intermolecular interactions and processes [13,36,37], as well as a basis for some sensing [38] and imaging [39,40] techniques.

2.1.3. Excited-state relaxation dynamics and fluorescence decay kinetics

The previous section (*Section 2.1.2*) discussed steady-state properties, i.e., FL spectrum represents emission integrated over time. Such a spectrum does not provide information on temporal evolution of the excited-state processes.

The temporal evolution of the population $N(t)$ of the excited state can be described by the following kinetic equation [34]:

$$\frac{dN(t)}{dt} = -kN(t), \tag{2.5}$$

where $\frac{d}{dt}$ denotes the operation of differentiation with respect to time, whereas k denotes the total relaxation rate constant, which is determined by both radiative and non-radiative processes.

The integration of Eq. 2.5 gives an exponential decay of the population of the state [34]:

$$N(t) = N_0 exp\left[{}^{-t}/_{\tau}\right], \quad (2.6)$$

where N_0 denotes the initial population of the state, and $\tau = 1/k$ denotes the lifetime of the state. It should be noted that the FL spectroscopy detects not the population of a state, but the intensity of the FL signal originating from this population. *However, the intensity of FL signal is proportional to the population of the state [34], therefore it obeys the same exponential decay law [34].* It should be noted that in complex molecular systems one can observe multi-exponential decays originating either from several emitting species or from different excited-state processes, such as excitation energy migration [18].

The efficiency of FL, i.e., FL quantum yield (QY), is defined as ratio of number of the emitted photons N_{em} to the number of absorbed N_{abs}. FL QY depends on the parameters characterizing the temporal evolution of the excited state as follows [12]:

$$QY = \frac{N_{em}}{N_{abs}} = \frac{k_r}{k} = \frac{\tau}{\tau_r}, \quad (2.7)$$

where k_r is the radiative rate constant, k is the total relaxation rate equal to the sum of the radiative and all the non-radiative relaxation rate constants, τ is FL lifetime, while $\tau_r = 1/k_r$ is the intrinsic radiative lifetime, i.e., lifetime of FL in the absence of the non-radiative relaxation processes.

Since FL lifetime and QY depend on rates of non-radiative relaxation processes, they provide useful information on intermolecular interactions and processes, for example on excitation energy migration processes [18,41].

2.2. Interactions in molecular systems

2.2.1. Van der Waals interactions

Van der Waals (vdW) interaction is a relatively weak non-covalent interaction between atoms, molecules or molecular systems arising from the interactions between their charge distributions. The interactions between these charge distributions can be described in terms of their electric dipole moments. Three main types of such interactions can be distinguished. The first one is the interaction between two permanent dipoles, which is referred to as the Keesom force [42]. The second one is the interaction between a permanent dipole and an induced one – Debye force [42]. London dispersion forces arise from the interaction between two fluctuating dipoles [42]. In such a case, an instantaneous dipole moment in one species induces a fluctuating dipole moment in a neighboring species, and their correlated fluctuations result in a mutual attraction. Therefore, London dispersion forces are present in all species containing electrons, including non-polar ones [43].

The dispersion energy E_{disp} between species A and B at the separation distance R between them can be expressed using the following asymptotic formula [44,45]:

$$E_{disp} = -\frac{C_6}{R^6}, \tag{2.8}$$

where C_6 denotes the system-specific dispersion coefficient, which is determined by polarizabilities of A and B species, while the negative sign ('$-$') indicates mutual attraction between the species.

Figure 2.3 schematically represents the dependence of dispersion energy on the distance between interacting species. According to Eq. 2.8, at relatively long distances species A and B are attracted to each other. However, at relatively short distances this equation is no longer valid due to significant overlap of the electronic wave functions of the interacting species. In such a case, with decreasing distance, the dispersion energy approaches a constant value [45]. Additionally, at short distances, the electronic clouds of the interacting species overlap, and, according to Pauli exclusion principle, the species start to repel each other [42].

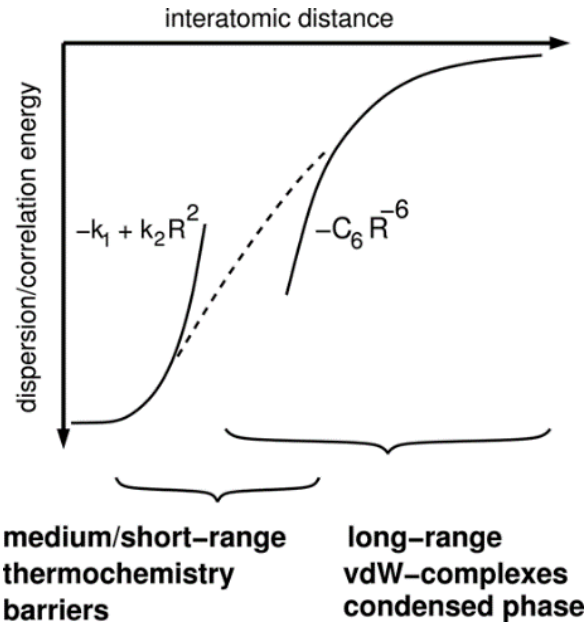


Figure 2.3. *The asymptotic behavior of the dispersion energy at relatively short and relatively long separation distances between interacting species.* C_6*, as well as* k_1 *and* k_2 *are system-specific constants* [45]. *Reprinted from Ref.* [46] *with the permission from John Wiley and Sons. Copyright © 2014, John Wiley and Sons.*

The vdW interactions in general, and dispersion forces in particular, play an important role in molecular packing and aggregation, as well as in chemical reactions and catalysis [43,47].

2.2.2. Molecular aggregates

A molecular aggregate is an assembly of identical or different molecular species stabilized by vdW forces, hydrogen bonding, π- π stacking, and other non-covalent interactions. Figure 2.4 (a) illustrates different geometries of π-π stacking using benzene dimer as an example, while Figure 2.4 (b) shows several examples of hydrogen bonding using acetic acid dimer, aromatic ring and cyclic water trimer.

The optical properties of molecular aggregates strongly depend on molecular packing and can either differ from those of the corresponding isolated molecule or remain unchanged [11]. Perhaps, one of the most pronounced aggregation-induced effects is changes in FL efficiency. The so-called aggregation-caused quenching (ACQ) [48] is observed in many molecular systems. In some fluorophores increasing molecular concentration leads to the formation of aggregate species that quench FL. The left panel of Figure 2.5 represent this effect using perylene as an example of a compound exhibiting such a phenomenon.

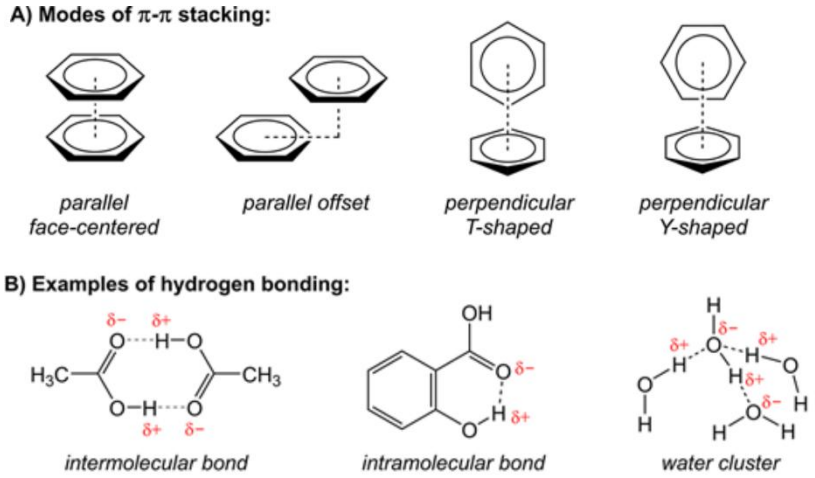


Figure 2.4. *a) Schematic illustration of the different modes of π-π stacking of the benzene dimer. b) Intermolecular hydrogen bond forming the dimer of acetic acid (left subpanel), intramolecular hydrogen bond in the aromatic ring (the central subpanel), and the formation of a cyclic water trimer stabilized by hydrogen bonds between water molecules (right subpanel). Both panels (a,b) are reprinted from Ref.* [42] *under the terms of the Creative Commons Attribution 4.0 International (CC BY 4.0) license.*

In contrast to ACQ, aggregation-induced emission (AIE) [49] is a phenomenon resulting in an enhanced FL of the compound in an aggregated form. It usually occurs due to restrictions in intramolecular motions – rotations and/or vibrations – in an aggregated compound compared with monomeric one [11]. The right panel in Figure 2.5 illustrates the AIE effect in hexaphenylsilole THF/water solution.

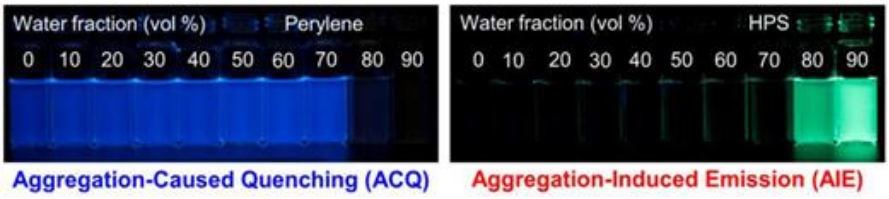


Figure 2.5. *The manifestation of aggregation-caused quenching of FL in perylene solution (left panel), and the manifestation of aggregation-induced emission effect in hexaphenylsilole THF/water solution (right panel) upon increasing the water fraction. Reprinted from Ref.* [11] *with the permission from American Chemical Society. Copyright © 2015 American Chemical Society.*

AIE is a promising phenomenon for various optoelectronic applications, for example photovoltaics or optical waveguides [11].

2.2.3. Excitonically-coupled aggregates: H- and J-aggregates

Close packing of molecules can result in significant intermolecular electronic interactions, which can affect both ground- and excited-state properties of an aggregate. This section describes such molecular systems in terms of the *Kasha model of molecular dimer* (see, for example, Refs. [50–52]).

The Coulomb coupling between two molecules in an aggregate using the point-dipole approximation can be expressed as follows [53]:

$$J_C^{pd} = \frac{\vec{\mu}_1 \cdot \vec{\mu}_2 - 3(\vec{\mu}_1 \cdot \hat{R})(\vec{\mu}_2 \cdot \hat{R})}{4\pi\varepsilon R^3}, \quad (2.9)$$

where $\vec{\mu}_1$ and $\vec{\mu}_2$ denote the vectors of transition dipole moments from the electronic ground state to the electronic excited state for the first and second molecules, respectively, $\hat{R}$ denotes the unit vector directed along the displacement vector with a magnitude R connecting the mass centers of two interacting molecules, as well as ε denotes the dielectric constant of a medium.

The Eq. 2.9 suggests the importance of the mutual orientation of transition dipole moments. Figure 2.6 (a) schematically represents the mutual orientation of transition dipole moments for a molecular homodimer. It should

be noted that the J_C^{pd} is equal to zero when the transition dipoles oriented relative to each other at the magic angel θ_M equal to 54.7 degrees [53]. The aggregates exhibiting so-called 'head-to-tail' ($\theta < \theta_M$) relative orientation of the transition dipoles are referred to as *J-aggregates* [53]. Such an orientation results in negative Coulomb coupling J_C^{pd} [53]. On the contrary, aggregates exhibiting 'side-by-side' orientation, i.e., $\theta_M < \theta < \pi/2$, exhibit positive Coulomb coupling J_C^{pd} and are called *H-aggregates* [53].

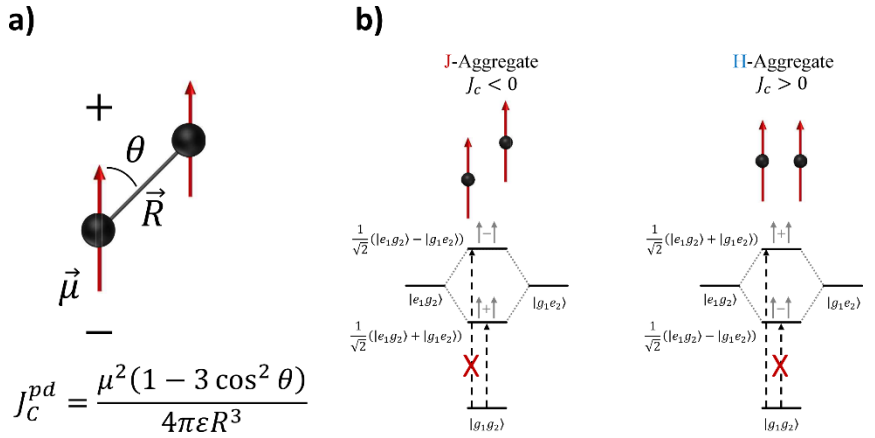


Figure 2.6. *a) The schematic representation of the relative orientation of transition dipole moments in a molecular dimer. b) The schematic representation of the electronic transitions in J- and H-aggregates. Both panels are reprinted from Ref.* [53] *with the permission from American Chemical Society. Copyright © 2018 American Chemical Society.*

The intermolecular electronic coupling results in the formation of two excitonic states, which can be expressed as follows [24,53]:

$$|\Psi_{\pm}\rangle = \frac{1}{\sqrt{2}}\,(|e_1g_2\rangle \pm \langle g_1e_2|). \tag{2.10}$$

In Eq. 2.10 $|\Psi_{\pm}\rangle$ denotes two ($|\Psi_+\rangle$ and $|\Psi_-\rangle$) excitonic states of a molecular dimer. The splitting of the excited state in a molecular aggregate is called *Davydov splitting* [9,24,53]. $|e_1g_2\rangle$ and $\langle g_1e_2|$ are the states corresponding to the excitation being localized on the first and second molecule, respectively. Therefore, Eq. 2.10 suggests *the delocalization of the electronic excitation* within a dimer. Such aggregates are referred to as *excitonically-coupled* aggregates.

The sign of Coulomb coupling significantly affects the photophysical properties of aggregates [53]: H- and J-aggregates exhibit different optical

properties. Figure 2.6 (b) represents the electronic transitions in J- and H-aggregates. The in-phase state ($|\Psi_+\rangle$) is characterized by the enhanced transition dipole moment value by a factor of $\sqrt{2}$ compared with that of monomer, whereas the electronic transition to the out-of-phase state ($|\Psi_-\rangle$) is forbidden, because transition dipole moments mutually cancel each other. The difference in optical properties of J- and H-aggregates is the following: the in-phase state of J-aggregate has lower energy than the energy of monomeric excited state, whereas that of H-aggregates exhibits higher energy. Therefore, J-aggregates usually exhibit red-shifted electronic absorption bands compared with monomers, while H-aggregates demonstrate blue-shifted absorption spectrum. Additionally, J- and H-aggregates exhibit different FL properties. H-aggregates usually exhibit significant decrease in FL intensities compared with that of monomers, therefore solutions and films containing big amount of them usually exhibit pronounced FL quenching [18]. In contrast, J-aggregates are usually emissive exhibiting accelerated intrinsic radiative decay by a factor of 2 [53].

2.3. Excitation energy transfer

2.3.1. Introduction to excitation energy transfer

Excitation energy transfer (EET) is either a radiative or a non-radiative process in which excitation energy is transferred from one molecular species (energy donor; D) to another (energy acceptor; A) [54]. EET occurs without net charge transfer and does not require significant spatial reorganization, whereas the total energy of the donor-acceptor system is conserved during the EET event [55]. The simple EET event can be expressed using the following equation [56]:

$$D^* + A \rightarrow D + A^*, \tag{2.11}$$

where the asterisk sign '*' denotes the excited species.

According to Eq. 2.11, following the initial excitation of donor species, the emission of light by the donor species [57] or interaction between donor and acceptor species – Coulombic and/or electron exchange interactions [55] – leads to the EET event, and donor species relaxes to the ground state, while acceptor species appears in an electronically excited one [56]. Figure 2.7 schematically represents EET event described with Eq. 2.11. It should be noted that EET processes can provide an additional non-radiative relaxation channel for an excited donor species, and the kinetic equation (Eq. 2.5) should therefore contain EET rate constant.

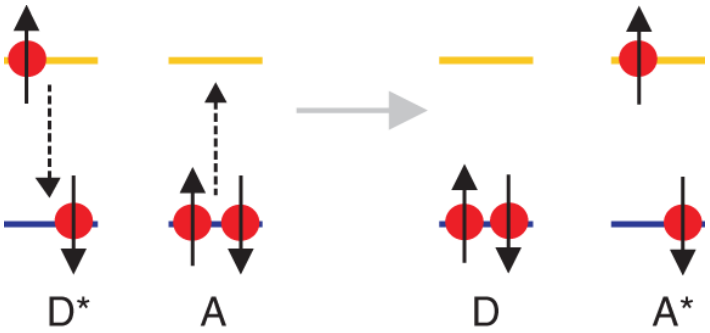


Figure 2.7. *The schematic representation of excitation energy transfer event denoted using Eq. 2.11. The blue horizontal lines represent the highest occupied molecular orbital (HOMO), while yellow horizontal lines represent the lowest unoccupied molecular orbital (LUMO) of both donor (D) and acceptor (A) species. Black vertical arrows indicate electron spin projections, while black dashed upwards and downwards arrows represent HOMO—LUMO and LUMO-HOMO electronic transitions, respectively. Reprinted from Ref.* [56] *with the permission from Wiley-VCH. Copyright © 2023 Wiley-VCH GmbH.*

EET processes play an important role in natural and artificial photosynthesis [1,58–60], as well as in some organic photovoltaic systems [15]. Additionally, systems exhibiting EET are considered to be suitable model systems for probing an efficiency of quantum computations with bosonic quantum devices [61].

2.3.2. Mechanisms of excitation energy transfer

This section concentrates mainly on non-radiative EET processes. However, firstly radiative EET process should be briefly introduced.

Radiative EET occurs through the following sequence of events: initially excited donor species emit photon, which is reabsorbed by acceptor species. The efficiency of this process depends on the intrinsic FL QY of donor species, molecular concentration of acceptor species, spectral overlap and geometrical sizes of a sample [57]. Such an effect results in a decrease in FL intensities exhibiting by donor species [57].

The non-radiative EET occurs through electronic interaction between donor and acceptor species without net photon emission. The non-radiative EET events can occur in coherent and incoherent regimes. In the incoherent regime, EET is usually referred to as a sequence of energy-hopping events [15]. This process can be described [15] in terms of Markov-type random walk

model [62]. In contrast, coherent EET process exhibits wave-like dynamics, in which excitation cannot be attributed to a particular species; it is considered to be delocalized within the interacting species [63]. Further we concentrate on *incoherent EET* processes.

Figure 2.8 schematically represents the sequence of events involved in *Dexter-type EET*. This EET mechanism involves electron exchange between the donor and acceptor species and therefore requires significant overlap of their electronic wave functions. Dexter EET occurs at low separation distances between donor and acceptor species: the distance at which this process is effective is usually not higher than 1 nm [24]. This process can be represented by the following sequence of events [56]:

$$\begin{matrix} |D^*A\rangle \rightarrow |D^+A^-\rangle \rightarrow |DA^*\rangle \\ |D^*A\rangle \rightarrow |D^-A^+\rangle \rightarrow |DA^*\rangle \end{matrix}, \tag{2.12}$$

where the upper equation corresponds to the first EET pathway with the formation of molecular cation D^+ and molecular anion A^-, whereas the lower equation corresponds to the second EET pathway with the formation of molecular anion D^- and molecular cation A^+.

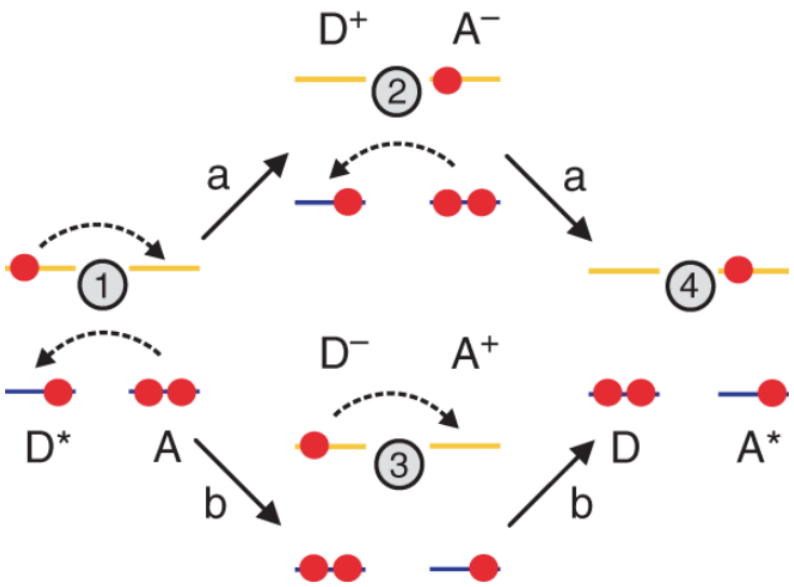


Figure 2.8. *The schematic representation of the excitation energy transfer process via Dexter mechanism. The pathway 'a' corresponds to the upper formula in Eq. 2.12, whereas the pathways 'b' corresponds to the lower formula in Eq. 2.12. Reprinted from Ref.* [56] *with the permission from Wiley-VCH. Copyright © 2023 Wiley-VCH GmbH.*

The rate of the EET event via a Dexter mechanism exponentially depends on the separation distance between donor and acceptor species [15,24,64], and can be expressed using the following equation [15]:

$$k_{EET}^{D} = KJ\exp\left[-\frac{2R}{L_{vdW}}\right], \tag{2.13}$$

where k_{EET}^{D} denotes the rate of EET event via Dexter mechanism, K is a parameter describing an orbital interaction, J is the spectral overlap integral between FL spectrum of donor species and absorption spectrum of acceptor species [15,24], whereas R is a separation distance between interacting species, and L_{vdW} is a van der Waals radius.

It should be noted that Dexter mechanism can involve non-emissive states and, consequently, not only singlet, but also triplet excitons [15,24].

2.3.3. Förster resonance energy transfer

Förster resonance energy transfer (FRET) [65] is a non-radiative EET mechanism arising from Coulombic interactions between donor and acceptor species. In contrast to the Dexter mechanism, FRET does not require overlap of wave functions and does not involve electron exchange. The typical FRET operation distances are up to approximately 20 nm [24,66].

In the simplest case – in the ideal dipole approximation – the donor and acceptor species are approximated as point transition dipoles interacting via Coulombic forces [67]. Figure 2.9 (upper panel) schematically represents the interaction between transition dipole moment of donor and acceptor species in an ideal point-dipole approximation. In such a case the coupling between interacting species can be denoted by the same equation used to express coupling in an excitonically-coupled dimer (see Eq. 2.9, *Section 2.2.3*) [12]. The FRET event requires energetic resonance between donor and acceptor species, which is reflected in a significant overlap between the emission spectrum of donor species and the absorption spectrum of acceptor species [67]. The middle panel in Figure 2.9 represents such a case. Additionally, it should be noted that since the donor-acceptor system is approximated as point transition dipoles, FRET rate strongly depends on the mutual orientation of the donor and acceptor transition dipole moments.

The rate of the FRET can be expressed as follows [12,24,55,67]:

$$k_{DA}^{FRET} = \frac{1}{\tau_D}\left(\frac{R_F}{R}\right)^6, \tag{2.14}$$

where k_{DA}^{FRET} denotes energy transfer rate via FRET mechanism, τ_D is an intrinsic fluorescence lifetime of a donor (as was defined in Eq. 2.7), R is a separation distance between donor and acceptor species, while R_F is Förster radius. This equation does not include the mutual orientation parameter κ^2,

which is omitted in this notation, corresponding to the orientationally-averaged approximation [12]. Eq. 2.14 shows that the rate constant of the FRET event depends on the separation distance R as R^{-6}, in contrast to the Dexter mechanism, which exhibits exponential dependence of the rate constant on the distance between donor and acceptor species.

Förster radius R_F is a system-specific parameter which is defined as the distance at which the FRET efficiency is equal to 0.5 (50%) [24]. The lower panel in Figure 2.9 represents the efficiency of FRET process: it strongly depends on the separation distance between donor and acceptor species and can be expressed as the ratio of donor FL lifetimes in and without the presence of acceptor species.

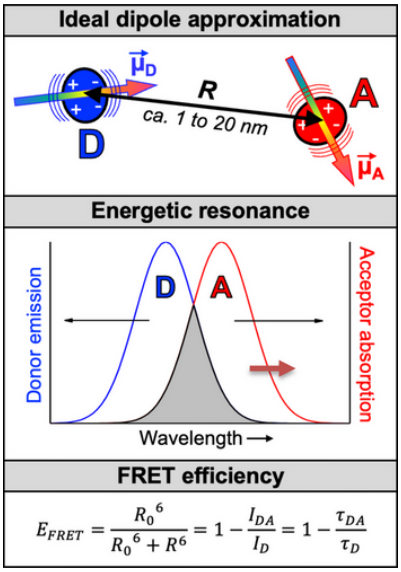


Figure 2.9. *The upper panel schematically represents the interaction between transition dipole moments of donor and acceptor species, and shows characteristic distances of the FRET process. The middle panel schematically represents the spectral overlap between FL spectrum of donor and absorption spectrum of acceptor. The lower panel indicates the dependence of FRET efficiency on different parameters of the system. In this scheme* R_0 *denotes Förster radius, whereas* τ_{DA} *denotes the donor FL lifetime in the presence of acceptors. Reprinted from Ref.* [66] *with the permission from Wiley-VCH. Copyright © 2025 Wiley-VCH GmbH.*

2.3.4. Concentration quenching of fluorescence

This section is dedicated to the discussion of mechanisms of concentration quenching of FL arising from EET from emissive species to non-emissive ones acting as excitation traps. In these traps excitation is lost and this results in a decrease in FL QY of a system. However, firstly *static* and *dynamic* FL quenching mechanisms should be briefly introduced [34]. According to *Lakowicz* [34], the difference between these FL quenching mechanisms is as follows. Dynamic quenching occurs, when a fluorophore being in an *electronically excited state* collides with some quenching species and, hence, non-radiatively loses some energy. In contrast, static quenching is a *ground-state* processes occurring when a fluorophore forms a stable molecular complex with some quenching species, resulting in the formation of molecular structures suppressing FL.

FL quenching arising from excitation energy migration from one species to another species is an alternative mechanism of the FL quenching. When the formation of the excitation trap species and, consequently, FL quenching efficiency is increased with the increasing molecular concentration of a fluorophore, such a phenomenon is referred to as concentration quenching (CQ) of FL.

Figure 2.10 represents two common models of the spatial distribution of the excitation trap species. The panels (a) and (c) represent so-called *random trap* model in a two- and three-dimensional geometries, respectively. The random trap model describes a case when any species can act as a trap. Figure 2.10 (b, d) represent the *statistical trap* model. In terms of this model any of the species separated from each other by the critical distance act as excitation traps. One should note, that none of these models specify the exact molecular origin of the trap species. In a general case, the molecular origin of the traps is not known, however most common of them are H-aggregates [68] and the species exhibiting charge transfer state [69].

The excitation reaches a trap via EET events [70,71]. Considering EET as a sequence of hopping events, one can model this process using a random walk model. Additionally, a simple model accounting for EET from a single donor species surrounded by an infinite number of acceptors (hereafter denoted as *'DA' model*) can be applied to some molecular systems. This model is based on the following assumptions: the acceptor species is considered to be infinitely energetically deep, i.e., the excitation cannot escape them, and additionally spatial and orientational distribution of the acceptor species are assumed to be uniform. In such a case, considering FRET as the EET mechanism, the kinetic Eq. 2.5 should be modified to include the FRET rate

constant. The following expression defines the probability $P(t)$ that the donor remains electronically excited [12,70]:

$$P(t) = \exp\left[-\frac{t}{\tau_D} - \left(\frac{t}{\tau_2}\right)^b\right], \tag{2.15}$$

where τ_D denotes the intrinsic FL lifetime of donor species without acceptor species, τ_2 represents the characteristic quenching time due to acceptor species, and b parameter depends on the system's dimensionality. Eq. 2.15 can be applied when the relative concentration of donor and acceptor species within the system is known [72–74], however its explanatory power is somewhat limited in case of solutions and films consisting of the only molecular species, because in such a case it is difficult to define the exact concentration of the acceptor species.

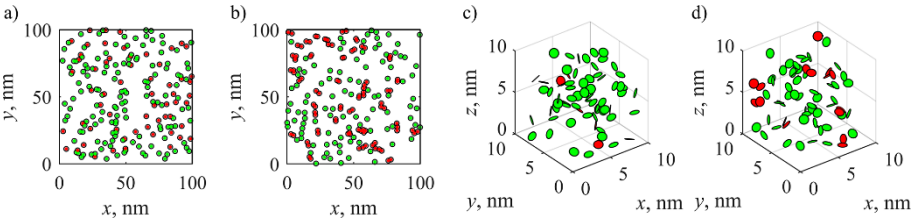


Figure 2.10. *The graphical representation of the random trap model (a,c) for the two- and three-dimensional geometries, respectively. The graphical representation of the statistical trap model (b,d) for the two- and three-dimensional geometries, respectively. Green dots indicate emissive species, while red dots indicate trap species. Reprinted from Ref.* [12] *under the terms of the Creative Commons Attribution 4.0 International (CC BY 4.0) license*.

CQ is observed in many natural and synthetic compounds, including, but not limited to chlorophylls [68,75,76], phthalocyanines [18], perylenes [77] , and other compounds. From a practical perspective, CQ is detrimental for the light-to-energy applications, including photovoltaics [15,16], optoelectronics [17,78], and artificial photosynthesis [58,60]. Nowadays researchers try to suppress FL quenching in the light-to-energy conversion architectures using so-called 'size-matching' principle [58,60,79]. However, it should be mentioned that CQ phenomenon can be useful for bioimaging [80] and biosensing [81] applications. This inspires the desire to deeply understand the molecular mechanisms governing this phenomenon.

3. MATERIALS AND METHODS

3.1. Materials

All the materials used in this research work, namely chloroform, 2,9,16,23-tetra-tert-butyl-29H,31H-phthalocyanine (TTBPc; $C_{48}H_{50}N_8$), zinc 2,9,16,23-tetra-tert-butyl-29H,31H-phthalocyanine (ZnTTBPc; $C_{48}H_{48}N_8Zn$), *trans*-stilbene (TS, $C_{14}H_{12}$), polystyrene (PS), and hexagonal boron nitride (hBN) were purchased from Sigma-Aldrich and were used as received without any purification.

3.2. Sample preparation

3.2.1. TTBPc and ZnTTBPc solutions

In this study firstly the stock 10 mmol/l (mM) chloroform solutions of both TTBPc and ZnTTBPc were prepared. The stock solutions were diluted with chloroform to obtain the solutions of 3 mM, 1 mM, 0.3 mM and 0.1 mM molecular concentrations.

For low concentrated solutions (up to 1 mM) electronic absorption spectra were measured via placing the solutions in circular quartz cuvettes with an optical path length of 0.1 mm (QS 124-0.1). However, high concentrated solutions (3 mM and 10 mM) exhibited too high intensities, therefore they were measured between two thin glass coverslips.

To minimize the influence of reabsorption effect [20] (see *Section 3.4.1* for details) fluorescence spectra as well as decay kinetics of all the solutions were measured between two circular glass cover slips (0.13–0.17 mm thick, 22 mm in diameter) sealed with nail polish. Although such a method effectively suppresses reabsorption, the optical path length cannot be determined somewhat precisely, because the thickness of the sample depends on the spacing between two coverslips and cannot be controlled. However, this limitation does not affect the fluorescence-decay analysis.

3.2.2. TS spin-coated films

The stock 30 mg/ml solution of PS in chloroform was prepared, after that this solution was diluted to obtain PS solutions with mass concentration of 15 mg/ml, 10 mg/ml, 5 mg/ml and 3 mg/ml. TS was dissolved in these solutions with the following TS:PS mass ratio in percent: 0.5%, 10%, 20%, 60% and 80%.

For electronic spectroscopy and atomic force microscopy (AFM), thin films were prepared on pre-cleaned with chloroform quartz substrates using

the KW-4A spin-coater in the following mode: 70 revolutions per minute (r/m) for 3 s and 1200 r/m for 30 s **[*Paper A2*]**.

The same spin-coater and the same operating mode was used to prepare samples for coherent anti-Stokes Raman Scattering (CARS) microscopy, however thin circular glass cover slip, i.e., the same one which was used to measure fluorescence of phthalocyanine solutions, was used as a substrate.

3.2.3. TS + hBN van der Waals complex

Purchased TS as well as hBN were ground in a mortar to obtain fine powder. This was done do reduce particle sizes to minimize possible scattering of light during optical spectroscopy measurements. To make TS + hBN van der Waals (vdW) complex the TS and hBN mixture (1:1 mass ratio, approximately 400 mg of each) was firstly put in chloroform. TS dissolved immediately, while hBN is not dissolved in chloroform in general. This suspension was left in a fume hood for 12 hours until chloroform evaporated. It was assumed that during the evaporation process TS was adsorbed on hBN surface.

TS and TS + hBN powders were pressed into 0.8 mm-thick tablets. It was impossible to obtain hBN tablet, therefore for FL measurements its powder was used. It should be noted, that 1:1 mass ratio of TS and hBN was selected, because i) it allowed the preparation of a mechanically stable TS + hBN tablet, ii) and it enabled the spectroscopic investigation of vdW interaction using equal masses of *bulk materials*.

Additionally, samples, which were used for supporting experimental methods, should be briefly discussed. For THz spectroscopy the same tablets as for FL measurements were used. However, it was decided not to measure THz spectrum of hBN in powder, therefore hBN was mixed with polyethylene (1:1 mass ratio) and pressed in a tablet. Polyethylene was chosen due to i) its ability to be pressed in a tablet and ii) because it has only one weak intensity band in THz region (see **[*Paper A3*]** and Ref. [82]). For Raman scattering powders of all the compounds were used as samples.

3.3. Electronic absorption measurements

All the electronic absorption spectra of all the samples were measured with Jasco V-670 spectrophotometer in a transmission mode, i.e., transmitted through a sample light was detected. For ZnTTBPc and TTBPc samples the absorption spectrum of chloroform was pre-measured and considered as a baseline, which was automatically removed by the device from the measured spectrum of the sample. For TS spin-coated films the absorbance of the PS film was considered as a baseline. The absorption spectrum of none of the

samples from **[*Paper A3*]** was recorded, since these bulk samples do not transmit light.

3.4. Steady-state fluorescence measurements

FL spectra of all the studied samples were measured with Edinburgh F920 spectrometer. TS thin films, bulk TS tablet, hBN and TS + hBN samples were excited with 300 nm picosecond pulsed diode, 2-nm spectral slit and 850 ps pulse duration. All the measured spectra were automatically corrected to the instrument sensitivity. ZnTTBPc and TTBPc chloroform solutions were excited with 375 nm pulsed diode laser having 70 ps pulse duration and the 4 nm spectral slit was chosen to obtain higher signal.

In addition to steady-state FL spectra, FL excitation spectra for TS thin films **[*Paper A2*]** were measured with Edinburgh FS5 spectrofluorometer. The samples were excited with a xenon lamp with emission spectral slit set as 0.15 nm, while excitation one was opened to 2 nm. FL excitation spectrum indicates how FL intensity at a specific emission wavelength depends on excitation wavelength and for some FL species it is the same as absorption one. Deviations of the excitation spectrum from the absorption one can indicate, e.g., the presence of optically dark states or the migration of excitation between species in the system [34].

3.4.1. Insights into minimizing the influence of reabsorption effect on ZnTTBPc and TTBPc fluorescence spectra

Reabsorption of the emitted light usually occurs when a fluorophore has i) high optical density (OD), i.e., OD > 0.1, and ii) when steady-state absorption and fluorescence spectra overlap. Reabsorption usually manifests in red shifted fluorescence peak compared to a sample with reasonably small OD. This effect can lead to the misinterpretation of the observed fluorescence spectrum and, for example, incorrect assumption of the presence of J-aggregates in the system, because they usually exhibit red shifted fluorescence peak compared with a monomeric compound [53].

Even though spin-coated films of TS can exhibit relatively high ODs (see, e.g., *Karpicz, et.al.* [13] or **[*Paper A2*]**), high Stokes shifts suggest the absence or, at least, negligible manifestation of the reabsorption effect in these compounds. However, absorption and fluorescence spectra of both free-base and metal phthalocyanines significantly overlap [[18,27,37,83], **[*Paper A1*]**]. Therefore, for correct interpretation of the results of fluorescence measurements, minimizing the manifestation of reabsorption effect, i.e., reducing the ODs of high concentrated samples, is of critical importance.

To achieve this goal samples for both steady-state fluorescence measurements as well as FL decay kinetics were prepared between two thinnest commercially available glass coverslips (diameter of this coverslip was 22 mm, while thickness was 0.13–0.17 mm according to the manufacturer VWR International). The sample preparation itself was simple: An Eppendorf pipette was used to place 10 µl of a solution on a glass, then second glass was pressed against the first one and sealed with a nail polish **[*Paper A1*]**. This sample preparation method allowed to minimize the manifestation of reabsorption effect on the one hand, and obtain reasonable FL intensities on the other hand. However, for low concentration samples ODs were very small to detect steady-state absorption spectrum, therefore it was measured in circular quartz cuvettes (QS 124-0.1). To demonstrate the manifestation of reabsorption effect, we also measured steady-state FL in this cuvette. In Figure 3.1 raw and normalized to unity steady-state FL spectra of both TTBPc and ZnTTBPc chloroform solutions measured in QS 124-0.1 quartz cuvette across the entire set of concentrations covering two orders of magnitude are presented. These measurements showed significant red shifts in FL spectra with the increase in molecular concentration of both phthalocyanines at high ODs. In Table 3.1. comparison between results obtained for samples measured in QS 124-0.1 cuvette and in glass cover slips (GCs) are presented. Samples measured in QS 124-01 cuvette exhibit artificially increased Stokes shifts compared with those measured in GC. These shifts are the result of the reabsorption effect. *Dhami, et.al.* [20] observed the same manifestation of the effect for different phthalocyanine compounds.

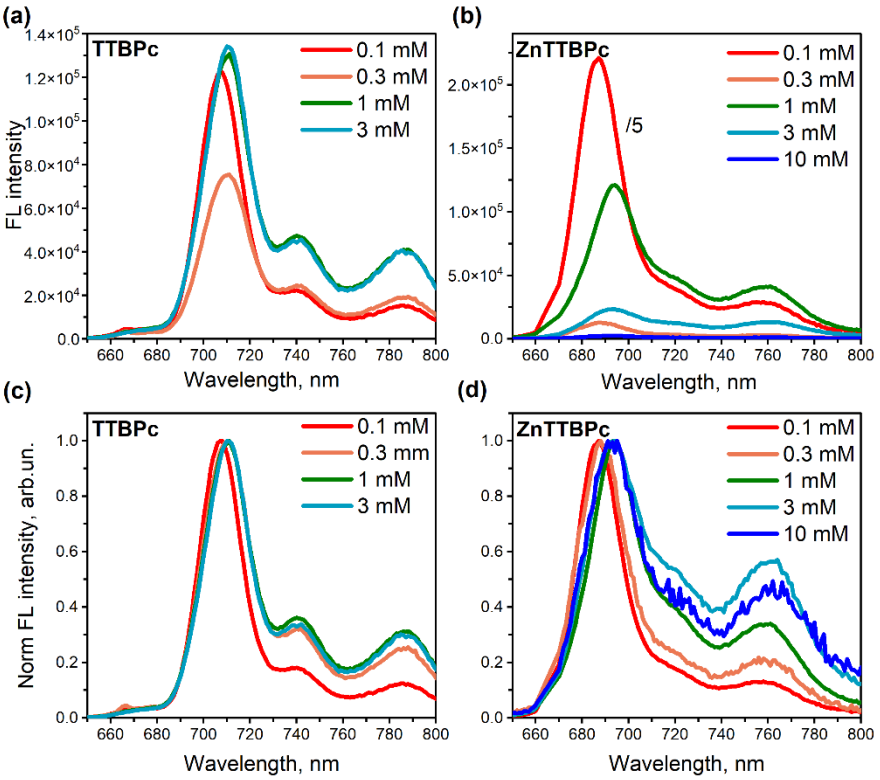


Figure 3.1. *Raw steady-state FL spectra of TTBPc (a) and ZnTTBPc (b) chloroform solutions measured in QS 124-0.1 quartz cuvette. For clarity spectrum of 0.1 mM ZnTTBPc solution was multiplied by the factor of 5. Normalized to unity steady-state FL spectra of TTBPc (c) and ZnTTBPc (d) chloroform solutions measured in QS 124-0.1 quartz cuvette. All the samples were excited at 375 nm. Adapted from* **[*Paper A1*]**, *with the permission of AIP Publishing.*

Table 3.1. *Main characteristics of fluorescence measurements in quartz cuvette (QC) of TTBPc and ZnTTBPc chloroform solutions. For comparison in this table results obtained for samples measured in glass cover slips (GC) are presented. Adapted from* **[*Paper A1*]**, *with the permission of AIP Publishing.*

	TTBPc				**ZnTTBPc**			
Conc, mM	Abs. peaks, nm	OD at 701 nm in QC	FL peak, nm (Stokes shift, nm) in GC	FL peak, nm (Stokes shift, nm) in QC	Abs peaks, nm	OD at 701 nm in QC	FL peak, nm (Stokes shift, nm) in GC	FL peak, nm (Stokes shift, nm) in QC
0.1	640, 664, 701	0.16	704 (3)	708 (7)	613, 648, 680	0.10	684 (4)	687 (7)
0.3	637, 664, 701	0.31	704 (3)	711 (10)	613, 648, 680	0.41	684 (4)	688 (8)
1	637, 664, 701	1.03	704 (3)	711 (10)	613, 647, 679	1.15	685 (6)	694 (15)
3	---	---	704 (3)	710 (9)	---	---	685 (6)	694 (15)
10	---	---	705 (4)	---	---	---	687 (8)	695 (16)

3.5. Fluorescence decay kinetics measurements

Fluorescence decay kinetics of all the samples were measured with the Edinburgh F920 spectrometer using time correlated single photon counting technique [34]. All the kinetics were recorded using the same parameters and conditions, as were used for the measurements of the steady-state FL spectrum of the corresponding sample.

All the kinetics were fitted with a convolution of different model functions, which were chosen according to the specific task, with the pre-measured instrument response function (IRF). To obtain better fit quality, IRF was fitted as a convolution of a Gaussian function with a single exponential decay:

$$\mathrm{IRF}\,(t) = \exp\left(-\frac{(t-t_0)^2}{2\sigma^2}\right) * \exp\left(-\frac{t}{\tau}\right), \tag{3.1}$$

where σ is a width of Gaussian, τ represents characteristic decay time of IRF, t_0 defines the difference between initial IRF and kinetics profiles, while asterisk symbol '$*$' denotes convolution operation. All the mentioned parameters had to be optimized during the fit of IRF.

3.6. Data processing and analysis

3.6.1. Data processing of steady-state spectroscopy

The obtained steady-state absorption and fluorescence data did not require difficult data processing, except horizontal background removal and/or smoothing in case they were noisy. These procedures were performed using *Python* packages *Pandas* [84], *NumPy* [85] and *SciPy* [86].

3.6.2. Target analysis of FL decay kinetics

The decay kinetics fittings with convolution of different model functions, namely, mono-, multi- and stretched-exponential decay functions, with IRF's approximation using Eq. 3.1. were performed with *Python* package *lmfit* [87] using the differential evolution algorithm [88].

It should be noted, that instead of applying Poisson weighting [34] to the time correlated single photon counting data and including horizontal background in the fits, the background was simply subtracted from the experimental spectra.

3.6.3. Global analysis of FL spectra and FL decay kinetics

In contrast to target analysis, global analysis is used when one needs not to obtain lifetimes or decompose each particular spectrum, but when common features and/or differences have to be found in the whole set of measurements [89]. Mathematically this task can be formulated in terms of multivariate curve resolution problem [90]. In a matrix form it can be written the following way [[89,91], ***Paper A2***]:

$$F(\lambda, n) = \sum_{i=1}^{n} S_i(\lambda) \cdot C_i(n), \tag{3.2}$$

where in general case $F(\lambda, n)$ represents matrix containing experimental results, $S_i(\lambda)$ is a basis matrix and $C_i(n)$ is a matrix of weights.

Usually so-called model-based methods are applied for global analysis. These models are used, for example, when one fits time-resolved fluorescence or transient absorption data and the time-resolved behavior, i.e., the form of $C_i(n)$ matrix, can be *a priori* assumed somewhat reasonably. The most widely used method is the decay-associated spectrum (DAS) [89,92] technique, when it is assumed that the spectra of the components exhibit single-exponential decay. For example, *Mascoli, et.al.* [93] applied this method to fit time-resolved fluorescence data of minor light-harvesting complexes of plants.

However, sometimes it may be more useful not to impose restrictions on the behavior of components. In such a case no parts in Eq. 3.2. are *a priori* known. In principle, in such a case infinite number of the solutions of Eq. 3.2. can be found. However, when one deals with fluorescence spectrum and/or decay kinetics it can be stated, that each element in Eq. 3.2. has non-negative value. In such a case non-negative matrix factorization (NNMF) [91] can be performed, assuming that *the components are spectroscopically independent*. This method, e.g., was successfully applied to fit time-resolved fluorescence of aggregates of light harvesting complex II [94] and fucoxanthin–chlorophyll protein complexes [95].

In **[*Paper A2*]** we applied multiplicative update algorithm [96] for NNMF to both the entire sets of steady-state FL spectra and FL decay kinetics to reveal the features of morphology-induced changes in optical properties of TS films.

3.7. Supporting experimental and theoretical methods

As stated in the *Section 1.8*, several additional experiments and theoretical calculations supporting the conclusions of this thesis were performed by the co-authors of the publications. This section briefly introduces the supporting techniques presented in the thesis.

3.7.1. TTBPc and ZnTTBPc chloroform solutions

To support conclusions based on **[*Paper A1*]**, quantum chemical calculations were performed for ZnTTBPc and TTBPc monomers and H-dimer structures. The structures themselves were optimized using density functional theory (DFT) on the LC-BLYP/6-31G(d) level. The calculations of transition dipole moments and excited-state energies of the corresponding molecules were performed using time-dependent density functional theory (TD-DFT) using LC-BLYP functional. All the details of the calculations can be found in **[*Paper A1*]**. ***All the calculations were performed by Dr. Andrius Gelzinis and Darius Likandrovas at the High-Performance Computing Center "HPC Saulėtekis", Vilnius University.***

3.7.2. TS spin-coated thin films

In the [***Paper A2***] *trans*- and *cis*-stilbene structures were optimized using DFT applying B3LYP and CAM-B3LYP functionals. All the details can be found in the **[*Paper A2*]**. ***These calculations were performed by Dr. Mindaugas Mačernis at the High-Performance Computing Center "HPC Saulėtekis", Vilnius University.***

The results of the coherent anti-Stokes Raman Scattering (CARS) microspectroscopy and of the atomic force microscopy (AFM) of the TS spin-coated films are discussed in the *section 4.2.3*. AFM-based characterization of

the films was performed using DimensionIcon system (Bruker). The image resolution for all the samples was not less than 128 pixels. The thicknesses of the films were evaluated by scratching some small area of the film until the substrate was reached, and the microscope image analysis was performed with the Nanoscope Analysis software (Bruker). ***AFM measurements were performed by Dr. Marija Jankunec at the Life Sciences Center of Vilnius University.***

Polarization-resolved CARS characterization using single-wavelength CARS system (see, for example, Ref. [97]). The CARS signal was obtained using laser pulses at the constant 1064 nm wavelength and tunable one at the 900 nm – 935 nm. Polarization-resolved measurements were performed by the rotating the placed in front of the studied sample AHWP05M-980 half-wave-plate (Thorlabs) in the range from -180° to +180°. The CARS images were recorded using IX microscope (Olympus) and P-517.3CL scanning system (Physik Instrumente). ***CARS measurements were performed by Dr. Andrej Dementjev using custom-built CARS microspectroscopy system at the Department of the Molecular Compound Physics (MDFS), State Research Institute Center for Physical Sciences and Technology (FTMC), Vilnius, Lithuania.***

3.7.3. TS + hBN van der Waals complex

DFT-based quantum chemical calculations were performed in the **[*Paper A3*]** to assign THz and Raman bands (see *Section 4.3.3*). All the structures in terms of Model I (see *Section 4.3.1* for details) were optimized and their THz and Raman spectra were calculated using cc-pVDZ basis set and B3LYP as well as BPW91 functionals. All the structures and spectra in terms of Model II (see *Section 4.3.1* for details) were calculated using PBE functional with ultrasoft pseudopotentials. All the details of the calculations can be found in the **[*Paper A3*]**. ***All the calculations were performed by Dr. Maksim Shundalau using supercomputer cluster at the University of Salerno, Italy***.

Raman spectroscopy measurements were performed using an inVia Raman microscope (Renishaw) using a green laser emitting at 532 nm with the laser power equal to 0.5 mW. To collect the spectra, an objective lens (50 ×/0.75 NA; Leica) was used, and the integration time was set to 500 s. The spectra were collected from a spot of approximately 1 μm in diameter. ***All the Raman spectroscopy measurements were performed by Dr. Martynas Talaikis from the Department of Organic Chemistry, FTMC.***

THz absorption spectra were measured using Terahertz time domain spectroscopy system T-SPEC 800 (Teravil). The obtained THz signals were averaged 256 times to obtain the final signal. ***All the THz spectroscopy***

measurements were performed by Dr. Daniil Pashnev together with Dr. Irmantas Kašalynas and Dr. Andžej Urbanovič from the Department of Optoelectronics, FTMC.

4. RESULTS AND DISCUSSION

4.1. Concentration quenching of fluorescence in phthalocyanine chloroform solutions

4.1.1. Initial remarks

This section is dedicated to the analysis of concentration-induced changes in the electronic properties of free-base and zinc-substituted phthalocyanine solutions. Varying molecular concentration of both **2,9,16,23-tetra-tert-butyl-29H,31H-phthalocyanine** [**TTBPc**; Molecular Formula is $C_{48}H_{50}N_8$; Figure 4.1 (a)] and **zinc 2,9,16,23-tetra-tert-butyl-29H,31H-phthalocyanine** [**ZnTTBPc**; Molecular Formula is $C_{48}H_{48}N_8Zn$; Figure 4.1 (b)] by two orders of magnitude from 0.1 mmol/L (mM) to 10 mM we investigated steady-state properties, i.e., absorption and fluorescence (FL), as well as FL decay kinetics, and examined changes with the increase in concentration.

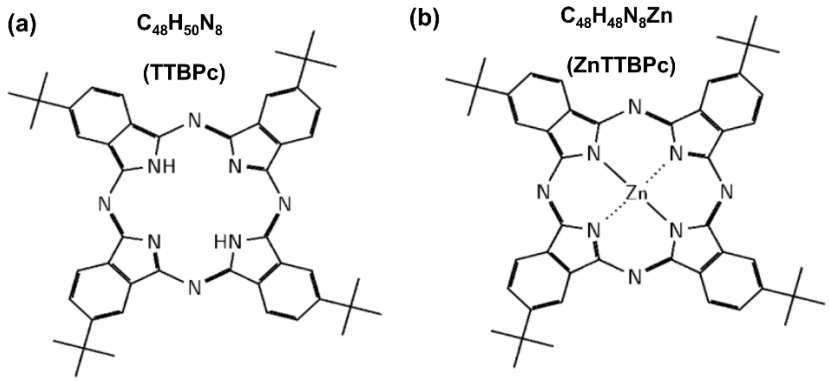


Figure 4.1. *Molecular structures of (a) TTBPc and (b) ZnTTBPc phthalocyanines. Adapted from* **[*Paper A1*]**, *with the permission of AIP Publishing.*

4.1.2. Short overview of phthalocyanine compounds applications and properties

Phthalocyanines are structural relatives of chlorophylls – natural plant pigments responsible for light harvesting in photosynthesis [1]. Therefore, one of the most straightforward fields of applications of phthalocyanine compounds is light-to-energy conversion systems, namely mimicking natural photosynthesis [59,98,99] and/or as components of artificial photosynthetic architectures [2,100], as well as organic photovoltaics devices [101]. In

addition, phthalocyanines nowadays have shown potential in optoelectronics [102–105], ecology due to their ability to purify water via generating singlet oxygen species [106], as well as in biomedical applications, for example, as photosensitizers in photodynamic cancer therapy [107] and in cardiology [108]. All these applications result in the growing interest and detailed study of the photophysical properties of different phthalocyanine compounds under different conditions [18,27,37,109–112].

Additionally, both free-base and metal phthalocyanines are known to exhibit aggregates formation with molecular concentration increase and, hence, aggregation-induced changes in electronic spectra [27,112,113]. *Therefore, nowadays phthalocyanine compounds are widely used as model systems for observing and studying different photophysical effects, such as quenching of fluorescence and/or excitation energy migration* [18,19,100,114]. *Tamošiūnaitė, et.al.* [18] *described* ***concentration quenching (CQ) of fluorescence*** *for ZnTTBPc spin-coated thin films, however concentration-dependent fluorescence dynamics in phthalocyanine solutions as well as photophysical processes governing CQ remain undescribed, which is crucial for present and possible future applications.*

4.1.3. Steady-state absorption and fluorescence of TTBPc and ZnTTBPc

Phthalocyanine monomeric compounds demonstrate two intense absorption bands, namely **Soret** or B_x and B_y **bands** ($S_0 \rightarrow S_3$ and $S_0 \rightarrow S_4$ electronic transitions) in the blue region of the spectrum, and two intense Q_x and Q_y **bands** ($S_0 \rightarrow S_1$ and $S_0 \rightarrow S_2$ electronic transitions) in the red region of the spectrum. This splitting happens due to different x- and y-polarizations of transition dipole moments. However, in the case of metal phthalocyanines an increase in symmetry from D_{2h} point group to D_{4h} point group leads to electronic bands degeneracy and, consequently, for metal phthalocyanines one can observe two (single ***B***- and single ***Q*-bands**) intense electronic bands with low intense vibronic features [109,113].

Figure 4.2 (a, b) illustrates normalized to unity steady-state absorption spectrum of zinc 2,9,16,23-tetra-tert-butyl-29H,31H-phthalocyanine (**ZnTTBPc)** and 2,9,16,23-tetra-tert-butyl-29H,31H-phthalocyanine (**TTBPc**) at different molecular concentrations. Since the core part of this part of the work is the analysis of *concentration dependent fluorescence* properties of phthalocyanine compounds, we present absorption spectra only at the *Q*-band region of the spectrum, which is usually the only electronic excited state responsible for fluorescence, according to *Kasha's rule* [31]. ZnTTBPc exhibits ~680 nm *Q*-band absorption over the entire range of the studied concentrations. It is worth noting that with the increase in molecular

concentration a subtle increase in bandwidth as well as in low intense vibronic bands are observed. Absorption spectra of TTBPc samples at the same set of molecular concentrations exhibit two non-degenerate peaks at approximately 664 nm (Q_y-band) and 701 nm (Q_x-band). In addition to two intense electronic peaks, free-base TTBPc has a strong vibronic band at 640 nm. Interestingly, the relative intensities of both the 640 nm and 664 nm absorption peaks monotonically increase upon increase in molecular concentration. *Tolbin, et.al.* [115] attributed the similar relative increase in intensities of *clamshell*-type phthalocyanine ligands to the formation of H-aggregates. Since ZnTTBPc exhibits similar dynamics, but in a weaker manner, the observed changes in its spectra might also be explained by the formation of H-aggregates, albeit to a lesser extent than in a free-base TTBPc case.

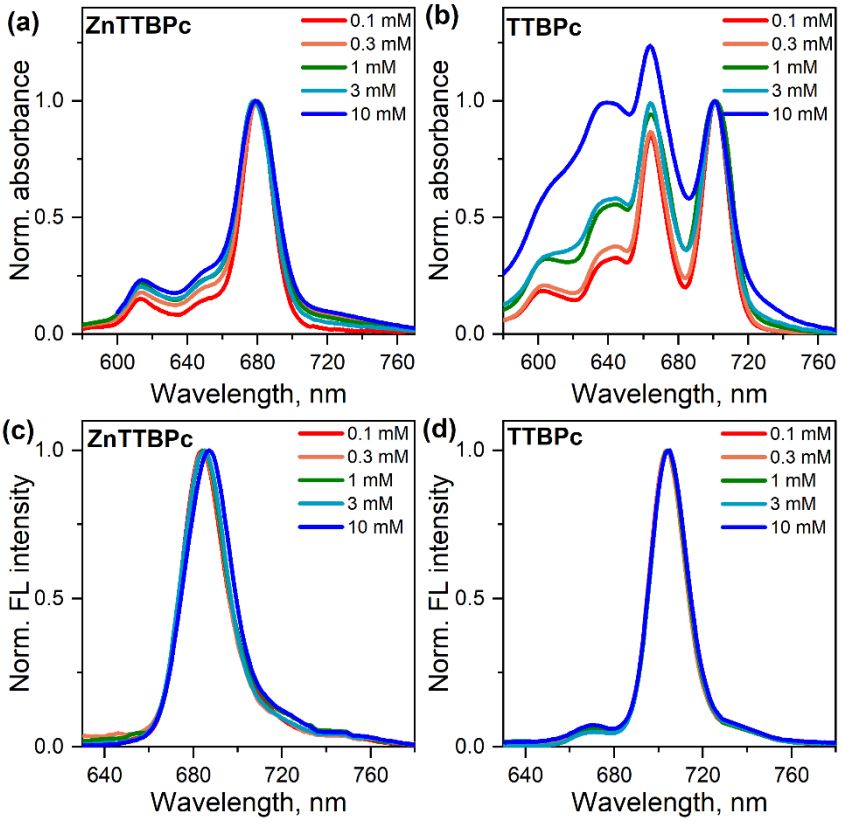


Figure 4.2. *The normalized Q-band electronic absorption spectra of (a) ZnTTBPc and (b) TTBPc. Normalized to the maximum steady-state fluorescence spectra of (c) ZnTTBPc and (d) TTBPc. For all the FL spectra* λ_{exc} *=375 nm. The set of molecular concentrations is [0.1 mM, 0.3 mM, 1 mM, 3 mM, 10 mM]. Adapted from* **[*Paper A1*]**, *with the permission of AIP Publishing.*

In Figure 4.2 (c, d) normalized to unity FL spectra of ZnTTBPc and TTBPc chloroform solutions measured across all the set of concentrations are presented. ZnTTBPc FL spectrum exhibits single dominating peak which is shifted from 684 nm (4 nm Stokes shift, see Table 4.1.) for the lowest concentrations (0.1 mM and 0.3 mM) to 687 nm (8 nm Stokes shift, Table 4.1.) for the highest 10 mM concentration. It is difficult to assign precisely the origin of the observed shift of FL band: on the one hand it can be caused by subtle manifestation of reabsorption effect [20], on the other hand the formation of some FL species leading to red shifted FL spectrum (such as small amount of J-type aggregates [53] present within the system) cannot be completely excluded based on only steady-state spectra evolution. It is worth mentioning that *Tamošiūnaitė, et.al.* [18] detected similar 3 nm shift of FL band of ZnTTBPc spin-coated films with the increase in molecular concentration, while ODs were relatively small. Similarly to ZnTTBPc, TTBPc also exhibits single-peak dominating FL spectrum centered at 704 nm (3 nm Stokes shift, Table 4.1.) for all the concentrations except 10 mM having single peak at 705 nm and, consequently, 4 nm Stokes shift. Relative intensities of vibronic features in TTBPc FL spectrum, as well as in ZnTTBPc spectrum, remain unchanged with the increase in concentrations.

Table 4.1. *Q-bands absorption peak positions, optical densities at the maximum and fluorescence peak positions of TTBPc and ZnTTBPc solutions in chloroform across 0.1–10 mM concentrations range. Adapted from* **[*Paper A1*]**, *with the permission of AIP Publishing.*

Conc, mM	**TTBPc**			**ZnTTBPc**		
	Abs peaks, nm	OD at 701 nm	FL peak, nm (Stokes shift, nm)	Abs peaks, nm	OD at 680 nm	FL peak, nm (Stokes shift, nm)
0.1	640, 664, 701	<0.01	704(3)	613, 648, 680	<0.01	684(4)
0.3	637, 664, 701	0.04	704(3)	613, 648, 680	0.01	684(4)
1	637, 664, 701	<0.01	704(3)	613, 647, 679	<0.01	685(6)
3	637, 664, 701	0.04	704(3)	613, 648, 679	0.09	685(6)
10	637, 664, 701	0.06	705(4)	613, 647, 679	0.13	687(8)

4.1.4. Concentration-dependent FL decay kinetics of TTBPc and ZnTTBPc

Figure 4.3. illustrates normalized FL decays of TTBPc and ZnTTBPc chloroform solutions at 0.1 – 10 mM concentrations range. Both compounds exhibit similar behavior with the increase in concentration, i.e., monotonic decrease in the average FL lifetimes (see Table 4.2). Firstly, at low concentrations (0.1 mM and 0.3 mM) both compounds have mono-exponential decays with the FL average lifetimes equal to 5.68 ns and 5.43 ns for TTBPc, respectively, as well as 3.20 ns and 3.06 ns for ZnTTBPc, respectively (average lifetimes obtained from exponential fits can be found in Table 4.2.). With further increase in concertation decays exhibit faster bi-exponential profiles (1 mM TTBPc solution exhibits FL decay with the average lifetime equal to 3.10 ns, while 1 mM ZnTTBPc has 1.25 ns decay). High concentrated solutions, i.e., 3 mM and 10 mM, exhibit even faster decays with 1.64 ns and 0.20 ns for TTBPc, respectively, as well as 0.58 ns and 0.27 ns for ZnTTBPc, respectively. The kinetics of 3 mM TTBPc solution is somewhat well described by bi-exponential decay, while three exponents are required to fit ZnTTBPc FL decay kinetics at the same concentration. However, this monotonic increase in the number of required exponents is broken when it comes to 10 mM samples. In case of TTBPc second exponential component has an amplitude equal to 8%, almost approaching mono-exponential profile, while 10 mM ZnTTBPc kinetics requires two exponents, in contrast to triple-exponential decay for 3 mM sample. This probably can be explained by the fact that these 10 mM kinetics almost approach IRF profile and, possibly, real decay components are faster than the detection limit of the setup.

However, the observed decay behavior can be described using stretched-exponential decay:

$$K(t) = a \cdot \exp[-(t/\tau)^b], \tag{4.1}$$

with average FL lifetime τ_{av} evaluated as follows:

$$\tau_{\mathrm{av}} = \tau \cdot \Gamma\left(1 + \frac{1}{b}\right), \tag{4.2}$$

In these formulas τ is an optimized lifetime, b is a stretching parameter and $\Gamma(\cdot)$ is a gamma-function.

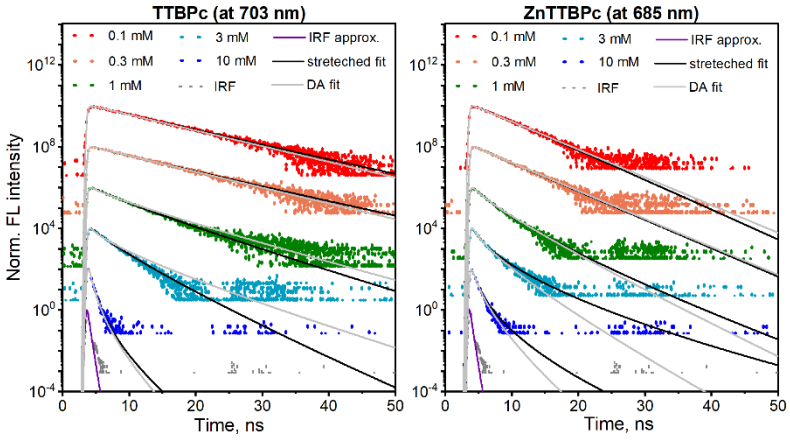


Figure 4.3. *Experimental FL decay kinetics (dots) of TTBPc and ZnTTBPc solutions in chloroform, measured across 0.1 mM – 10 mM range of concentrations at 703 nm and 685 nm, respectively. All the samples were excited using 375-nm laser. Black and light grey lines represent the fits using the stretched-exponential function (Eq. 4.1) and the single donor, surrounded by infinite number of acceptors model (DA model, Eq. 4.3), respectively. All the kinetics are shifted by the factor of* 10^2*. For clarity, at the bottom of each graph the laser IRF as well as its approximation with Eq. 3.1 are presented. Adapted from* **[*Paper A1*]***, with the permission of AIP Publishing.*

The obtained fits are presented as black lines in Figure 4.3, while Table 4.2 contains fitting parameters. The evolution of stretching parameter b from 1 for low-concentrated samples to 0.5 for the highest concentrations (see Table 4.2) represents monotonic changes from mono-exponentiality to multi-exponentiality in time-resolved behavior of the system. It is worth mentioning that the similar b-parameter evolution with the increase in molecular concentration of the ZnTTBPc spin-coated thin films was obtained by *Tamošiūnaitė, et.al.* [18]. However, this evolution does not provide any physical insights into the origin of the CQ phenomenon in phthalocyanine compounds. Therefore, in the following section deeper analysis of the observed changes in FL decay kinetics is provided.

Table 4.2. *Lifetimes, relative amplitudes and average lifetimes of FL decay kinetics of TTBPc and ZnTTBPc chloroform solutions obtained from multi-exponential fits as well as the parameters of the stretched-exponential fits with Eq. 4.1 and their average lifetimes computed with Eq. 4.2. Adapted from* **[*Paper A1*]***, with the permission of AIP Publishing.*

Conc, mM	Exponential decay				Stretched exponential decay		
	τ_1, ns	τ_2, ns	τ_3, ns	τ_{av}, ns	τ	b	τ_{av}, ns
TTBPc							
0.1	5.68 (100%)			5.68	5.59	0.97	5.66
0.3	5.43 (100%)			5.43	5.29	0.95	5.40
1	3.76 (69%)	1.61 (31%)		3.10	2.86	0.89	3.03
3	2.01 (75%)	0.51 (25%)		1.64	1.50	0.85	1.63
10	0.70 (8%)	0.15 (92%)		0.20	0.05	0.50	0.10
ZnTTBPc							
0.1	3.20 (100%)			3.20	3.26	1.02	3.22
0.3	3.06 (100%)			3.06	3.05	0.99	3.06
1	1.76 (65%)	0.31 (35%)		1.25	1.11	0.77	1.29
3	2.65 (5%)	0.97 (39%)	0.12 (56%)	0.58	0.39	0.59	0.61
10	0.64 (25%)	0.13 (75%)		0.27	0.09	0.50	0.17

4.1.5. CQ in ZnTTBPc and TTBPc due to excitation energy migration to trap species

The observed concentration-dependent picture, i.e., no significant changes in both steady-state absorption and FL spectra, and decrease in FL lifetimes as well as monotonic transition from mono-exponential decay to multi-exponential one, is less likely to occur due to the presence of multiple emissive species, such as monomers exhibiting long-lived FL and aggregates having short one. In such a case one would observe constant bi-exponential decay with the same decay components and different amplitudes over the entire concentration range. In our case lifetime components, as well as amplitudes, exhibit chaotic values across all the concentrations, making bi-exponential decay suitable mathematical model to describe the detected

kinetics, but not physical one. Such bimolecular reactions, as either excimer formation or collisional quenching, cannot somewhat reasonably describe the observed CQ picture. Usually, these quenching mechanisms can be detected at nanosecond timescales [116,117], but in our case FL lifetimes of high concentrated samples are 0.1 – 0.3 ns (see Table 4.2).

Therefore, most likely these phthalocyanine solutions have the only dominant FL species at all the concentrations and CQ happen due to excitation energy migration from monomeric species to excitation traps.

To verify this assumption the simplest possible model of the Förster-like energy transfer between two species can be applied, i.e., single donor surrounded by infinite number of acceptors (DA) model:

$$P(t) = \exp\left[-\frac{t}{\tau_A} - \left(\frac{t}{\tau_B}\right)^{1/2}\right]. \quad (4.3)$$

This formula represents the probability $P(t)$ of a donor species being excited after time t, while τ_A is an intrinsic FL lifetime of a donor species, as well as $\tau_B = 9/(16\pi^3 C n_A^2)$ represents characteristic decay time due to excitation traps; n_A here is a mean acceptor concentration. This equation is adapted from the Eq. 2.15 for the three-dimensional geometry.

The fits of the experimental kinetics with the DA model are presented in a Figure 4.3 with light grey lines. Table 4.3 represents τ_B parameter values. It was assumed that the solutions of the lowest concentration of both compounds are pure monomeric, hence do not contain any trap species. Therefore, FL lifetime of donor species τ_A can be fixed for both compounds as a FL lifetime obtained from mono-exponential fits of the 0.1 mM samples. The '∞' values at 0.1 mM, i.e., lowest concentrations, indicate the absence of quenching. At the same time, at the highest concentrations τ_B being equal to approximately 0.1 ns indicate the prevalence of the excitation migration processes via FRET to non-emitting traps. The intermediate concentrations exhibit monotonic decrease in τ_B values with the increase in concentrations indicating sequential enhancement of the quenching.

The provided analysis allows to explain the observed concentration-dependent changes in FL decay kinetics in terms of excitation migration from monomeric phthalocyanine species to excitation traps. However, the molecular origin of these traps remains unclear. In principle, phthalocyanine compounds due to their planar structure are known to form H-aggregates [27]. As discussed previously (see *Section 2.2.3*), H-aggregates can serve as excitation trap species usually being almost non-fluorescent [53]. To verify this assumption Dr. Andrius Gelzinis and Darius Likandrovas in the **[*Paper A1*]** performed quantum chemical calculations of the structures and electronic

transition dipole moments of both monomeric and dimeric structures of TTBPc and ZnTTBPc compounds (see Figure 4.4 and Table 4.4).

Table 4.3. *τ_B values, obtained by fitting FL decay kinetics of TTBPc and ZnTTBPc chloroform solutions with DA model using Eq. 4.3. Reprinted from* **[*Paper A1*]**, *with the permission of AIP Publishing.*

Concentration, mM	τ_B, ns	
	TTBPc	ZnTTBPc
0.1	∞	∞
0.3	1189	691
1	6.35	1.66
3	1.28	0.50
10	0.05	0.11

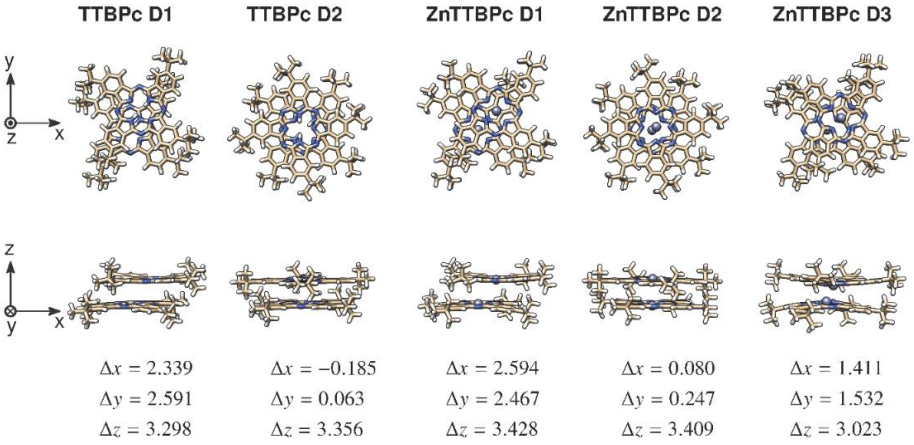


Figure 4.4. *The upper panel presents top views of the molecular structures of TTBPc and ZnTTBPc H-dimers. The middle panel presents side views of the corresponding structures. The lower panel shows the relative displacements of the corresponding monomers along the x, y and z axes. The initial H-dimer structures – prior to optimization – were generated by placing the two monomers on top of each other with a relative orientation of 0° or 45° about the z axis. All the structures were optimized at the LC-BLYP/6-31G(d) level of theory using the GaussView program. Reprinted from* **[*Paper A1*]**, *with the permission of AIP Publishing. / Computations were performed by Dr. Andrius Gelzinis and Darius Likandrovas (both FTMC).*

And indeed, the calculations show that both compounds can form stable H-type dimers, namely there are three stable H-type dimer geometries for ZnTTBPc and two stable H-type geometries for TTBPc (see Figure 4.4). The details of quantum chemical calculations can be found in the **[*Paper A1*]** and its supplementary material, while here the main trends are provided. Firstly, both TTBPc and ZnTTBPc exhibit similar transition energies $E_1 - E_0$ (see Table 4.4) at monomeric and dimeric configurations, which supports the assumption of possible monomer – H-dimer Förster energy transfer. Secondly, monomers of both compounds exhibit higher (from approximately 3 to approximately 10 times) transition dipole moments to the first electronic excited states than H-dimers (see Table 4.4). This probably does not make the obtained dimeric structures to be ideal optically dark, but suggests significant decrease in FL quantum yield (QY) of these species compared with monomers.

Table 4.4. *The transition energy to the first electronic excited state $E_1 - E_0$, and the corresponding electronic transition dipole moment $\mu_{0\to1}$ for each of the monomeric (M) species as well as the obtained stable dimers (D1, D2, D3) structures. All the computations were performed using Time-Dependent Density Functional Theory with LC-BLYP functional. Adapted from* **[*Paper A1*]**, *with the permission of AIP Publishing. / Computations were made by Dr. Andrius Gelzinis and Darius Likandrovas (both FTMC).*

Compound	$E_1 - E_0$, cm^{-1}	$\mu_{0\to1}$, D
TTBPc		
M	17087	9.4
D1	16455	1.8
D2	14066	2.5
ZnTTBPc		
M	14065	10.5
D1	13986	3.7
D2	11984	0.6
D3	14595	1.0

4.1.6. Current limitations and unresolved questions

Although the provided analysis enables complete description of CQ picture in phthalocyanine solutions, it has several limitations and leaves unresolved questions.

Firstly, it does not allow to evaluate Förster radius R_F of monomer – H-dimer system. In such a case for precise R_F computation exact concentration of acceptor species is required, but in our case, it is impossible to estimate it somewhat precisely. In principle, dependence of the concentration of acceptor species n_A on quenching parameter τ_B is known, namely being $\tau_B^{-1/2} \propto n_A$. Therefore, it might still be useful to analyze dependence of τ_B quenching parameter (see Table 4.3) on the molecular concentration of the solution (see Figure 4.5). The obtained dependence is almost linear for the lowest concentrations, while exhibit significant deviations from linearity for 10 mM samples. This observation supports the proposed CQ mechanism, i.e., energy migration to H-dimers, but additionally suggests some additional intermolecular processes happening at high concentrations, such as formation of higher aggregates. It should be noted, that the evaluated R_F would indicate the efficiency of excitation energy migration in this system and, consequently, the efficient FL quenching distance, making this knowledge crucial for practical purposes.

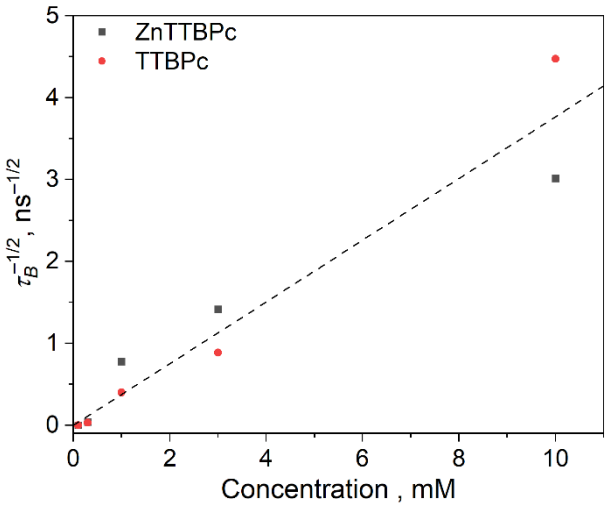


Figure 4.5. *Dependence between the parameter* $\tau_B^{-1/2}$ *and molecular concentration of the ZnTTBPc and TTBPc chloroform solutions. Adapted from* **[*Paper A1*]**, *with the permission of AIP Publishing.*

Additionally, it would be interesting to compare the observed CQ pictures in solutions and spin-coated thin films [18]. Interestingly, in Ref. [18] simple DA model (Eq. 2.15) did not describe FL decay kinetics of ZnTTBPc thin films somewhat precisely, therefore more complicated model taking into

account back transfer from traps to donor species had to be applied. It obviously states the difference in intermolecular processes in solutions and films, and, consequently, possible different efficiency in aggregates formation, however it is impossible to state this clearly at the current level of knowledge.

4.1.7. Summarizing remarks

i) The present section explores concentration quenching of fluorescence in the chloroform solutions of ZnTTBPc and TTBPc. Both compounds exhibit the same CQ dynamics. Steady-state spectra, i.e., absorption and fluorescence, of both compounds remain unchanged, while monotonic acceleration of decay kinetics as well as change from mono-exponential decay to multi-exponential one is observed. To explain these dynamics the simple model of excitation migration from donor to acceptor species was employed, while quantum chemical calculations suggested that the acceptor species, i.e., excitation traps, are H-aggregates of the compounds.

ii) The results of this study were published in **[*Paper A1*]** and presented at the following conferences: **[*Conferences C1, C2, C4, C7, C11, C13, C14*]**.

iii) The provided findings led to the ***first statement*** of the thesis:

Phthalocyanine solutions in chloroform exhibit concentration quenching of fluorescence, governed by Förster-type excitation energy migration from monomeric species to H-dimers. It manifests only in the time-resolved fluorescence decay kinetics through their monotonic acceleration and a smooth transition from mono-exponential to non-exponential decay with increasing concentration, making this technique the most efficient way to observe and study such type of the phenomenon.

4.2. Morphology-induced changes in FL properties of *trans*-stilbene thin films

4.2.1. Initial remarks

This section explores morphology-induced spectroscopic changes in *trans*-stilbene [TS; $C_{14}H_{12}$; Figure 4.6 (a)] spin-coated thin films. Varying both mass concentration of TS with respect to polystyrene (PS) matrix from 0.5% to 80%, as well as the thickness of the film from 45 nm to 670 nm, we explored the spectroscopic features of TS disordered aggregates as well as highly structured mono-crystallites (single crystals), applying atomic force microscopy (AFM), coherent anti-Stokes Raman scattering (CARS) microspectroscopy, as well as such electronic spectroscopy techniques, as steady-state Uv/vis absorption, FL excitation spectroscopy, steady-state FL

and FL decay kinetics. To get deeper insight into morphology-induced changes in optical properties, global analysis via non-negative matrix factorization (NNMF; Eq. 3.2) was applied to both steady-state FL and FL decay kinetics.

4.2.2. Short overview of stilbene compounds applications and properties

Stilbene is an organic compound with structural formula $C_6H_5CH{=}CHC_6H_5$ ($C_{14}H_{12}$). The most well-known feature of this compound is photochemical *trans*-*cis* photoisomerization (Figure 4.6) [118–120], which occurs under ultraviolet light in gas and liquid phases. *Cis*-stilbene (CS) nowadays serves as a useful model system to study ultrafast dynamics of photoisomerization, e.g., *Wang, et.al.* [121] observed vibrational coherences during photoisomerization of both gas and liquid CS. At the same time, such isomerization is less likely to occur in a solid state due to steric constraints [13,36,122], with *trans*-stereoisomer being more stable. TS can be applied in sensing and screening [14], for UV-irradiation detection[123,124] or for neutron irradiation detection [125–127].

TS has been widely characterized across infra-red [128,129] and Uv/visible [13,36,130] regions of spectrum. It should be noted, that the findings creating basis of this thesis increased the characterization range of TS molecules to THz **[*Paper A3*]** spectral region. It is worth mentioning that **[*Paper A3*]** showed that TS, being non-polar molecule, is an ideal candidate to be a model system for studying pure non-covalent, i.e., van der Waals, interactions between two-dimensional materials and organic compounds adsorbed on them (see *Section 4.3* for details).

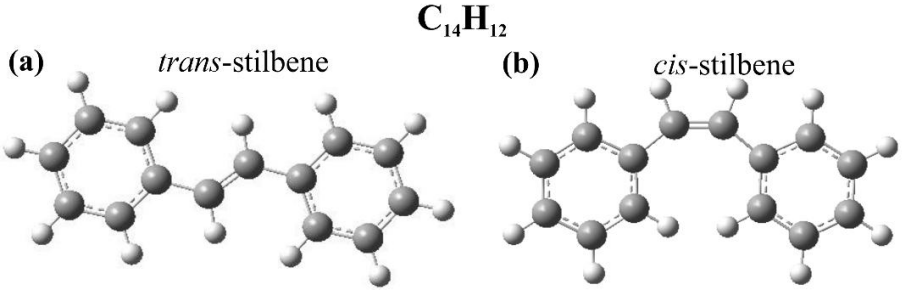


Figure 4.6. *Chemical structures of a) trans- and b) cis-stilbene compounds. Adapted from* **[*Paper A2*]** *under the CC BY 4.0 license. /Chemical structures were drawn using GaussView program by Dr. Mindaugas Mačernis (Vilnius University).*

TS stable thin films has been recently characterized by the means of SEM [13] and XRD [131]. *Karpicz, et.al.* [13] observed that increasing of TS concentration relative to the polymer matrix in a thin film leads to TS molecules clusterization and significant changes in FL spectra. *However precise three-dimensional morphology of such films as well as dynamics of optical properties governed by the changes in morphology with concentration and thickness increase remain underexplored, while this knowledge might help to manipulate the structure and properties of TS films, which might be useful for various applications.*

4.2.3. Structural transitions in TS thin films observed via CARS and AFM

Before analyzing possible morphology-induced changes in optical properties of TS thin films, it is necessary to explore films' morphology itself.

Figure 4.7 presents CARS microscopy images in false colors, corresponding spectra at several points and polarization-resolved spectra. For comparison, films of the same thickness, namely 670 nm, were examined by CARS [Figure 4.7 (a–c)], and additionally for the highest concentration of 80% an intermediate thickness [Figure 4.7 (d)] was measured with CARS microspectroscopy. All the films exhibit similar CARS spectra with two intense vibrational bands centered at approximately 1600 cm^{-1} – 1605 cm^{-1} and 1645 cm^{-1} – 1650 cm^{-1}, predominantly associated with C–H bending and C=C double-bond stretching, respectively **[*Paper A2*]**. CARS microscopy revealed formation of the μm-sized TS clusters for 60% and 80% films (see Figure 4.7). However, CARS microscopy of 20% TS film exhibits just constant background, either due to low signal or due to very small for being resolved size of TS clusters. To get deeper insight into the structure of the films, polarization-resolved measurements were applied. These measurements may help reveal the molecular ordering of a sample. A highly ordered molecular system would exhibit the following dependence between the intensity of CARS signal $I^{(\mathrm{CARS})}$ and polarization angle θ [132]:

$$I^{(\mathrm{CARS})} \propto \cos^6\theta. \tag{4.4}$$

All the detected polarization-resolved curves were fitted using Eq. 4.4. The signal from 20% TS sample cannot be fitted with this equation, indicating that this film most-likely consist of unstructured TS species: TS monomers, aggregates or their combination; while highly concentrated films – both 60% and 80% – exhibit spectra which can be well approximated with $\cos^6\theta$ and, consequently, contain highly ordered structures – most likely μm-sized TS single crystals. Taking into account both microscopy images and the quality of the fits with the Eq. 4.4, it can be stated that TS film of 80% concentration

and 670 nm thickness [Figure 4.7 (c)] consist mainly of TS single crystals, while films of both lower TS concentration [60%; Figure 4.7 (b)] and thickness [TS 80% 175-nm film; Figure 4.7 (d)] contain both highly-ordered single crystals and disordered aggregates and/or TS polycrystals which are partially disordered.

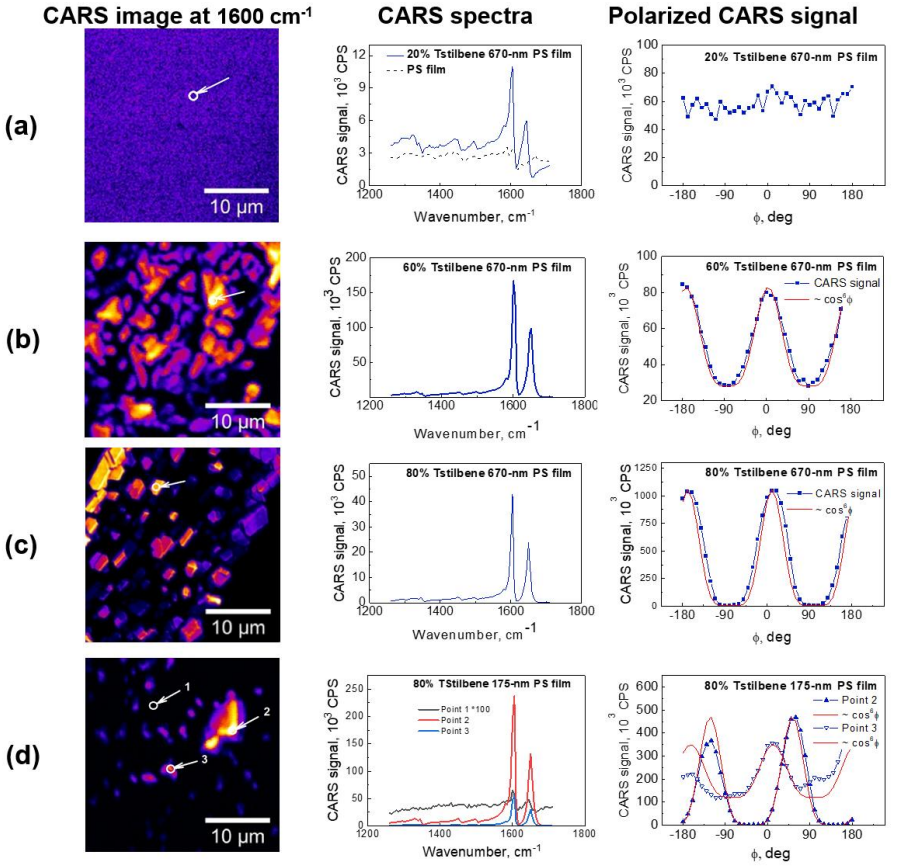


Figure 4.7. *The left panel presents CARS microscopy images (false colors) of TS thin films with different concentrations and thicknesses, recorded at 1600 cm^{-1}. The middle panel presents CARS spectra measured at the selected points. The spectra contain two Raman-active vibrational bands: one centered at 1600 cm^{-1} – 1605 cm^{-1} (dominated by C–H bending vibrations), and the other at approximately 1645 cm^{-1} – 1650 cm^{-1} (dominated by C=C stretching vibrations). The right panel shows polarization-resolved CARS spectra of different TS films measured at the corresponding points. Reprinted from* **[*Paper A2*]** *under the CC BY 4.0 license. / CARS measurements were performed by Dr. Andrej Dementjev (FTMC).*

Atomic force microscopy (AFM) was applied i) to measure the thicknesses of the studied films and ii) to probe the films' surface. Figure 4.8 (a) demonstrates surface topography of TS films of different concentrations and thicknesses. AFM reveals the following feature of TS self-organization, i.e., aggregates (TS 80% 45-nm film) and highly-ordered crystals (TS 80% 670-nm film) are formed on the films' surface. Comparison of CARS and AFM images of 0.5% TS sample suggests absence of (dis-) ordered structures both at the film's surface and throughout its volume.

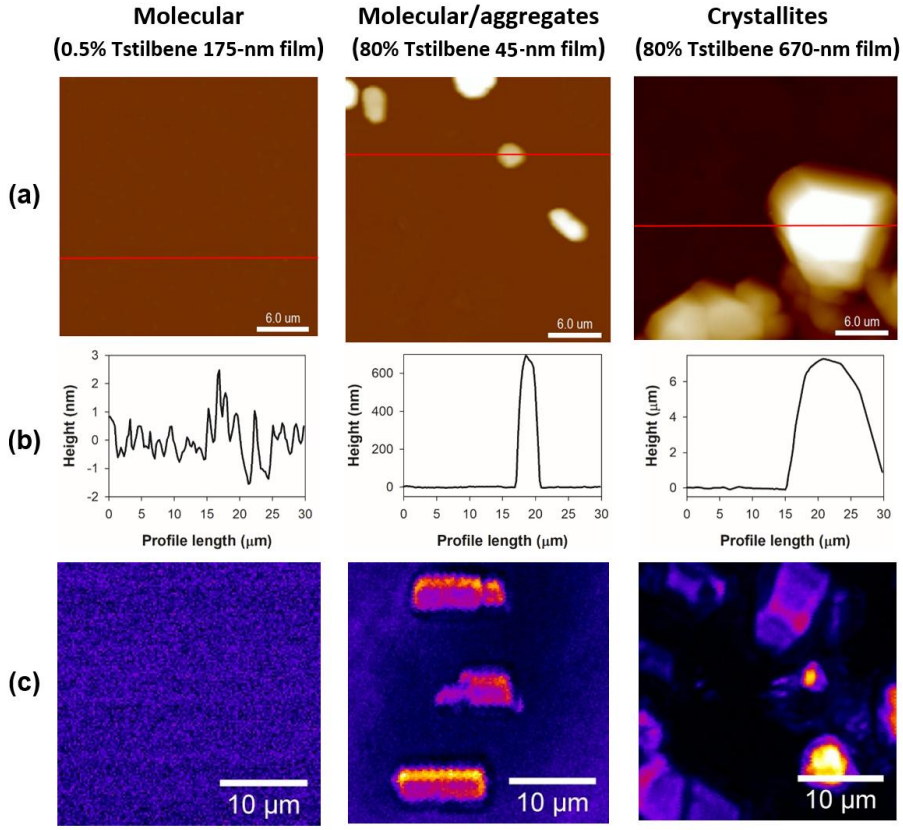


Figure 4.8. *a) 30 μm × 30 μm AFM surface scan of TS thin films. b) The height of the TS clusters, i.e., the distance from the film surface in the vertical direction along the red line shown in a). c) 30 μm × 30 μm CARS images of the same films. Reprinted from* **[*Paper A2*]** *under the CC BY 4.0 license. / AFM measurements were performed by Dr. Marija Jankunec (Vilnius University), while CARS measurements were performed by Dr. Andrej Dementjev (FTMC).*

Altogether, these findings suggest smooth transition from monomeric (pure molecular) morphology of TS films for the lowest concentration to the films consisting predominantly of disordered TS aggregates at the intermediate concentrations, and, finally, to the morphology which is dominated by the highly ordered TS monocrystals at the highest concentration. Additionally, it can be stated that the films' thickness regulates the amount and the size of these crystals (see Figure 4.7).

4.2.4. Steady-state electronic spectroscopy of TS thin films

Karpicz, et.al. [13,36] described electronic properties of TS compounds for both spin-coated thin films and bulk samples. It was stated, that *trans-cis* photoisomerization might still play an important role in photophysics of low concentrated – predominantly molecular – TS thin films, while with an increase in molecular concentration of TS thin films bulky species are formed and photoisomerization does not happen due to steric constraints. It was reported [13], that steady-state FL spectra of TS thin films exhibit red shifts with an increase in molecular concentration, while (normalized) electronic absorption spectra remain unchanged.

Figure 4.9 shows optical spectra, namely Uv/vis absorption, FL excitation and FL emission, varying both molecular concentration of TS at the fixed thickness of the films [see Figure 4.9 (a)], as well as the thickness of the film at the fixed molecular concentration of TS with respect to polystyrene (PS) matrix [see Figure 4.9 (b)]. Similarly to previous studies [13], normalized absorption, i.e., absorption bands positions, remain almost unchanged with the increase in concentration (see Figure 4.9 and Table 4.5). Increase in films' thickness also does not influence absorption shapes; increase in both concentration and thickness lead only to increases in ODs (see Table 4.5).

Increase in molecular concentration from 0.5% to 80% at a fixed 175 nm film thickness also does not influence FL excitation spectra [orange lines in the Figure 4.9 (a)], however FL excitation spectra corresponding to the highest thickness sample [TS 80% 670-nm film; see Figure 4.9 (b)] exhibit significant deviations from the electronic absorption spectrum. Most probably, the intense peak at the reddest region of the FL excitation spectrum (344 nm; see Table 4.5) of this sample originates from TS single crystal phase. This assumption can be supported by the structural analysis provided in the previous section (CARS and AFM images in the Figures 4.7 and 4.8). Therefore, the deviations from the corresponding electronic absorption spectrum might mean that this crystal-attributed band is optically dark.

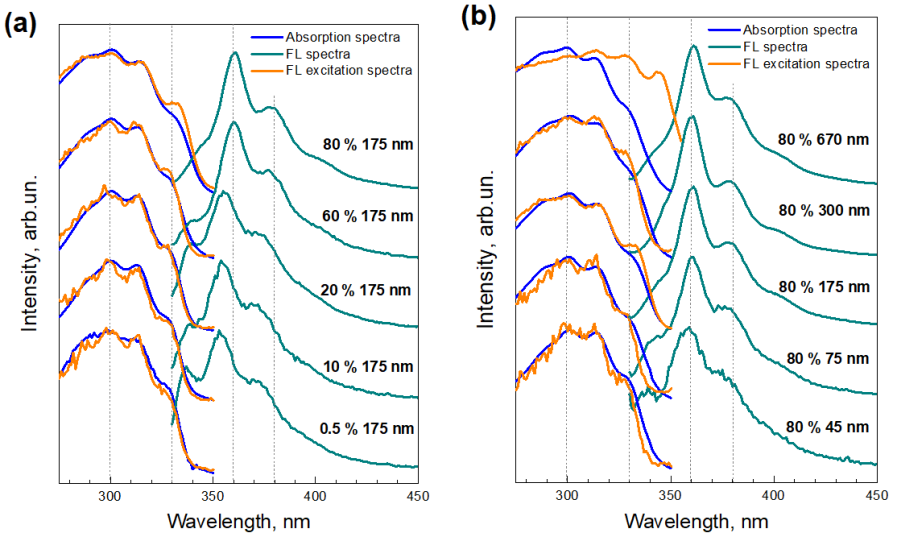


Figure 4.9. *a) Uv/vis absorption spectra (blue lines), FL excitation spectra (orange lines) and FL spectra (dark teal lines) of 175-nm thick TS thin films at different TS concentrations. b) Uv/vis absorption spectra (blue lines), FL excitation spectra (orange lines) and FL spectra (dark teal lines) of 80% TS thin films at different film thicknesses. For all the FL measurements 300 nm diode was used as an excitation source. Reprinted from* **[*Paper A2*]** *under the CC BY 4.0 license.*

In contrast to steady-state absorption, FL spectra exhibit pronounced changes with both increase in concentration and thickness of the film. When TS concentrations are relatively small (0.5%, 10% and 20%) FL spectrum exhibit 3 bands with the most intense one centered at 353 – 355 nm (see Figure 4.9 (a) and Table 4.5). At high concentrations (60% and 80%) the dominating peak is shifted to 360 – 361 nm and, additionally, one can observe redistribution in relative intensities of the two remaining peaks [see Figure 4.9 (a)]. At the lowest concentration bluest peak (336 nm) is more intense than the reddish one (372 nm), while at the intermediate concentrations the intensities of these peaks (340 nm and 374 – 375 nm, respectively) become almost equal, and with the further increase in concentration up to 80% the reddish FL peak (380 nm) becomes more intense. These features, supported by the microscopy results, may indicate that at the lowest (0.5%) and highest (60% and 80%) concentrations FL spectra are dominated by different TS species – most likely TS monomers and crystallites, respectively. Similar shifts from 359 nm to 361 nm of the dominating FL band can also be observed when increasing a thickness of the film at the fixed 80% concentration. However, relative intensities of bluest and reddish bands remain the same, while their positions

are shifted to the blue direction with an increase in a thickness. This most likely suggests, that these films have the same dominating FL species – TS crystallites – while films of lower thicknesses might also contain some amount of TS aggregates.

Table 4.5. *Characteristics of steady-state absorption and FL emission spectra, as well as FL excitation spectra of TS at different concentrations and films' thicknesses. Adapted from* **[*Paper A2*]** *under the CC BY 4.0 license.*

TS conc. in PS, % wt.	Film thickness, nm	Absorption bands, nm	OD at 300 nm	FL Excitation bands, nm	FL bands, nm
0.5%	175	300, 313,328	0.02	299, 313, 327	336, 353, 372
10%	175	289, 299, 313, 328	0.17	290, 299, 313, 327	340, 354, 374
20%	175	289, 300, 313, 328	0.30	299, 313, 327	340, 355, 375
60%	175	290, 300, 313, 329	0.38	299, 313, 327	341, 360, 380
80%	45	288, 300, 314, 328	0.11	288, 300, 314, 327	339, 359, 376
80%	75	290, 300, 314, 328	0.29	290, 299, 313, 327	341, 360, 376
80%	175	291, 300, 315, 329	0.68	290, 300, 315, 328	342, 360, 380
80%	300	291, 301, 315, 329	0.76	299, 313, 328	347, 360, 380, 404
80%	670	290, 300, 314, 329	1.53	300, 314, 330, 344	347, 361, 380, 405

4.2.5. FL decay kinetics of TS thin films

Figure 4.10 (a) and (b) represents FL decay kinetics of TS spin-coated films, while Table 4.6 contains the main characteristics of these decays. The film of the lowest concentration exhibits mono-exponential decay with FL lifetime being equal to 0.71 ns (see Table 4.6). Mono-exponential origin of the kinetics remains at the intermediate concentrations (10% and 20%), however the lifetimes are significantly shorter (approximately 0.30 ns) compared with that of the 0.5% sample. Similarly to our results, *Karpicz, et.al.*

[13] observed CQ of FL for low concentrated TS thin films. However, CQ picture in the case of TS thin films differs from the one exhibited by phthalocyanine solutions (see section 4.1 and **[*Paper A1*]**): in contrast to phthalocyanine case, all the discussed kinetics of TS exhibit mono-exponential decay. *Therefore, most likely FL decay kinetics of 0.5% TS and of 10% as well as 20% are dominated by different species. Taking into account the results of the steady-state FL and CARS as well as AFM microscopies, these species most likely are pure TS molecules and disordered aggregates, respectively. These assumptions suggest that the static quenching mechanism is predominant in this case.* However, it should be noted, that kinetics of 10% and 20% samples almost approach IRF profile, therefore they might exhibit in reality even faster decay components, than the detection limit of the setup.

The subsequent increase in a molecular concentration (60% and 80% 175-nm TS films) of TS results in a slower (average lifetimes are 0.48 ns and 0.90 ns, respectively) bi-exponential FL decay. Interestingly, both kinetics have a fast component (0.19 ns and 0.51 ns, respectively) with relatively high amplitudes (80% and 61%, respectively; see Table 4.6) and almost the same slow component with a ~1.6 ns lifetime (see Table 4.6). These results are consistent with the steady-state FL spectroscopy and AFM and CARS microscopies, suggesting presence of the disordered aggregates within the films and highly-ordered TS crystals exhibiting longer FL.

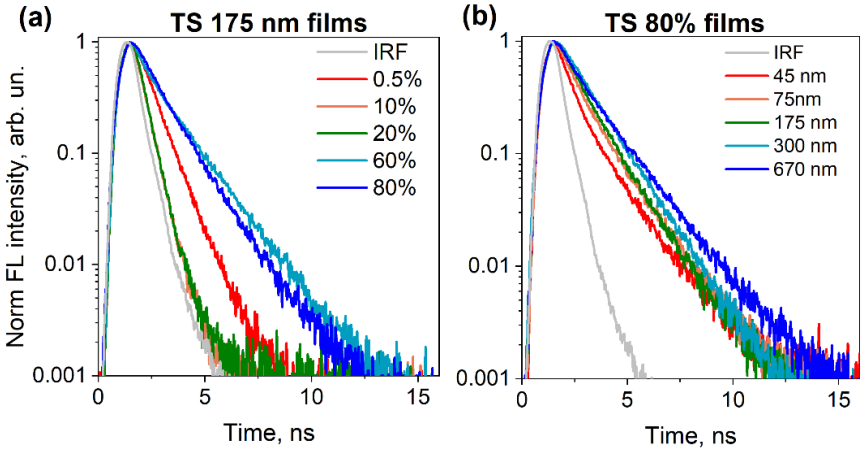


Figure 4.10. *FL decay kinetics of TS spin-coated thin films at the fixed a) thickness (175 nm) and b) concentration of the film (80%).* $\lambda_{exc} = 300\ nm$.

The thinnest sample (45 nm) at the 80% of TS concentration exhibit bi-exponential decay with an average FL lifetime equal to 0.48 ns. The consistent

increase in the film's thickness from 75 nm to 670 nm results in monotonic increase in the average FL lifetime values from 0.69 ns for 75-nm film to 1.60 ns for 670-nm film. Additionally, the thickest 670-nm film exhibit pure mono-exponential FL decay, while all the rest samples, i.e., thinner films, at 80% of concentration exhibit bi-exponential FL decay with faster (from 0.19 ns to 0.51 ns) to slower (1.48 ns – 1.65 ns) components, and at the same time with an increase in thickness of the film an amplitude of the faster component decreases, while that of slower one increases. *This decay dynamics suggests the presence of two FL species, namely these two components in the FL decays can be attributed to the disordered TS aggregates and TS single crystals. It is hard to explain differences in the values of the fast components, which varies from 0.19 ns to 0.51 ns (see Table 4.6). It might be the case, that the thickness of the film affects size of the formed aggregates and, consequently, larger aggregates might exhibit longer fluorescence lifetimes.*

Table 4.6. *Characteristics of the mono- and bi-exponential FL decays of TS thin films. Adapted from* **[*Paper A2*]** *under the CC BY 4.0 license.*

TS conc. in PS, % wt.	**Film thickness, nm**	**λ_{FL}, nm**	**τ_1, ns (%)**	**τ_2, ns (%)**	**τ_{av}, ns**
0.5%	175	353	0.71 (100%)	---	0.71
10%	175	355	0.26 (100%)	---	0.26
20%	175	357	0.28 (100%)	---	0.28
60%	175	361	0.19 (80%)	1.65 (20%)	0.48
80%	45	360	0.30 (87%)	1.68 (13%)	0.48
80%	75	361	0.38 (75%)	1.62 (25%)	0.69
80%	175	361	0.51 (61%)	1.50 (39%)	0.90
80%	300	361	0.51 (36%)	1.48 (63%)	1.12
80%	670	361	---	1.60 (100%)	1.60

4.2.6. Observation of structural transitions via global analysis of FL spectra and kinetics

The observed monotonic changes in both steady-state FL and FL decay kinetics, as well as target analysis of FL decay kinetics provided in the previous section suggest the presence of the several FL species in the TS thin films: TS monomers, TS disordered aggregates and TS mono-crystals.

The Figure 4.11 represents the results of two-component global analysis using the non-negative matrix factorization (NNMF; Eq. 3.2) method. Figure 4.11 (a) shows the results obtained for the steady-state FL. To make this global decomposition algorithm more physically meaningful, it was assumed that the 0.5% 175-nm TS film does not contain either disordered aggregates or highly-structured crystallites, but rather consists predominantly of pure molecular TS species, therefore the FL spectrum of this film was fixed and kept unchanged during the entire algorithm. Table 4.7 shows the weights of the obtained spectral components presented in Figure 4.11 (a). This analysis allows to distinguish between only two components, i.e., two FL species. The first one [golden line in Figure 4.11 (a)], as was stated before, belongs to pure molecular species and its influence decreases with an increase in TS concentration. Regarding analysis of the thickness dependent spectra at the fixed concentration of 80%, the picture is similar. The FL spectrum of the thinnest film contain 60% of monomers according to the decomposition, and this amount decreases with an increase in thickness. The second component [green line in Figure 4.11 (a)] might be attributed to the FL spectrum of TS crystallites. Interestingly, according to this NNMF decomposition, no spectra – even 80% 300-nm (87%) and 670-nm (89%) – consist only of crystallite TS species.

Figure 4.11 (b) shows the results of the decomposition of FL decay kinetics applying the same technique as was applied for the steady-state FL. However, in this case two-component decomposition is not so straightforward. Two components are not enough to adequately fit the entire set of the kinetics. However, if mono-exponential kinetics of the lowest concentrated sample (0.5% 175-nm TS film) is excluded from the fit, it becomes possible to decompose all the remaining kinetics into two components. The first of them is the fast one with the average lifetime equal approximately to 0.27 ns [blue curve in Figure 4.11 (b)]. This kinetic component can be attributed to the fast FL of disordered TS aggregates. This component dominates the kinetics of 10% and 20% 175-nm films as well as 80% 45-nm film. The second – long-lived (1.60 ns) – component [green curve in Figure 4.11 (b)] may be attributed to the mono-exponential kinetics of TS

single crystals. Interestingly, none of the kinetics can be completely described by this component.

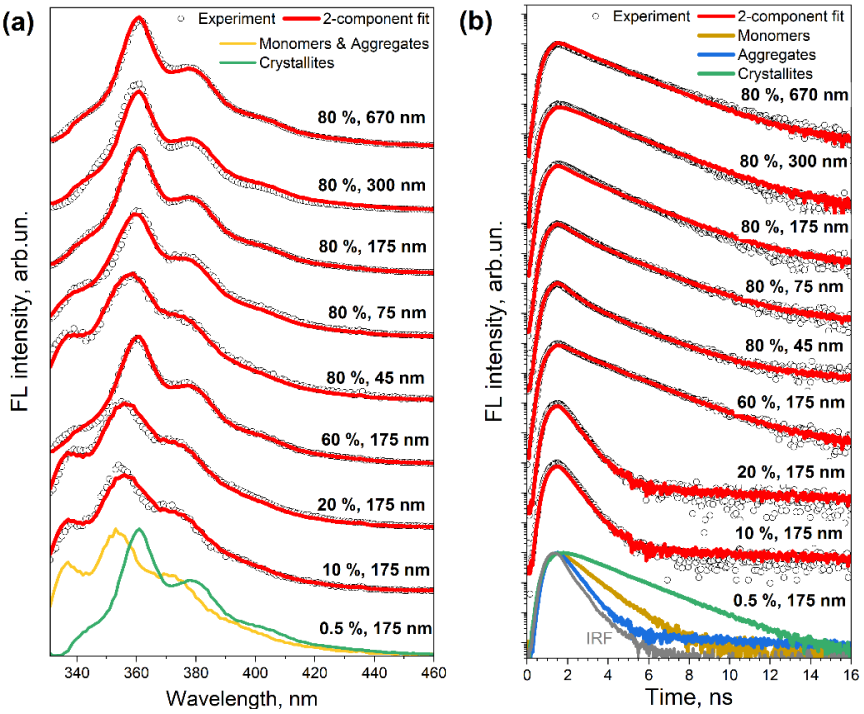


Figure 4.11. *Results of the global analysis of a) steady-state FL spectra and b) FL decay kinetics using multivariate curve resolution via non-negative matrix factorization (Eq. 3.2). Adapted from* **[*Paper A2*]** *under the CC BY 4.0 license.*

Altogether, the presented global analysis via NNMF suggests the following: steady-state FL spectra has two components – pure monomers and single crystals – and all the rest spectra contain both features; while time-resolved FL decay kinetics, in principle, contain three components: pure molecular, and the components originating from disordered aggregates and single crystals.

Table 4.7. *Characteristics of the global analysis of the steady-state FL spectra and FL decay kinetics using multivariate curve resolution via non-negative matrix factorization (Eq. 3.2).*

		Steady-state FL		**FL decay kinetics**	
TS conc, %wt.	Film thickness, nm	Relative weight of monomers, %	Relative weight of crystallites, %	Relative weight of aggregates, %	Relative weight of crystallites, %
0.5%	175	100	0	---	---
10%	175	73	27	100	0
20%	175	71	29	99	1
60%	175	21	79	39	61
80%	45	60	40	75	25
80%	75	38	62	60	40
80%	175	17	83	50	50
80%	300	13	87	24	76
80%	670	11	89	38	62

4.2.7. Current limitations and unresolved questions

Although the presented results provide deep insights into structural, surface and optical properties of TS spin-coated thin films, i.e., steady-state and time-resolved FL properties are governed by monomer → aggregates → crystallites structural transitions, some questions, *especially regarding TS aggregates*, still remain unresolved.

For example, in spite of the fact, that NNMF clearly stated presence of aggregates-attributed FL components, therefore stating that TS disordered aggregates are FL species, minor changes in spectra with the increase in molecular concentration of a compound accompanied by a notable acceleration in FL decay kinetics is a classical picture of CQ due to excitation energy migration to non-fluorescent/weakly-fluorescent traps. Such an analysis using different energy transfer models could be performed for low concentrated films exhibiting CQ, however explanatory power of such an analysis in this case is limited, because the kinetics of 10% and 20% samples are very fast, almost approaching the IRF profile and it is impossible to extract the needed temporal components responsible for quenching using simple FL spectrometer.

In addition, the present analysis does not provide enough information about the structural properties of low and intermediate concentration, as well low thickness films – films, which most likely contain TS aggregates of

different sizes and, probably, shapes. As was shown in Table 4.6, these films exhibit a fast FL component, whose FL lifetime differs by a factor of approximately 2.5 between the samples. This difference might be caused by sizes and/or shapes of different TS aggregates.

4.2.8. Summarizing remarks

i) The present section explores morphology-induced changes in the optical properties, mainly FL, of *trans*-stilbene (TS) polystyrene thin films by varying both TS concentration with respect to the matrix and the thickness of the film. CARS showed that disordered TS aggregates are formed at low and intermediate TS concentrations, while highly ordered single crystals are formed at high concentrations. Via varying thickness of the film, one can somewhat precisely regulate the relative amount of the formed crystals as well as their sizes. Global analysis of steady-state FL showed that steady-state properties are dominated by two components, where the first one originates from TS molecules and the second can be attributed to TS single crystals. Time-resolved properties are also *mainly* determined by two compounds, i.e., fast FL of disordered aggregates and the slow FL of TS single crystals. FL decay of the lowest concentrated sample is *fully* determined by pure molecular properties, making molecular-attributed decay the third component.

ii) The results of this study were published in **[*Paper A2*]** and presented at the following conferences: **[*Conferences C2, C4, C5, C6, C8, C9, C10, C14, C15*]**.

iii) The provided findings led to the ***second statement*** of the thesis:

Trans-stilbene in spin-coated films exhibit monomer → disordered aggregates → highly ordered single crystallites structural transitions with an increase in molecular concentration. Both the steady-state fluorescence spectra and fluorescence decay kinetics undergo smooth and monotonic changes governed by these transitions, therefore fluorescent properties of trans-stilbene in thin films can be fine-tuned by sample preparation conditions.

4.3. Manifestation of van der Waals interaction between *trans*-stilbene and hexagonal boron nitride

4.3.1. Initial remarks

This section explores spectroscopic manifestation of the van der Waals (vdW) interaction between *trans*-stilbene (TS) and hexagonal boron nitride (hBN). The selected TS + hBN model system is a suitable one for studying such type of interactions, because both TS and hBN are non-polar compounds,

thus suggesting the London dispersion forces being the governing mechanism of vdW binding between TS and hBN surface. TS and hBN separately, as well as their mixture with 1:1 mass ratio (see *Chapter 3* for sample preparation details) were studied via THz and Raman spectroscopies to obtain insights into the manifestation of the interaction at the vibrational level and confirm the formation of the complex itself. Steady-state FL as well as time-resolved FL decay kinetics were used to probe the manifestation of vdW interaction at the electronic level.

To support experimental results Dr. Maksim Shundalau (University of Salerno) performed DFT-based quantum chemical calculations using two structural models. The first model (Model I) describes a single isolated TS molecule, a $B_{27}N_{27}H_{18}$ quantum dot (BNQD) and the TS + BNQD vdW complex as isolated molecular systems. Empirical dispersion correction [133] was used for the TS + hBN vdW complex to take into account London dispersion forces between TS molecule and BNQD. The optimized structures based on Model I can be found in Figure 4.12. The second structural model (Model II) uses periodic boundary conditions to calculate the structure and properties of an isolated TS molecule, a two-dimensional (2D) hBN monolayer, a three-dimensional (3D) TS single crystal and isolated TS molecules adsorbed on a 2D hBN layer. The structures of the latter three systems optimized based on Model II can be found in Figure 4.12. The distance between TS molecules and hBN was predicted in terms of both models, being equal to 2.9 Å and 4.2 Å, respectively. It should be noted that in this dissertation these calculations are used to support the experimental results. A detailed explanation of these calculations can be found in the **[*Paper A3*]** and its supplementary material.

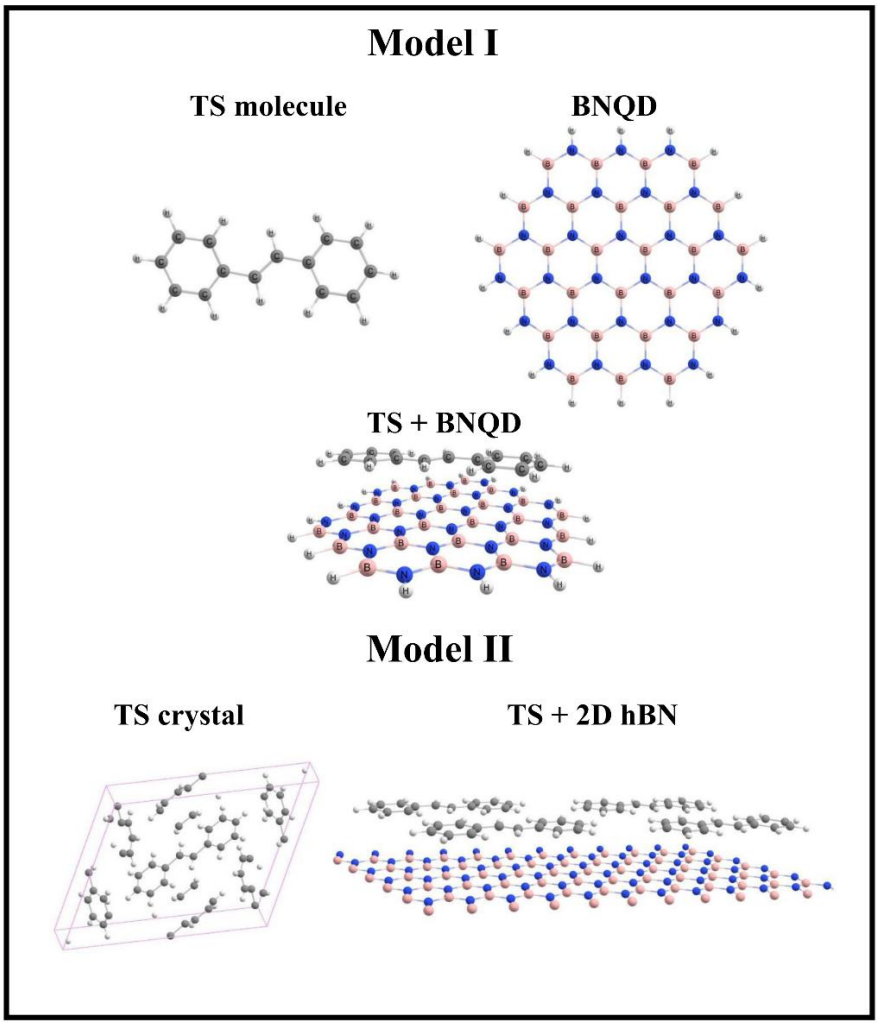


Figure 4.12. *Scheme of the two structural models, namely Model I and Model II, which were applied to compute THz and Raman spectra of TS isolated molecule, BNQD, TS + BNQD vdW complex (all Model I) and TS isolated molecule, TS single crystal, 2D hBN mono-layer and isolated TS molecules adsorbed on hBN surface (all Model II). Adapted from* **[*Paper A3*]**. *Copyright 2025 American Chemical Society.*

4.3.2. Short overview of hexagonal boron nitride applications and properties

It should be noted that the main reason of choosing hexagonal boron nitride (hBN) for this study is its non-polarity and planar 2D structure. Therefore, hBN can serve as a good model system to explore vdW interaction between an organic compound and 2D material.

Nevertheless, it would be remiss not to mention wide range of hBN applications. Two-dimensional (2D) hexagonal boron nitride (hBN) nanosheet is a material of high chemical stability and of high thermal stability and conductivity [134–136]. 2D hBN nanosheet is a structural relative of graphene. However, in contrast to graphene, it is an insulator [134,135], and it has already been successfully applied as a dielectric layer in a field effect transistor [135,137], as well as a protective cover layer in various devices [135]. Additionally, it is worth mentioning that hBN showed potential for photonics applications, for example for ultraviolet detectors and emitters [137].

Although in the present study (see **[*Paper A3*]** for details) BNQD is used only as a model system for quantum chemical computations (Model I), it is still useful to briefly discuss some of their applications. Zero-dimensional (0D) BNQDs are nanoscale substrates [136,138–140]. Being biocompatible, they are promising compounds for a variety of biomedical tasks, such as bioimaging [141,142], biosensing [142] and target drug delivery [143].

Consequently, understanding the mechanisms and magnitudes of interactions between various organic compounds and different forms of boron nitride is an important for the mentioned applications. Recently, the spectroscopic manifestations of vdW interaction and adsorption-related phenomena have been investigated both theoretically and experimentally for doxorubicin adsorbed on 2D hBN nanoflakes [144], as well as for thiacarbocyanine dyes [21], and various porphyrin or phthalocyanine compounds [10,22,102,103,145] adsorbed on hBN. *However, the insights into vibrational and electronic properties of the adsorbed compounds as well as manifestation of vdW interaction between organic compounds and hBN surface still remains poorly described.*

4.3.3. Observation of vdW interaction between TS and hBN via vibrational spectroscopy

Usually, the first step in describing some kind of molecular complex with spectroscopic methods is to measure Raman or infra-red spectrum. However, THz absorption spectrum can provide additional information about weak interactions in molecular complexes, such as intermolecular H-bond formation or weak vdW interaction between parts of a complex [146–149]. While infra-red region of the spectrum contains information about vibrational properties of each particular molecule (part of molecular complex), THz one may contain low-frequency vibrations of one part of a complex relative to another – so-called libration bands.

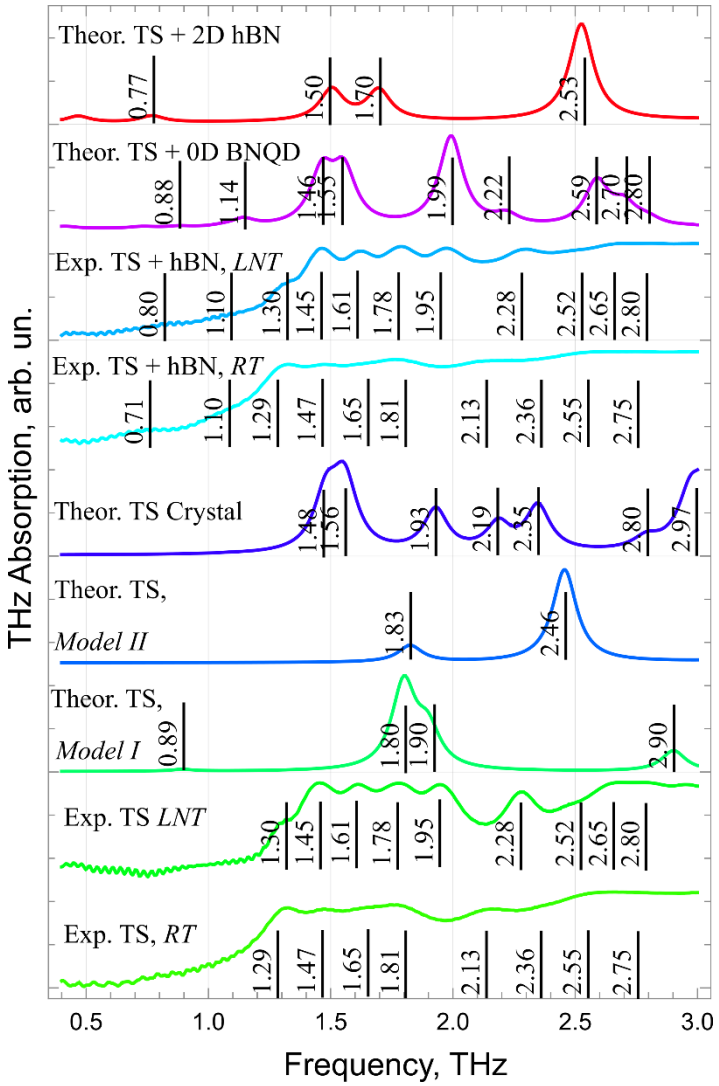


Figure 4.13. *Experimental and calculated (Model I and Model II) THz spectra of TS and TS + hBN complex. Peak positions are labeled in all the spectra. 'RT' denotes 'Room Temperature', while 'LNT' denotes 'Liquid Nitrogen Temperature'.* ***The assignment of THz bands is presented in Table 4.8****. Adapted from* **[*Paper A3*]**. *Copyright 2025 American Chemical Society. / THz experiments were conducted by Dr. Daniil Pashnev (FTMC), while all the computations were performed by Dr. Maksim Shundalau (University of Salerno).*

Figure 4.13 represents experimental and theoretical THz spectra of TS and TS + hBN complex. The measurements were performed both at the room and the liquid nitrogen temperatures. Table 4.8 presents frequencies and

assignment of the experimental THz absorption bands of both TS and TS + hBN compounds. At the room temperature, experimental THz absorption spectrum contains eight bands at the region from 1.29 THz to 2.75 THz (see Figure 4.13 and Table 4.8), while decreasing temperature to the liquid nitrogen one results in approximately 0.15 THz blue shifts in vibrational frequencies of high frequency vibrations (1.8 THz – 3 THz) and in the appearance of ninth THz band centered at 1.30 THz (Figure 4.13). Most likely, the corresponding band presents also at the room temperature spectrum, but its intensity is lower than the level of noise. Interaction between TS and hBN does not lead to the changes in TS-belonged THz frequencies at both room and liquid nitrogen temperature, but two additional bands at the low frequency region (0.71 THz and 1.10 THz for the room temperature spectrum and 0.80 THz and 1.10 THz for the liquid nitrogen spectrum) appear in the spectrum. These two bands belong to librations, i.e., low frequency motion of TS relative to hBN surface, thus confirming the formation of the complex. Calculations of THz spectrum of both TS and TS + hBN complex were made to confirm experimental trends and to assign the bands. While deep analysis of the calculations results is presented in **[*Paper A3*]**, here we concentrate on the main trends. Firstly, the bands are assigned to the skeleton in-plane (i.p.) and out-of-plane (o.o.p.) vibrations, as well as intermolecular (i.m.) vibrations. Secondly, DFT-based quantum chemical calculations support experimental data, as two weak intensity bands at 0.88 THz and 1.14 THz (Model I) and 0.77 THz and 1.50 THz (Model II) appear in the TS + hBN vdW complex compared with pure TS (see Figure 4.13). It should be noted that hBN has a single low intense THz band centered at approximately 1.5 THz, but its intensity is negligible compared with the intensities of TS and TS + hBN samples, therefore it is not shown and does not participate in the analysis. Discussion of the hBN THz spectra can be found in the **[*Paper A3*]** and the supplementary material for it, as well as in the Ref. [150].

Table 4.8. *Assignment of the experimental THz bands of TS and TS + hBN complex, measured at the room and the liquid nitrogen temperatures.*

Frequency, THz		**Band assignment[$]**
Room Temperature	**Liquid Nitrogen Temperature**	
0.71*	0.80*	Libration*
1.10*	1.10*	Libration*
1.15[#]	1.30	i.m.
1.29	1.45	o.o.p.
1.47	1.61	i.m.
1.65	1.78	i.m.
1.81	1.95	o.o.p.
2.13	2.28	i.m.
2.36	2.52	o.o.p.
2.55	2.65	i.p.
2.75	2.80	i.p.

[$]i.m. – intermolecular vibration; o.o.p. – out-of-plane deformation vibration; i.p. – in-plane deformation vibration. [*]Libration bands correspond only to TS + hBN sample. [#]This band is not observed in the experimental spectrum, however is assumed to present in the spectrum based on the noise level and DFT calculations.

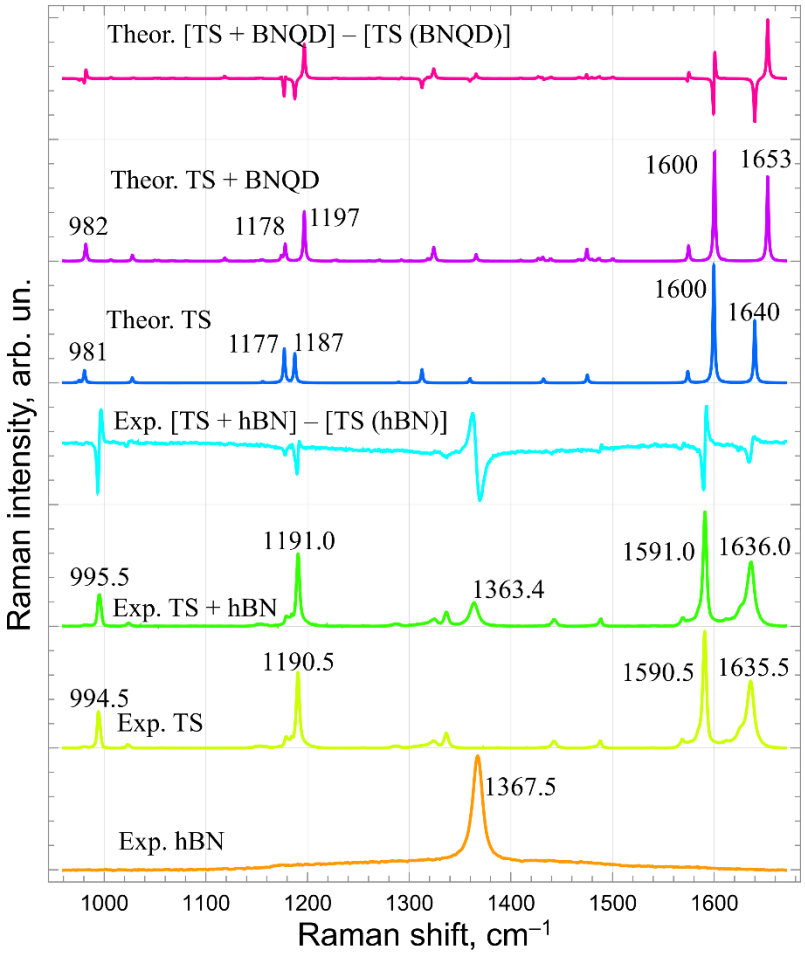


Figure 4.14. *Experimental and calculated (Model I) Raman spectra of TS and TS + hBN complex. For comparison, experimental Raman spectrum of hBN is presented. For clarity, difference spectra between TS and TS + hBN vdW complex is shown for both experimental and calculated Raman spectra. Peak positions are labeled in all the spectra.* ***The assignment of Raman bands is presented in Table 4.9****. Adapted from* **[*Paper A3*]**. *Copyright 2025 American Chemical Society. / Raman measurements were performed by Dr. Martynas Talaikis (FTMC), while all the computations were performed by Dr. Maksim Shundalau (University of Salerno).*

After examining the features of vdW interaction between TS and hBN at the inter-compound level, it is useful to observe changes in the vibrational properties of each particular part of the complex – TS and hBN compounds. Therefore, the infra-red region of the spectrum needs to be analyzed. It is worth mentioning, that infra-red (IR) absorption spectrum cannot be used for

this analysis, since the measured spectra of TS + hBN complex contain broad and intense hBN band, that overlaps with all the other bands (see **[*Paper A3*]** and also Refs. [151,152]). Figure 4.14 presents experimental and calculated (Model I) Raman spectra of hBN, TS and TS + hBN. Similarly to calculations of THz spectra, the deep analysis of the calculation results of Raman spectra can be found in **[*Paper A3*]** and the supplementary material for it, while here the main trends are provided. The experimental manifestation of vdW interaction between TS and hBN results in in 0.5 – 1 cm^{-1} blue shifts of some of the TS-attributed Raman bands, while hBN band exhibits 4 cm^{-1} red shift, thus confirming the formation of the complex. Table 4.9 presents the Raman frequencies and attribution of the selected shifted vibrational bands of hBN, TS and TS + hBN complex. This trend is completely confirmed by the results of computations based on both Model I.

Table 4.9. *Assignment of the shifted due to vdW interaction experimental Raman bands of hBN, TS and TS + hBN complex. Adapted from the* **[*Paper A3*]**. *Copyright 2025 American Chemical Society.*

Raman frequency, cm^{-1}			**Band assignment**
TS	**hBN**	**TS + hBN**	
994.5		995.5	Ring in-plane trigonal deformation
1190.5		1191.0	C–ring stretching
	1367.5	1363.5	E_{2g} hBN mode (BN stretching)
1590.5		1591.0	Ring stretching
1635.5		1636.0	C=C stretching

Summing up the results of THz and Raman spectroscopies it can be stated, that the formation of vdW complex is confirmed by the changing in Raman frequencies and appearance of low frequency libration bands in the THz spectra. Furthermore, in the case of this particular complex the vdW interaction results in an increase in stretching and in-plane deformation vibrational modes, while the frequencies of out-of-plane deformation modes decrease.

4.3.4. Electronic manifestation of vdW interaction between TS and hBN

Figure 4.15 (a) represents steady-state FL of the hBN powder, pressed TS and TS + hBN complex. Due to its high bandgap hBN exhibits intrinsic FL at the deep UV region, therefore with exciting it at 300 nm, one can observe only defects-caused FL [153,154]. The studied hBN powder exhibit broad FL spectrum with two overlapping bands centered at 352 nm and 364 nm (see Table 4.10). Bulk TS exhibits broad FL spectrum centered at 380 nm with minor features at 345 nm, 365 – 367 nm, 404 nm (see Table 4.10). It should be noted, that FL bands approximately at the positions corresponding to these minor features are present as (more) intense peaks in the spectra of TS spin-coated thin films (see Figure 4.9 and Table 4.5); the most intense FL band of bulk TS [Figure 4.15 (a)] is red shifted with respect to the one of TS spin-coated films (Figure 4.9). This difference can be explained by the different dominating FL species, i.e., this spectrum is dominated by TS polycrystals and governed by the bulk properties of TS, while the spectrum of spin-coated films originates from the pure TS molecules, molecular aggregates and/or μm-sized single crystals. The experimentally observed spectrum is in a good agreement with the previous reports of bulk TS FL [36,130]. The vdW interaction between TS and hBN does not result in any notable blue or red shifts of the FL bands of TS + hBN sample, however it manifests in quenching of FL intensities compared with pure TS (see Table 4.10). In addition, 365-nm band – the one, that, in principle, can be assigned to FL of both hBN and TS species – exhibits relative increase in intensity compared with pure TS. On the one hand, this increase can be caused by the FL of hBN, however it is less likely to be the case, because FL intensity of pure hBN (see Table 4.10) is much weaker than the one of pure TS. On the other hand, this increase in the intensity can be caused by the subtle deformation of the TS crystals' surface or their reorientation and, consequently, subtle changes in electronic cloud of TS, thus subtle changes in FL spectrum.

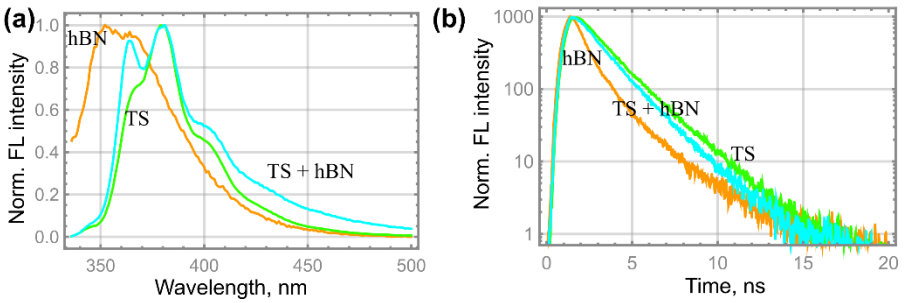


Figure 4.15. *a) steady-state FL spectra and b) FL decay kinetics of hBN, TS and TS + hBN vdW complex. In all the measurements λ_{exc} = 300 nm. Adapted from* **[*Paper A3*]**. *Copyright 2025 American Chemical Society.*

Figure 4.15 (b) represents normalized-to-unity and averaged across all the listed in Table 4.10 FL emission wavelengths time-resolved FL decay kinetics of hBN, TS and TS + hBN complex. Pure hBN exhibits fast bi-exponential decay with the average lifetime τ_{av} increasing from 0.35 ns (λ_{em} = 345 nm) to 0.70 ns (λ_{em} = 420 nm). This difference in lifetimes by a factor of two might probably be explained by the influence of different hBN defects. hBN decay is dominated by the fast (0.29 ns – 0.42 ns) component. Similarly to hBN, bulk TS also exhibits b-exponential decay with the average lifetime τ_{av} equal to 1.18 ns at the FL maximum (380 nm; see Table 4.10). This result differs from the one observed for hot-pressed and sublimated bulk TS samples, when they exhibited mono-exponential decay with the FL lifetime equal to 2.8 ns – 2.9 ns [36]. Most likely, this FL quenching can be explained in terms of different sample preparation procedure, i.e., in our case TS tablet most likely contain TS polycrystals of different sizes which might exhibit different FL properties. This assumption is somewhat well confirmed by the examining of decay components at different emission wavelengths (see Table 4.10): for the high emission wavelengths (starting from 380 nm) domination of the shorter component decreases with the increasing the emission wavelength, being in agreement with red shifted FL of bigger TS crystallites. TS + hBN vdW complex also exhibits bi-exponential decays (τ_{av} = 0.92 ns) at the maximum of the emission (380 nm; Table 4.10). The vdW interaction between TS and hBN results in subtle quenching of FL at both 365 nm (from 1.14 ns to 0.94 ns) and 380 nm (from 1.18 ns to 0.92 ns) emission wavelengths. Interestingly, FL decay of the complex is dominated by the fast component which is faster than the corresponding one of pure TS, and its amplitude does not decrease notably with an increase in the emission wavelength, compared with the case of pure TS. This probably *partly*, i.e., not *completely*, can be attributed to the fast FL of pure hBN, since the fast component observed in TS + hBN sample

is almost equal (up to 405 nm emission) to τ_{av} of pure hBN (see Table 4.10). The longer component in TS + hBN kinetics is attributed to FL of TS species. This longer component i) increases in lifetime with an increase in emission wavelength (except emission at 365 nm) and ii) is faster than the corresponding slow component of pure TS. It might indicate, that hBN prevents formations of bigger TS crystallites if compare with pure TS sample. Additionally, all the observed changes in time-resolved FL decay kinetics can be explained – as in the case of steady-state FL spectra – by the subtle change in electronic clouds of TS when it interacts with hBN.

Table 4.10. *Characteristics of the steady-state FL and time-resolved FL decay kinetics properties of hBN, TS and TS + hBN compounds. Adapted from the* **[*Paper A3*]**. *Copyright 2025 American Chemical Society.*

	hBN			**TS**			**TS + hBN complex**		
Steady-state FL									
FL bands, nm	352, 364			345, 367, 380, 404			364, 380, 405		
FL intensity at 365 nm	17920			245700			85950		
FL decay kinetics									
Band, nm	τ_1, ns	τ_2, ns	τ_{av}, ns	τ_1, ns	τ_2, ns	τ_{av}, ns	τ_1, ns	τ_2, ns	τ_{av}, ns
345	0.29 (97%)	2.45 (3%)	0.35	0.63 (84%)	1.67 (16%)	0.80	0.35 (83%)	1.51 (17%)	0.54
352	0.35 (97%)	2.70 (3%)	0.42	0.68 (65%)	1.81 (35%)	1.07	0.41 (73%)	1.90 (27%)	0.82
364	0.33 (94%)	2.31 (6%)	0.44				0.53 (70%)	1.88 (30%)	0.94
367				0.70 (68%)	2.10 (32%)	1.14			
380	0.33 (93%)	2.24 (7%)	0.47	0.70 (70%)	2.23 (30%)	1.18	0.47 (70%)	1.94 (30%)	0.92
405	0.40 (90%)	2.41 (10%)	0.60	0.68 (61%)	2.23 (39%)	1.29	0.44 (72%)	2.09 (28%)	0.90
420	0.42 (88%)	2.83 (12%)	0.70	1.02 (57%)	2.48 (43%)	1.65	0.60 (74%)	2.69 (26%)	1.14

4.3.5. Current limitations and unresolved questions

Although this section provides deep insights into the changes in vibrational and electronic properties of non-polar TS and hBN caused by van der Waals interaction between them, some questions remain unresolved.

Even though the successful formation of the complex is confirmed by the means of vibrational (THz and Raman) spectroscopy and it is assumed that the complex is uniformly formed within the sample, the origin of the blue shifts of TS Raman bands remains unexplained.

Additionally, present study does not allow to attribute the observed quenching of FL to the specific mechanism. Most likely, it is a static quenching due to TS interaction with boron nitride (changes in TS electronic cloud) and less active formation of bigger TS crystals (faster FL), however possible quenching mechanism mediated by excitation energy migration processes (both Dexter and Förster mechanisms) cannot be explored based on the results obtained in this study: either faster techniques or more concentrations (varying amount of TS relatively to hBN) are required.

4.3.6. Summarizing remarks

i) The present section explores the manifestation of vdW interaction between TS and 2D hBN surface using THz, Raman and FL spectroscopies. The interaction results in appearance of two additional low frequency bands in the THz spectrum of the complex compared with the spectrum of pure TS. These two bands are assigned to the librations of TS relative to hBN surface. In Raman spectra one can observe blue shifts of some of the TS-assigned and red shift of the hBN-assigned Raman bands. The vdW interaction results in a relative increase in intensity of one (365 nm) band in the TS + hBN FL spectrum compared with pure TS spectrum, and subtle quenching of FL decay kinetics. These changes might be attributed to the changes in electronic cloud of TS and less effective formation of TS crystals.

ii) The results of this study were published in **[*Paper A3*]** and presented at the following conferences: **[*Conferences C3, C4, C6, C12, C14, C16, C17*]**.

iii) The provided findings led to the ***third statement*** of the thesis:

Van der Waals interaction between non-polar hexagonal boron nitride and trans-stilbene results in an increased intensity of one fluorescence band and a slight acceleration of fluorescence decay. The combination of steady-state and time-resolved fluorescence might serve as a useful supporting technique for exploring extremely weak intermolecular interactions.

5. CONCLUSIONS AND OUTLOOK

5.1. Conclusions

This dissertation explores changes in optical spectra associated with different types of intermolecular interactions.

Both free-base and zinc-phthalocyanine exhibit concentration quenching (CQ) of fluorescence. Neither compound shows notable changes in the steady-state fluorescence spectra with increasing molecular concentration of the solution, whereas the fluorescence decay kinetics exhibit significant acceleration and a monotonic transition from mono-exponential decay at low concentrations to multi-exponential decay at higher concentrations. This behavior was attributed to the fluorescence quenching governed by Förster-type excitation energy migration to non-emissive or weakly emissive excitation traps. DFT-based quantum chemical calculations further suggested that these trap species are H-dimers.

Trans-stilbene (TS) thin films also exhibit CQ at relatively low concentrations (from 0.5 % TS films to 20 % TS films). However, in contrast to the phthalocyanine solutions, their fluorescence decays remain mono-exponential. Most likely, this quenching originates from the formation of weakly emissive TS aggregates, which are the main emissive species in the films. This behavior differs from that of phthalocyanines, where even at highest concentrations the observed emission originated from monomeric species.

In general, TS thin films exhibit more complex behavior with increasing molecular concentration. CQ at relatively low concentrations is followed by slower bi-exponential decay kinetics at higher concentrations. Increasing thickness of the films leads to slowing of the decays, and the thickest film (TS 80% 670 nm) exhibits slow mono-exponential decay with the lifetime of 1.60 ns. The steady-state fluorescence spectra exhibit smooth changes with increasing molecular concentration. This behavior is explained by structural transitions in the TS thin films, which were observed by the means of CARS and AFM microscopies. In general, the three structural forms are detected: pure TS molecules, TS disordered aggregates and TS single crystals. The relative amount of each TS structural form can be controlled by molecular concentration, whereas the size of TS aggregates and crystals can be controlled by film thickness. All three TS structural forms exhibit different steady-state and time-resolved fluorescent properties. Therefore, fine control of sample preparation conditions enables the fine control of the fluorescent properties, making both steady-state fluorescence and time-resolved decay

kinetics suitable and effective techniques for analyzing such morphology-dependent phenomena.

Fluorescence quenching is also observed in the van der Waals complex of bulk TS and two-dimensional (2D) hexagonal boron nitride (hBN) compared with a pure TS tablet. This quenching may be attributed to the subtle interaction-induced deformation of TS crystal structure upon interaction with hBN. The steady-state fluorescence spectra also exhibit changes, namely a relative increase in the intensity of one band, which most likely has the same origin as the quenching of fluorescence.

In general, the van der Waals (vdW) interaction between non-polar TS and hBN manifests itself in the THz, infra-red and visible spectral regions, thus making TS + hBN complex a suitable model system for exploring the features of vdW interaction between organic compounds and 2D non-polar material. In such a case Raman spectra exhibit adsorption-related shifts and, consequently, serves as the most efficient technique to detect and characterize such type of interactions.

Overall, the obtained results reveal distinct spectroscopic signatures of different types of intermolecular interactions, including H-aggregate formation, morphology-dependent molecular organization, and van der Waals interaction between two non-polar compounds. Although FL quenching is observed in all the investigated systems, its origin differs depending on the nature of intermolecular interactions and molecular organization, reflecting differences in the ground- and excited-state processes governing the photophysical response of the studied systems.

5.2. Outlook

The obtained results (*Chapter 4*) and the formulated conclusions (*Section 5.1*) provide valuable insights into the photophysical properties of the molecular aggregates, including excitonically coupled ones, crystallites and van der Waals complexes composed of non-polar compounds. Additionally, they demonstrate the applicability of several useful data-analysis techniques for extracting information about such systems: target analysis of fluorescence (FL) decays with stretched-exponential functions, which may indicate, for example, quenching arising from excitation energy migration to non-FL species, as well as global analysis of both steady-state FL and time-resolved FL decay kinetics, when the system is assumed to contain multiple FL species. Based on these findings, several directions for the future research can be proposed.

The most straightforward continuation of the present research is to shed light on the remaining unresolved questions:

i) Although excited-state properties of zinc phthalocyanine have already been explicitly studied using transient absorption (TA) spectroscopy [27], such properties of highly concentrated solutions remain underexplored. Since quantum chemical calculations (see Figure 4.4 and Table 4.4) suggest presence of *non-ideal* H-aggregates, it is important to apply ultra-fast techniques – streak-camera-based ultra-fast time-resolved FL (TRFL) and TA – to detect possible low-emissive species and charge transfer processes – especially for highly concentrated solutions, which might contain higher order aggregates. Such an analysis can possibly provide additional insights into excitation energy migration dynamics and, consequently, on the origin of energy losses within these systems, which is crucial for applications.

ii) Even though the changes in both steady-state and time-resolved photophysical properties of TS thin films are well-described by the morphological changes with increasing concentration, some additional knowledge on the photophysical behavior of TS disordered aggregates can be obtained applying the same techniques – TRFL and TA – to the low (0.5%) and intermediate (10% – 20%) concentrated TS thin films. At this set of the concentrations the films exhibit CQ effect, which cannot be explicitly studied using simple FL spectrometer, since FL decay kinetics of the samples almost approach IRF profile (see Figure 4.10). This knowledge can possibly provide additional insights into the excited-state dynamics of TS aggregates.

iii) Changes in both steady-state and time-resolved FL properties of bulk TS when it interacts with hBN were explained by subtle deformation of TS crystal. Additional insights into excited-state processes occurring in such a system, such as possible excitation energy migration between TS and hBN, might be studied using TRFL technique.

iv) TS + hBN complex is a suitable model system for exploring the features of van der Waals (vdW) interaction between non-polar 2D materials and organic molecules. However, functional groups used in preparation of 0D boron nitride quantum dots (BNQDs) may change the spectroscopic manifestation of the interaction, therefore it would be reasonable to experimentally study vdW complex of BNQDs and some organic compound. To come closer to biomedical

applications, instead of TS, its derivatives exhibiting anti-cancer activities [155] – resveratrol and pterostilbene – can be used. Such a complex would be an interesting model system, where a drug delivery platform (BNQD) exhibits vdW interaction with the anti-cancer agent, potentially being a valuable insight for biomedicine.

Additionally, it would be interesting to analyze the manifestation of aggregation-induced phenomena and vdW interaction at the same time. For example, vdW complex of 2D hBN and porphyrin- or phthalocyanine-like compound can be chosen as a model system. On the one hand, porphyrins and phthalocyanines are promising compounds for energy and biomedical applications; on the other hand, they exhibit well-studied aggregation-induced behavior, including quenching of FL, resulting in undesirable energy losses. However, the formation of vdW complex might result in a suppressed formation of aggregates and, thus, changes in both ground- and excited-state properties, which might be beneficial for photophysics and photochemistry applications, including artificial photosynthesis, photocatalysis, optoelectronics and bioimaging [33,156]. Firstly, steady-state FL and FL decay kinetics should be measured and FL decay dynamics should be analyzed. Then faster processes, such as excitation energy migration and other excited-state relaxation pathways, could be investigated using TA and TRFL by comparing the compounds in the presence and absence of hBN.

6. AI STATEMENT

The author of the thesis declares that the generative AI was used during writing of this thesis. *GPT-5.6 Sol* model (ChatGPT, OpenAI) was used to correct grammar and to improve the readability of the English language, as well as to assist in translating the thesis summary into Lithuanian language. No AI tools were used to create scientific content. All scientific statements, interpretations, and conclusions were formulated by the author of the thesis.

7. SANTRAUKA

7.1. Įvadas

Šviesos ir medžiagos sąveika atlieka esminį vaidmenį daugelyje gamtos ir technologinių procesų. Pavyzdžiui, ji yra svarbi fotosintezėje – natūraliame vyksme augaluose, dumbliuose ir samanose, kurio metu saulės šviesa yra sugeriama ir paverčiama chemine energija. Ji taip pat atlieka svarbų vaidmenį kuriant tvarios energetikos technologijas, tokias kaip dirbtinė fotosintezė [2] ir fotovoltika [3]. Šviesos ir medžiagos sąveiką nagrinėjamuose tyrimuose sukauptos žinios paskatino naujų cheminės fizikos krypčių, tokių kaip kvantinė biologija [4] ar poliaritoninė chemija [5], plėtrą. Be to, šviesos ir medžiagos sąveika atlieka svarbų vaidmenį ligų diagnostikoje, įskaitant tokias šiuo metu sparčiai besivystančias sritis kaip biojutikliai [6], biovaizdinimas [7] bei fotodinaminė vėžio terapija [8].

Paprastai šviesa sąveikauja ne su izoliuotomis molekulėmis, bet su tam tikromis *molekulinėmis sistemomis* – dažniausiai tai yra *molekuliniai agregatai*, *kristalitai* arba *ant paviršiaus adsorbuotos molekulės*, stabilizuojamos dėl įvairių *tarpmolekulinių sąveikų*. Tokios sąveikos paprastai lemia reikšmingus šių sistemų fotofizikinių savybių skirtumus, palyginti su izoliuotomis molekulėmis [9–12].

Optinė spektroskopija yra veiksmingas metodas tokioms tarpmolekulinėms sąveikoms tirti. Tiek sugerties, tiek fluorescencijos stacionariuosiuose spektruose gali būti stebimi požymiai, siejami su agregatų formavimusi arba molekulių adsorbcija. Fluorescencijos gesimo kinetikų matavimai yra dar vienas naudingas metodas tokiems reiškiniams analizuoti. Be gesimo komponenčių, kurios gali būti priskirtos skirtingoms fluorescuojančioms rūšims ir taip patvirtinti jų buvimą, šis metodas gali atskleisti tokius tarpmolekulinius procesus kaip sužadinimo energijos pernaša tarp skirtingų rūšių molekulių.

Tarpmolekulinių sąveikų supratimas įvairiose molekulinėse sistemose yra svarbus daugeliui taikymo sričių. Viena vertus, tokių sąveikų pasireiškimas gali būti naudingas praktiniams taikymams: pavyzdžiui, jos kartais lemia ryškius struktūrinius virsmus [13], todėl tokios sistemos yra perspektyvios jutiklių technologijoms [14], arba sustiprina šviesos emisiją, kas yra naudinga taikymams, kai svarbi intensyvi šviesos emisija ar efektyvi šviesos energijos konversija. Kita vertus, tokios sąveikos kartais sumažina emisijos efektyvumą ir dėl to padidina energijos nuostolius, o tai yra nepalanku fotovoltinių technologijų [15,16] ir optoelektronikos [17] taikymams.

Nepaisant jų svarbos praktiniams taikymams, tokios molekulinės sąveikos ir reiškiniai kaip agregatų, įskaitant eksitoniškai susietus agregatus, bei kristalitų susidarymas, taip pat van der Waalso sąveikos pasireiškimas ir jų lemiami fotofizikiniai pokyčiai įvairiomis sąlygomis iki šiol išlieka nepakankamai ištirti.

7.1.1. Disertacijos tikslas

Šios disertacijos tikslas – atskleisti ir išanalizuoti spektroskopinius pokyčius, susijusius su skirtingų tipų tarpmolekulinėmis sąveikomis: H tipo agregatų susidarymu, nuo morfologijos priklausoma molekuline organizacija ir van der Waalso sąveika tarp dviejų nepolinių junginių.

7.1.2. Tyrimo uždaviniai

Siekiant įgyvendinti išsikeltą disertacijos tikslą, buvo suformuluoti šie uždaviniai:

1. Ištirti koncentracijos sukeltą fluorescencijos gesinimą ftalocianinų molekulių chloroformo tirpaluose ir susieti stebimą gesinimo dinamiką su konkrečiu gesinimo mechanizmu.
2. Ištirti morfologijos sukeltų pokyčių trans-stilbeno molekulių plonųjų plėvelių optiniuose spektruose spektroskopinius požymius.
3. Ištirti van der Waalso sąveikos tarp trans-stilbeno molekulių ir heksagoninio boro nitrido spektroskopinius požymius.

7.1.3. Tyrimo užduotys

Pirmoji tyrimo dalis buvo skirta fluorescencijos koncentraciniam gesinimui bemetalio ir cinko ftalocianino molekulių chloroformo tirpaluose. Sugerties ir fluorescencijos spektrai buvo matuojami molekulių koncentraciją keičiant per dvi eiles, siekiant nustatyti nuo koncentracijos priklausomus spektrinius pokyčius, o fluorescencijos gesimo kinetikos buvo registruojamos atitinkamai sužadintosios būsenos dinamikai apibūdinti. Gesimo profiliai buvo analizuojami taikant monoeksponentinius, biekspontentinius ir ištemptosios eksponentės modelius. Apjungus stacionariųjų ir laikinės skyros matavimų duomenis, stebėta fluorescencijos gesinimo elgsena buvo susieta su konkrečiu gesinimo mechanizmu.

Antroji tyrimo dalis buvo skirta nuo morfologijos priklausomoms *trans*-stilbeno molekulių plonųjų plėvelių optinėms savybėms apibūdinti. Sugerties ir fluorescencijos spektrai kartu su fluorescencijos gesimo kinetikomis buvo išmatuoti plėvelėms, pasižyminčioms skirtingomis *trans*-stilbeno koncentracijomis ir storiais. Tikslinė slopimo kinetikų analizė buvo taikoma charakteringoms fluorescencijos gyvavimo trukmėms nustatyti, o visų

stacionariosios fluorescencijos spektrų ir gesimo kinetikų rinkinių globalioji analizė – skirtingų *trans*-stilbeno struktūrinių formų indėliams atskirti. Šie spektroskopiniai rezultatai buvo interpretuojami kartu su koherentinės anti-Stokso Ramano sklaidos mikrospektroskopijos ir atominės jėgos mikroskopijos duomenimis, siekiant nustatyti ryšį tarp plėvelių morfologijos ir optinių savybių.

Trečiojoje tyrimo dalyje buvo nagrinėjamos van der Waalso sąveikos tarp *trans*-stilbeno ir heksagoninio boro nitrido spektroskopinės apraiškos. Stacionariosios ir laiko skyros fluorescencijos matavimai buvo atlikti tūriniam *trans*-stilbenui, hBN ir jų van der Waalso kompleksui, o fluorescencijos gesimo kinetikos buvo analizuojamos taikant bieksponentinius modelius, siekiant nustatyti vidutines fluorescencijos gyvavimo trukmes. Sąveikos sukelti fluorescencijos pokyčiai buvo nagrinėjami kartu su kvantinės chemijos skaičiavimais, Ramano spektroskopijos ir THz spektroskopijos duomenimis. Ši kompleksinė analizė buvo naudojama įvertinti, kaip van der Waalso sąveika tarp dviejų nepolinių medžiagų pasireiškia THz, infraraudonojoje ir regimojoje spektro srityse.

7.1.4. Ginamieji teiginiai

I) Ftalocianinų molekulių chloroformo tirpaluose yra stebimas koncentracinis fluorescencijos gesinimas, kurį lemia Försterio tipo sužadinimo energijos pernaša iš pavienių molekulių į molekulinius H-dimerus. Išmatuotose fluorescencijos gesimo kinetikose šis reiškinys pasireiškia per monotonišką gesimo spartėjimą ir tolygų perėjimą nuo vieneksponentinio prie neeksponentinio gesimo didėjant koncentracijai, todėl šis metodas yra ypač veiksmingas tokiam reiškiniui stebėti ir tirti.

II) Sukimo būdu suformuotose trans-stilbeno molekulių plėvelėse didėjant molekulinei koncentracijai vyksta struktūriniai pokyčiai: nuo pavienių molekulių per netvarkingus agregatus iki labai tvarkingų monokristalų formavimosi. Tiek stacionariosios fluorescencijos spektrai, tiek fluorescencijos gesimo kinetika kinta tolygiai ir monotoniškai, priklausomai nuo šių virsmų. Todėl trans-stilbeno plonųjų plėvelių fluorescencines savybes galima tiksliai valdyti keičiant mėginių paruošimo sąlygas.

III) Van der Waalso sąveika tarp nepolinio heksagoninio boro nitrido ir trans-stilbeno lemia vienos fluorescencijos juostos intensyvumo padidėjimą ir nežymų fluorescencijos gesimo pagreitėjimą. Stacionariosios ir laikinės skyros fluorescencijos derinys gali būti

naudingas papildomas metodas itin silpnoms tarpmolekulinėms sąveikoms tirti.

7.1.5. Mokslinis naujumas

Pagrindinis šios disertacijos mokslinis naujumas yra susijęs su chemine fizika, nes joje pateikiama naujų įžvalgų apie šiuos iki šiol neišspręstus klausimus:

1. Nors fluorescencijos koncentracinis gesinimas stebimas įvairiose molekulinėse sistemose, jo molekulinė kilmė ir šį gesinimą lemiantys fizikiniai procesai dar nėra iki galo suprasti. Ftalocianinų junginiai yra tinkama modelinė sistema šiam reiškiniui tirti [18,19], tačiau tikslūs eksperimentiniai šio reiškinio tyrimai atliekami retai dėl reikšmingų pakartotinės sugerties efektų esant didelėms molekulių koncentracijoms [20]. Šioje disertacijoje naudojamos ploniausios komerciškai prieinamos stiklo kiuvetės, siekiant išvengti pakartotinės sugerties efektų arba juos kiek įmanoma sumažinti. Tai leidžia teisingai interpretuoti fluorescencijos koncentracinio gesinimo reiškinį didelės koncentracijos (iki 10 mmol/l) bemetalių ir cinko ftalocianinų tirpaluose. Koncentracinis gesinimas didelės koncentracijos tirpaluose siejamas su sužadinimo energijos gaudyklių nulemtu mechanizmu, atsirandančiu dėl H-dimerų susidarymo esant didelėms koncentracijoms.
2. Didėjant molekulinei koncentracijai, *trans*-stilbeno plonųjų plėvelių optinių savybių pokyčiai anksčiau buvo stebėti *Karpicz ir kt.* darbuose [13]. Šiame darbe ši tema nagrinėjama išsamiau, keičiant tiek plėvelių molekulinę koncentraciją, tiek jų storį. Globaliosios analizės taikymas kartu su mikroskopijos metodais leidžia tiksliai nustatyti skirtingų *trans*-stilbeno struktūrinių formų stacionariosios laikinės skyros fluorescencijos savybes. Be to, šiame darbe parodyta, kad *trans*-stilbeno plonųjų plėvelių fluorescencines savybes galima valdyti keičiant mėginių paruošimo sąlygas, t. y. molekulinę koncentraciją ir plėvelės storį.
3. Van der Waalso sąveikos spektroskopinės apraiškos iki šiol eksperimentiškai tiriamos palyginti retai. Daugeliu atvejų daugiau dėmesio skiriama su adsorbcija susijusiems reiškiniams ir atitinkamiems spektriniams pokyčiams [10,21–23]. Tuo tarpu šioje disertacijoje daugiausia dėmesio skiriama pačios van der Waalso sąveikos tarp nepolinių junginių spektroskopinėms ypatybėms, kaip modelinę sistemą naudojant trans-stilbeno (TS) ir dvimačio (2D) heksagoninio boro nitrido (hBN) kompleksą. Parodoma, kad van der

Waalso sąveikos sukelti pokyčiai gali būti stebimi terahercinėje (THz), infraraudonojoje ir regimojoje spektro srityse. Taip pat pademonstruojama, kad Ramano spektroskopija yra veiksmingiausias metodas tokiam kompleksui tirti, o THz spektroskopija ir stacionariosios bei laikinės skyros fluorescencijos matavimų derinimas gali suteikti papildomos informacijos. Šis kompleksas yra tinkama modelinė sistema van der Waalso sąveikų tarp organinių junginių ir dvimačių medžiagų ypatybėms tirti.

7.2. Metodologija

7.2.1. Mėginiai

Visos šiame tyrime naudotos medžiagos, būtent chloroformas, 2,9,16,23-tetra-tert-butil-29H,31H-ftalocianinas (TTBPc; $C_{48}H_{50}N_8$), cinko 2,9,16,23-tetra-tert-butil-29H,31H-ftalocianinas (ZnTTBPc; $C_{48}H_{48}N_8Zn$), *trans*-stilbenas (TS, $C_{14}H_{12}$), polistirenas (PS) ir heksagoninis boro nitridas (hBN) buvo įsigytos iš „Sigma-Aldrich“ ir naudotos tokios, kokios buvo gautos, be papildomo gryninimo.

[*Paper A1*] buvo tiriami ZnTTBPc ir TTBPc chloroformo tirpalai, keičiant molekulinę koncentraciją dviem dydžio eilėmis – nuo 0.1 mmol/L (mM) iki 10 mM.

[*Paper A2*] buvo tiriamos sukimo būdu suformuotos plonosios TS plėvelės, keičiant tiek TS koncentraciją PS matricoje (nuo 0.5 % iki 80 %), tiek plėvelių storį (nuo 45 nm iki 670 nm).

[*Paper A3*] buvo tiriami tūrinės formos TS, hBN ir TS + hBN mėginiai. Fluorescencijos ir THz matavimams buvo naudojamos presuotos TS ir TS + hBN tabletės. Ramano eksperimentams buvo naudojami junginių milteliai. hBN THz spektrui gauti buvo naudojamas hBN ir polietileno mišinys, kurio masių santykis buvo 1:1. hBN fluorescencijos spektrui gauti buvo naudojami gryni hBN milteliai.

7.2.2. Elektroninė spektroskopija

Elektroninės sugerties spektrai buvo išmatuoti naudojant Jasco V-670 spektrofotometrą. Tirpiklio **[*Paper A1*]** arba polimero **[*Paper A2*]** sugerties spektrai buvo naudojami kaip bazinė linija, kuri buvo atimta iš mėginių spektrų.

Visų tirtų mėginių fluorescencijos (FL) spektrai buvo išmatuoti naudojant Edinburgh F920 spektrometrą. TS plonosios plėvelės, tūrinė TS tabletė, hBN ir TS + hBN mėginiai buvo žadinami 300 nm pikosekundiniu impulsiniu diodu, naudojant 2 nm spektrinį plyšį ir 850 ps impulso trukmę. Visi išmatuoti

spektrai buvo automatiškai pakoreguoti atsižvelgiant į prietaiso jautrį. ZnTTBPc ir TTBPc chloroformo tirpalai buvo žadinami 375 nm impulsiniu diodiniu lazeriu, kurio impulso trukmė buvo 70 ps, o didesniam signalui gauti buvo pasirinktas 4 nm spektrinis plyšys.

Visų mėginių fluorescencijos slopimo kinetika buvo išmatuota naudojant Edinburgh F920 spektrometrą ir laike koreliuoto pavienių fotonų skaičiavimo metodą [34]. Visos kinetikos buvo registruojamos naudojant tuos pačius parametrus ir matavimo sąlygas, kurie buvo taikomi atitinkamo mėginio stacionariosios fluorescencijos spektrui matuoti. Iš visų išmatuotų kinetikų buvo pašalintas horizontalus foninis signalas. Visos kinetikos buvo aproksimuotos skirtingų modelinių funkcijų, parinktų pagal konkrečią užduotį, sąsūka su iš anksto išmatuota prietaiso atsako funkcija (IRF). Siekiant pagerinti aproksimacijos kokybę, IRF buvo aproksimuota Gauso funkcijos ir vieno eksponentinio slopimo sąsūka:

$$\text{IRF}\,(t) = \exp\left(-\frac{(t-t_0)^2}{2\sigma^2}\right) * \exp\left(-\frac{t}{\tau}\right), \tag{7.1}$$

čia σ yra Gauso funkcijos plotį apibūdinantis parametras, τ žymi charakteringą IRF slopimo laiką, t_0 apibrėžia laiko poslinkį tarp pradinio IRF ir kinetikos profilio, o žvaigždutės simbolis '$*$' žymi sąsūkos operaciją.

7.2.3. Duomenų analizė

Gautiems stacionariosios sugerties ir fluorescencijos duomenims nereikėjo sudėtingo duomenų apdorojimo, išskyrus horizontalaus foninio signalo pašalinimą ir (arba) glodinimą tais atvejais, kai duomenys buvo triukšmingi. Šios procedūros buvo atliekamos naudojant *Python* paketus *Pandas* [84], *NumPy* [85] ir *SciPy* [86].

Slopimo kinetikų aproksimavimas, naudojant skirtingų modelinių funkcijų sąsūką su IRF aproksimacija pagal (7.1) lygtį, buvo atliktas naudojant *Python* paketą *lmfit* [87] ir diferencialinės evoliucijos algoritmą [88].

Straipsnyje **[*Paper A2*]** globalioji analizė, taikant multiplikatyvaus atnaujinimo algoritmą [96] neneigiamos matricos faktorizacijai [91], buvo pritaikyta tiek visam stacionariųjų fluorescencijos spektrų rinkiniui, tiek visam fluorescencijos slopimo kinetikų rinkiniui, siekiant atskleisti morfologijos sukeltų TS plėvelių optinių savybių pokyčių ypatumus:

$$F(\lambda, n) = \sum_{i=1}^{n} S_i(\lambda) \cdot C_i(n), \tag{7.2}$$

čia $F(\lambda, n)$ žymi matricą, kurioje pateikti eksperimentiniai rezultatai, $S_i(\lambda)$ yra bazinė matrica, o $C_i(n)$ – svorių matrica.

7.3. Rezultatai ir aptarimas

7.3.1. Ftalocianinų chloroformo tirpalų fluorescencijos koncentracinis gesinimas

Fluorescencijos koncentracinis gesinimas – tai reiškinys, kai didėjant molekulinei koncentracijai mažėja fluorescencijos kvantinė išeiga. Paprastai dėl šio reiškinio didėja energijos nuostoliai, todėl praktiniuose taikymuose jį būtina kontroliuoti ir riboti.

Koncentracinis fluorescencijos gesinimas paprastai vyksta dėl sužadinimo energijos migracijos iš emituojančių rūšių į optiškai tamsius spąstus. Anksčiau buvo parodyta, kad ftalocianinų junginiai yra tinkama modelinė sistema šiam reiškiniui tirti [18].

7.1 pav. a ir b dalyse atitinkamai parodyti ZnTTBPc ir TTBPc sugerties (ištisinės linijos) ir fluorescencijos (taškai) spektrų pokyčiai, molekulinei koncentracijai padidėjus dviem dydžio eilėmis. ZnTTBPc atveju nei stacionariosios sugerties, nei fluorescencijos spektruose reikšmingų pokyčių nepastebėta. Tuo tarpu TTBPc sugerties spektruose, didėjant koncentracijai, santykinai didėja ties 640 nm ir 664 nm esančių sugerties juostų intensyvumas. Labiausiai tikėtina, kad tokį elgesį galima sieti su H agregatų susidarymu [115].

7.1 pav. c ir d dalyse atitinkamai pateiktos ZnTTBPc ir TTBPc fluorescencijos slopimo kinetikos, išmatuotos esant toms pačioms koncentracijoms. Abiem junginiams būdinga panaši dinamika: esant mažoms koncentracijoms (0.1 mM ir 0.3 mM), slopimo kinetikos gerai aprašomos viena eksponentine komponente (žr. 7.1 lentelę). Tačiau didėjant molekulinei koncentracijai abiejų junginių fluorescencijos slopimas tampa neeksponentinis.

Siekiant paaiškinti tokį sudėtingą elgesį, visoms slopimo kinetikoms aproksimuoti buvo taikyta ištemptosios eksponentės slopimo funkcija:

$$K(t) = a \cdot \exp[-(t/\tau)^b], \tag{7.3}$$

o vidutinė fluorescencijos gyvavimo τ_{av} trukmė buvo apskaičiuota taip:

$$\tau_{\text{av}} = \tau \cdot \Gamma\left(1 + \frac{1}{b}\right). \tag{7.4}$$

Šiose formulėse τ yra optimizuojama fluorescencijos gyvavimo trukmė, b – ištempimo parametras, o $\Gamma(\cdot)$ – gama funkcija.

Gautos aproksimacijos 7.1 pav. pateiktos juodomis linijomis, o aproksimavimo parametrai pateikti 7.1 lentelėje. Ištempimo parametro β\beta kitimas nuo 1 mažos koncentracijos mėginiams iki 0,5 didžiausios koncentracijos mėginiams atspindi monotonišką sistemos laiko skyros elgsenos kitimą nuo mono-eksponentinio prie daugia-eksponentinio slopimo.

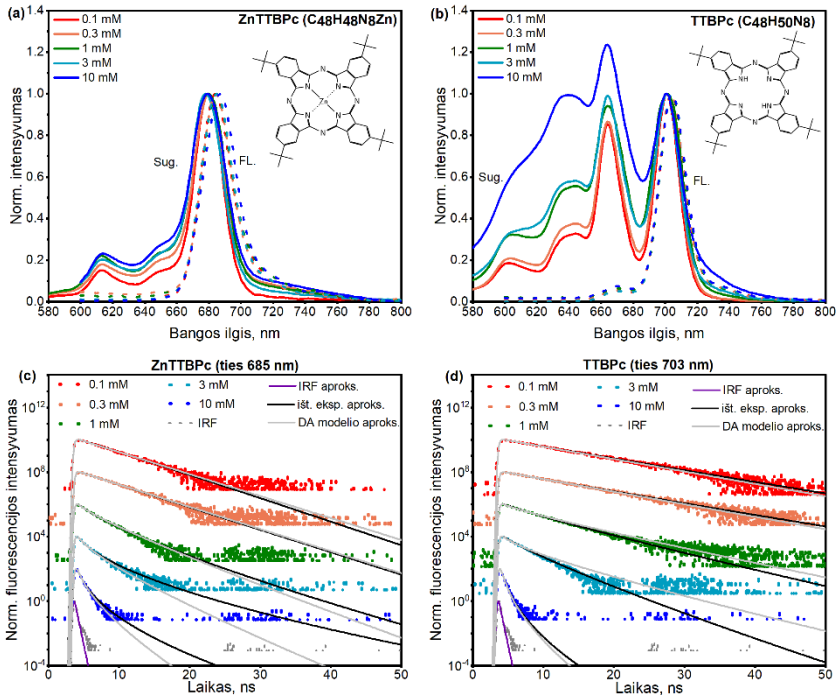
Tačiau toks kitimas nesuteikia fizikinės informacijos apie ftalocianinų junginiuose stebimo koncentracinio fluorescencijos gesinimo kilmę.

Tokia nuo koncentracijos priklausoma dinamika leidžia manyti, kad fluorescencijos gesinimą lemia spąstų sąlygotas mechanizmas. Šiam procesui aprašyti taikomas paprastas Försterio teorija pagrįstas sužadinimo energijos migracijos modelis, kuriame viena donoro rūšis yra apsupta begalinio skaičiaus akceptorių (DA modelis) [12,70]:

$$P(t) = \exp\left[-\frac{t}{\tau_A} - \left(\frac{t}{\tau_B}\right)^{1/2}\right]. \quad (7.5)$$

Ši formulė aprašo tikimybę $P(t)$, kad donoro rūšis išliks sužadinta praėjus laikui t, kur τ_A yra donoro rūšies fluorescencijos gyvavimo trukmė, o τ_B – charakteringas slopimo laikas, susijęs su sužadinimo spąstais.

Darant prielaidą, kad mažiausios koncentracijos (0.1 mM) abiejų junginių mėginiuose nėra spąstų rūšių, eksperimentines kinetikas galima aproksimuoti nustatant τ_A reikšmę lygią atitinkamo mažiausios koncentracijos mėginio fluorescencijos gyvavimo trukmei. Aproksimacijos, gautos taikant DA modelį, 7.1 pav. pateiktos šviesiai pilkomis linijomis, o optimizuotos τ_B reikšmės pateiktos 7.1 lentelėje. '∞' reikšmės esant 0.1 mM, t. y. mažiausiai koncentracijai, rodo, kad gesinimas nevyksta. Tuo tarpu esant didžiausioms koncentracijoms τ_B reikšmės, siekiančios maždaug 0.1 ns, rodo, kad vyrauja sužadinimo energijos migracijos į neemituojančius spąstus per FRET procesai. Tarpinių koncentracijų atveju, didėjant koncentracijai, τ_B reikšmės monotoniškai mažėja, o tai rodo nuoseklų fluorescencijos gesinimo stiprėjimą.

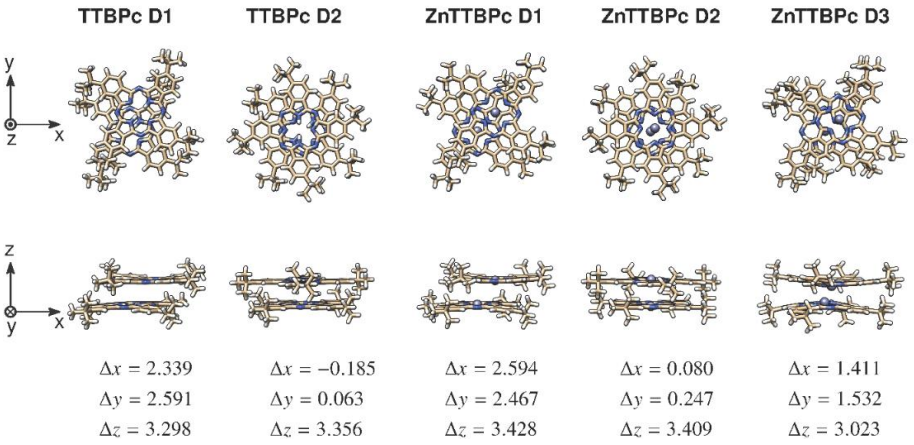


7.1 pav. *a–b) ZnTTBPc ir TTBPc chloroformo tirpalų sugerties (spalvotos ištisinės linijos) ir fluorescencijos (punktyrinės linijos) spektrai, išmatuoti atitinkamai 0,1–10 mM koncentracijų intervale. Aiškumo dėlei abiejuose grafikuose pateiktos atitinkamos molekulinės struktūros. c–d) ZnTTBPc ir TTBPc chloroformo tirpalų fluorescencijos gesimo kinetikos (spalvoti taškai). Juodos linijos žymi aproksimacijas, gautas taikant ištemptosios eksponentės funkciją ((7.3) lygtis), o šviesiai pilkos linijos – aproksimacijas, gautas taikant DA modelį ((7.5) lygtis). Aiškumo dėlei kinetikos paslinktos vertikaliai jas padauginant iš 100. Abiejuose grafikuose taip pat pateikta išmatuota IRF (pilki taškai) ir jos aproksimacija pagal (7.1) lygtį. Visi mėginiai buvo žadinami ties* λ_{exc} *= 375 nm. Adaptuota pagal* **[*Paper A1*]**, *gavus „AIP Publishing“ leidimą.*

Pažymėtina, kad ši analizė neleidžia nustatyti spąstų rūšių molekulinės kilmės. Šiam tikslui buvo atlikti kvantiniai cheminiai skaičiavimai. Jie parodė, kad tiek ZnTTBPc, tiek TTBPc chloroforme gali sudaryti stabilias H-dimerų struktūras, kurios, labiausiai tikėtina, veikia kaip sužadinimo energijos spąstai.

7.1 lentelė. *Fluorescencijos gesimo kinetikų aproksimavimo charakteristikos taikant mono-eksponentinio arba ištemptosios eksponentės aprašymą ((7.3) lygtis) ir DA modelį ((7.5) lygtis). Vidutinės fluorescencijos gyvavimo trukmės apskaičiuotos iš ištemptosios eksponentės aproksimacijų pagal (7.4) lygtį. Adaptuota pagal* **[*Paper A1*]** *, gavus „AIP Publishing“ leidimą.*

Koncentracija, mM	**Mono-eksponentinis gesimas**	**Ištemptosios eksponentės gesimas**			**DA modelis**
	τ_1, ns	τ	b	τ_{av}, ns	τ_B, ns
ZnTTBPc					
0.1	3.20	3.26	1.02	3.22	∞
0.3	3.06	3.05	0.99	3.06	691
1		1.11	0.77	1.29	1.66
3		0.39	0.59	0.61	0.50
10		0.09	0.50	0.17	0.11
TTBPc					
0.1	5.68	5.59	0.97	5.66	∞
0.3	5.43	5.29	0.95	5.40	1189
1		2.86	0.89	3.03	6.35
3		1.50	0.85	1.63	1.28
10		0.05	0.50	0.10	0.05



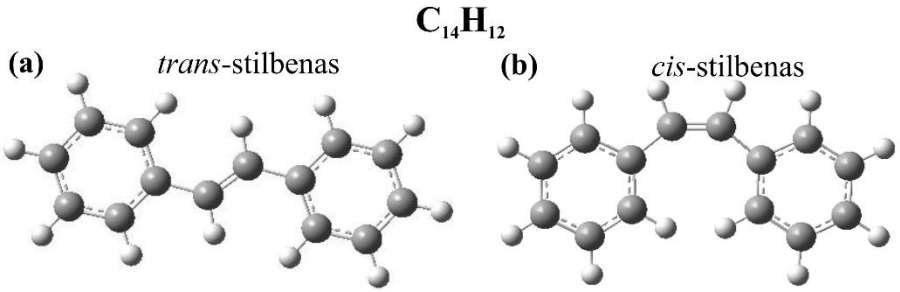
7.2 pav. *Viršutinėje dalyje pateikti TTBPc ir ZnTTBPc dimerų molekulinių struktūrų vaizdai iš viršaus. Vidurinėje dalyje pateikti atitinkamų struktūrų vaizdai iš šono. Apatinėje dalyje parodyti atitinkamų monomerų santykiniai*

poslinkiai x, y ir z ašių kryptimis. Pradinės H-dimerų struktūros prieš optimizavimą buvo sudarytos uždedant du monomerus vieną ant kito, kai jų tarpusavio orientacija z ašies atžvilgiu buvo 0° arba 45°. Visos struktūros buvo optimizuotos LC-BLYP/6-31G(d) teorijos lygmeniu, naudojant programą „GaussView“. Perspausdinta iš ***[Paper A1]****, gavus AIP Publishing leidimą. / Skaičiavimus atliko dr. Andrius Gelzinis ir Darius Likandrovas (abu iš FTMC).*

7.3.2. Morfologijos sukelti *trans*-stilbeno plonųjų plėvelių fluorescencinių savybių pokyčiai

Stilbenas ($C_{14}H_{12}$) yra organinis junginys, kurio geriausiai žinoma savybė yra *trans–cis* fotoizomerizacija [118–120]. Fotoizomerizacija vyksta veikiant ultravioletinei spinduliuotei tiek skystojoje, tiek dujinėje fazėje. 7.3 pav. a ir b dalyse atitinkamai pavaizduotos stilbeno *trans* ir *cis* stereoizomerų struktūros. Tačiau kietojoje stilbeno būsenoje izomerizacija nevyksta dėl sterinių apribojimų [13,36,122].

Kietasis *trans*-stilbenas (TS) gali būti taikomas jutiklių ir atrankos sistemose [14], UV spinduliuotei aptikti [123,124] arba neutroninei spinduliuotei registruoti [125–127]. Stabilios TS plonosios plėvelės pastaruoju metu buvo charakterizuotos naudojant SEM [13] ir XRD [131]. *Karpicz ir kt.* [13] parodė, kad didėjant TS koncentracijai polimerinėje matricoje, TS molekulės pradeda telktis į klasterius, o fluorescencijos spektruose atsiranda reikšmingų pokyčių. Tačiau tiksli tokių plėvelių trimatė morfologija, taip pat optinių savybių kitimo dinamika, susijusi su morfologijos pokyčiais keičiant koncentraciją ir plėvelės storį, vis dar nėra pakankamai ištirta. Tokios žinios galėtų padėti valdyti TS plėvelių struktūrą ir savybes, o tai gali būti naudinga įvairiems praktiniams taikymams.

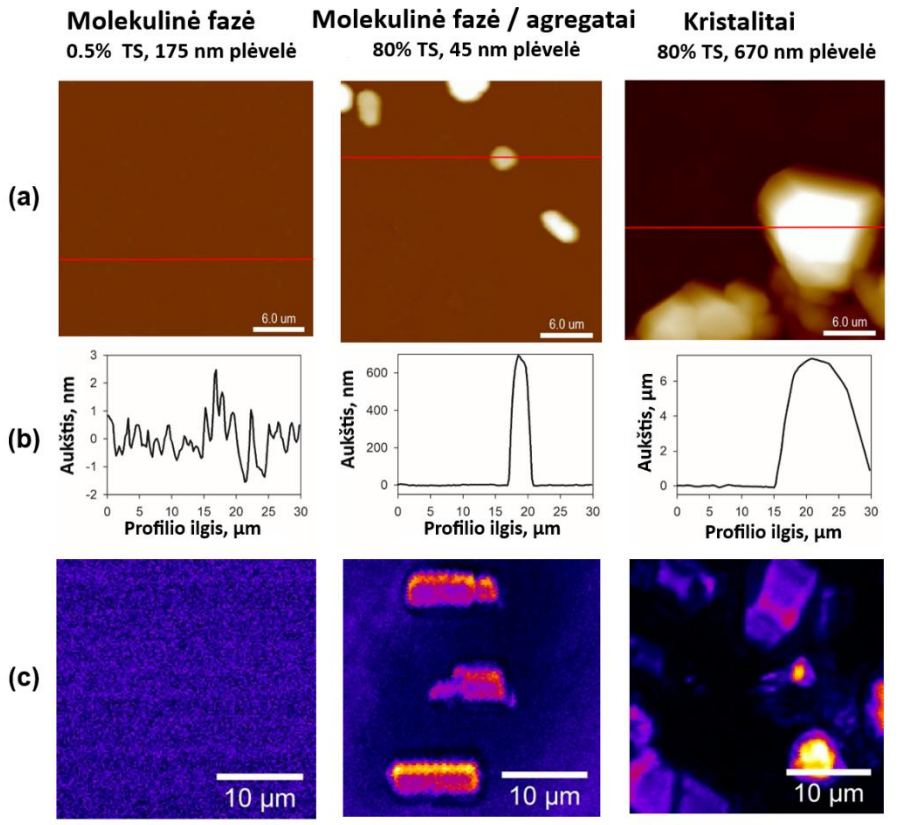


7.3 pav. *Cheminės a) trans- ir b) cis-stilbeno junginių struktūros. Adaptuota pagal* **[*Paper A2*]**, *laikantis CC BY 4.0 licencijos sąlygų. /Chemines struktūras, naudodamas „GaussView“ programą, nubraižė dr. Mindaugas Mačernis (Vilniaus universitetas).*

7.4 pav. pateikti trijų TS plonųjų plėvelių, pasižyminčių skirtingomis TS koncentracijomis ir plėvelės storiais, AFM (7.4 pav. a) ir CARS (7.4 pav. c) vaizdai. Remiantis ankstesniais tyrimais [13], mikroskopijos rezultatai rodo, kad didėjant koncentracijai vyksta TS klasterizacija. Esant mažiausiai koncentracijai (0.5 %), stebima monomerinė, t. y. grynai molekulinė, TS plėvelės morfologija. 80 % koncentracijos ir 670 nm storio TS plėvelėse yra labai tvarkingų TS monokristalų, o 80 % koncentracijos ir 45 nm storio mėginį, labiausiai tikėtina, sudaro tiek netvarkingi TS agregatai, tiek TS monokristalai. AFM tyrimai parodė, kad TS kristalai susidaro plėvelės paviršiuje.

7.5 pav. a dalyje pateikti TS plonųjų plėvelių stacionariosios fluorescencijos spektrai, išmatuoti esant skirtingoms TS koncentracijoms ir plėvelių storiams. *Karpicz ir kt.* [13] arodė, kad TS klasterizacija lemia subtilius TS plonųjų plėvelių fluorescencinių savybių pokyčius. Iš tiesų, keičiant tiek TS koncentraciją, tiek plėvelės storį, stebimi laipsniški fluorescencijos spektrų pokyčiai (žr. 7.5 pav. a ir 7.2 lentelę).

Siekiant išsamiau suprasti šiuos pokyčius, visam fluorescencijos spektrų rinkiniui buvo atlikta globalioji analizė, taikant NNMF metodą (7.2 lygtis). Dviejų komponenčių skaidymo rezultatai 7.5 pav. a dalyje pateikti raudonomis linijomis. Buvo daroma prielaida, kad 0.5 % koncentracijos ir 175 nm storio TS plėvelėje nėra nei netvarkingų agregatų, nei labai tvarkingų kristalitų ir kad ją daugiausia sudaro grynai molekulinės TS rūšys. Todėl šios plėvelės fluorescencijos spektras viso algoritmo metu buvo fiksuotas ir nekeičiamas. Ši analizė leidžia išskirti dvi fluorescencines rūšis. Pirmoji komponentė (auksinė linija 7.5 pav. a dalyje) priskiriama grynai molekulinėms TS rūšims, o jos indėlis mažėja didėjant TS koncentracijai. Analizuojant nuo plėvelės storio priklausančius spektrus, kai TS koncentracija buvo pastovi ir lygi 80 %, stebima panaši tendencija. Pagal skaidymo rezultatus ploniausios plėvelės fluorescencijos spektre monomerinių rūšių indėlis siekia apie 60 %, o didėjant plėvelės storiui šis indėlis mažėja. Antroji komponentė (žalia linija 7.5 pav. a dalyje) gali būti priskirta TS monokristalams. 7.5 pav. b dalis rodo, kad didėjant tiek TS koncentracijai, tiek plėvelės storiui, kristalams priskiriamos komponentės santykinis svoris fluorescencijos spektruose didėja.



7.4 pav. *a) 30 µm × 30 µm TS plonųjų plėvelių paviršiaus AFM vaizdai. b) TS klasterių aukštis, t. y. atstumas nuo plėvelės paviršiaus vertikalia kryptimi išilgai raudonos linijos, parodytos a dalyje. c) Tų pačių plėvelių 30 µm × 30 µm CARS vaizdai. Adaptuota pagal* ***[Paper A2]****, laikantis CC BY 4.0 licencijos sąlygų. / AFM matavimus atliko dr. Marija Jankunec (Vilniaus universitetas), o CARS matavimus – dr. Andrej Dementjev (FTMC).*

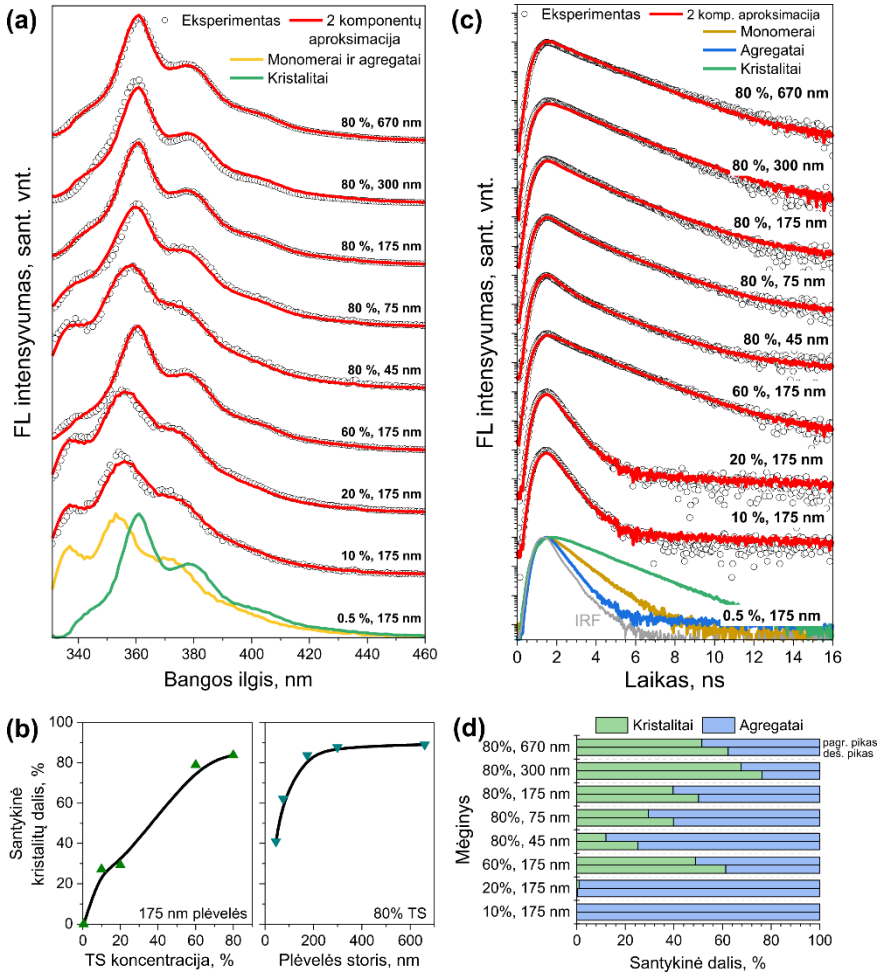
Didėjant TS koncentracijai, fluorescencijos slopimo kinetikose iš pradžių (iki 10 % ir 20 %) stebimas fluorescencijos gesinimas (žr. 7.5 pav. c ir 7.2 lentelę). Tačiau toliau didėjant koncentracijai, monotoniškai ilgėja fluorescencijos gyvavimo trukmės ir didėja komponenčių, reikalingų kinetikoms tinkamai aproksimuoti, skaičius. Keičiant plėvelės storį esant pastoviai TS koncentracijai, taip pat stebimas gyvavimo trukmių ilgėjimas. Didžiausios TS koncentracijos ir didžiausio storio plėvelė (80 % TS, 670 nm) pasižymi lėtu mono-eksponentiniu slopimu, kurio gyvavimo trukmė yra 1,60 ns, o tai rodo, kad šiame mėginyje vyrauja TS monokristalai.

7.2 lentelė. *Skirtingos koncentracijos ir storio TS plonųjų plėvelių stacionariosios fluorescencijos ir fluorescencijos slopimo kinetikų charakteristikos, įskaitant fluorescencijos juostų padėtis ir fluorescencijos slopimo kinetikų biekspontentinio aproksimavimo parametrus. Adaptuota pagal* **[*Paper A2*]**, *laikantis CC BY 4.0 licencijos sąlygų.*

TS koncentracija PS matricoje, mas., %.	**Plėvelės storis, nm**	Stacionariosios fluorescencijos savybės	Fluorescencijos slopimo kinetikos savybės			
		FL juostos, nm	λ_{FL}, **nm**	τ_1, **ns (%)**	τ_2, **ns (%)**	τ_{av}, **ns**
0.5%	175	336, 353, 372	353	0.71 (100%)	---	0.71
10%	175	340, 354, 374	355	0.26 (100%)	---	0.26
20%	175	340, 355, 375	357	0.28 (100%)	---	0.28
60%	175	341, 360, 380	361	0.19 (80%)	1.65 (20%)	0.48
80%	45	339, 359, 376	360	0.30 (87%)	1.68 (13%)	0.48
80%	75	341, 360, 376	361	0.38 (75%)	1.62 (25%)	0.69
80%	175	342, 360, 380	361	0.51 (61%)	1.50 (39%)	0.90
80%	300	347, 360, 380, 404	361	0.51 (36%)	1.48 (63%)	1.12
80%	670	347, 361, 380, 405	361	---	1.60 (100%)	1.60

Visas fluorescencijos slopimo kinetikų rinkinys buvo globaliai išanalizuotas taikant tą patį metodą, kuris buvo naudotas stacionariosios fluorescencijos spektrams. Skaidymo rezultatai 7.5 pav. c dalyje pateikti raudonomis linijomis. Šiuo atveju dviejų komponenčių skaidymas nėra toks vienareikšmis: dviejų komponenčių nepakanka visam kinetikų rinkiniui tinkamai aproksimuoti. Tačiau iš aproksimavimo pašalinus mažiausios koncentracijos mėginio (0.5 % TS, 175 nm) monoeksponentinę kinetiką, visas likusias kinetikas tampa įmanoma išskaidyti į dvi komponentes. Pirmoji yra greitoji komponentė, kurios vidutinė gyvavimo trukmė yra maždaug 0.27 ns (mėlyna kreivė 7.5 pav. c dalyje). Ši kinetinė komponentė gali būti priskirta greitai netvarkingų TS agregatų fluorescencijai. Ji vyrauja 10 % ir 20 %

koncentracijos 175 nm storio plėvelių, taip pat 80 % koncentracijos 45 nm storio plėvelės kinetikose. Santykinis šios komponentės svoris kiekvienoje fluorescencijos slopimo kinetikoje 7.5 pav. d dalyje parodytas mėlynu stulpeliu. Antroji, ilgaamžė, 1.60 ns gyvavimo trukmės komponentė (žalia kreivė 7.5 pav. c dalyje) gali būti priskirta TS monokristalų monoeksponentinei slopimo kinetikai. Santykinis šios komponentės svoris kiekvienoje fluorescencijos slopimo kinetikoje 7.5 pav. d dalyje parodytas žaliu stulpeliu. Įdomu tai, kad nė viena iš kinetikų negali būti visiškai aprašyta vien šia komponente.



7.5 pav. *Globaliosios analizės rezultatai: a) stacionariosios fluorescencijos spektrų ir c) fluorescencijos slopimo kinetikų analizė, taikant daugiamatės kreivių skiriamosios analizės metodą, pagrįstą neneigiamos matricos faktorizacija ((7.2) lygtis). b) ir d) dalyse atitinkamai parodytas santykinis TS*

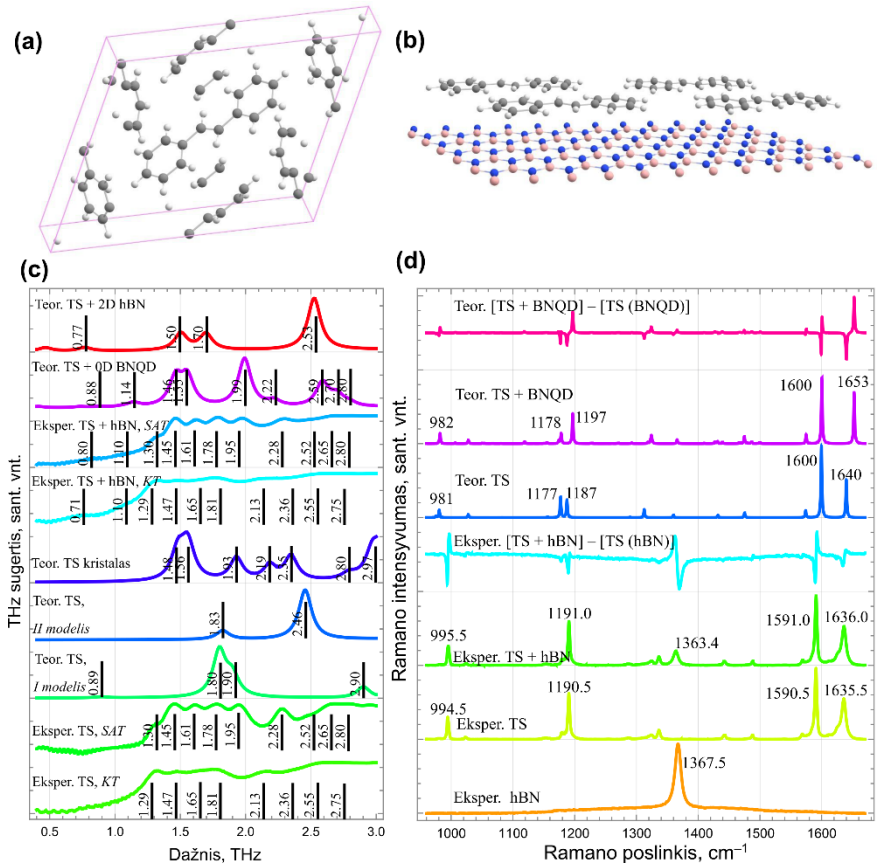
monokristalų indėlis plėvelių stacionariosios fluorescencijos spektruose bei santykiniai TS agregatų ir monokristalų indėliai plėvelių fluorescencijos slopimo kinetikose. Adaptuota pagal ***[Paper A2]****, laikantis CC BY 4.0 licencijos sąlygų.*

7.3.3. Van der Waals sąveikos tarp *trans*-stilbeno ir heksagoninio boro nitrido pasireiškimas

Dvimačio (2D) heksagoninio boro nitrido (hBN) nanosluoksnis yra medžiaga, pasižyminti dideliu cheminiu ir šiluminiu stabilumu bei dideliu šiluminiu laidumu [134–136]. 2D hBN yra izoliatorius [134,135] ir jau buvo sėkmingai pritaikytas kaip dielektrinis sluoksnis lauko tranzistoriuose [135,137], aip pat kaip apsauginis dengiamasis sluoksnis įvairiuose įrenginiuose [135]. Be to, verta paminėti, kad hBN yra perspektyvus fotonikos taikymams, pavyzdžiui, ultravioletinės spinduliuotės detektoriams ir emiteriams [137]. Įvairių organinių junginių sąveikos su skirtingomis boro nitrido formomis mechanizmų ir stiprumo supratimas yra svarbus minėtiems taikymams. Pastaruoju metu van der Waals sąveikos spektroskopinės apraiškos ir su adsorbcija susiję reiškiniai buvo tiriami tiek teoriškai, tiek eksperimentiškai doksorubicino, adsorbuoto ant 2D hBN nanodribsnių [144], atveju, taip pat tiakarbocianino dažikliams [21] ir įvairiems porfirinų bei ftalocianinų junginiams [10,22,102,103,145], adsorbuotiems ant hBN. Tačiau žinios apie adsorbuotų junginių vibracines ir elektronines savybes, taip pat apie grynos van der Waals sąveikos tarp organinių junginių ir hBN paviršiaus pasireiškimą vis dar yra nepakankamos.

Šiame skyriuje nagrinėjama van der Waals sąveika tarp tūrinio nepolinio TS ir hBN. Atsižvelgiant į abiejų medžiagų nepolinį pobūdį, galima manyti, kad pagrindinis jų tarpusavio sąveikos mechanizmas yra Londono dispersinės jėgos. 7.6 pav. a ir b dalyse atitinkamai pateiktos DFT metodu optimizuotos TS kristalo struktūros ir atskirų TS molekulių, adsorbuotų ant 2D hBN sluoksnio, struktūros.

7.6 pav. c dalyje pateikti tiek eksperimentiniai TS ir TS + hBN van der Waals komplekso THz-TD spektrai, išmatuoti kambario temperatūroje ir skysto azoto temperatūroje, tiek apskaičiuoti spektrai (išsamiau žr. **[*Paper A3*]**). Galima teigti, kad vdW sąveika tarp TS ir hBN lemia dviejų papildomų juostų atsiradimą TS + hBN spektre, palyginti su gryno TS spektru. Šios juostos yra žemų dažnių srityje: 0,71 THz kambario temperatūroje ir 0,80 THz skysto azoto temperatūroje, taip pat ties 1,10 THz abiem temperatūroms. Jos priskiriamos libraciniams virpesiams, t. y. TS virpesiams hBN paviršiaus atžvilgiu, ir taip patvirtina komplekso susidarymą. Šią tendenciją patvirtina ir DFT skaičiavimų rezultatai.



7.6 pav. *a–b) Atitinkamai optimizuota TS kristalo struktūra ir atskiros TS molekulės, adsorbuotos ant hBN. c) Eksperimentiniai ir apskaičiuoti TS bei TS + hBN komplekso THz spektrai. Visuose spektruose pažymėtos smailių padėtys. „KT“ reiškia kambario temperatūrą, o „SAT“ – skysto azoto temperatūrą. d) Eksperimentiniai ir apskaičiuoti TS bei TS + hBN komplekso Ramano spektrai. Palyginimui pateiktas eksperimentinis hBN Ramano spektras. Aiškumo dėlei tiek eksperimentiniams, tiek apskaičiuotiems Ramano spektrams taip pat pateikti skirtuminiai TS ir TS + hBN vdW komplekso spektrai. Visuose spektruose pažymėtos smailių padėtys. Adaptuota pagal* **[*Paper A3*]**. *Autorių teisės 2025 m. „American Chemical Society“. / THz eksperimentus atliko dr. Daniil Pashnev (FTMC), Ramano matavimus – dr. Martynas Talaikis (FTMC), o visus skaičiavimus atliko dr. Maksim Shundalau (Salerno universitetas).*

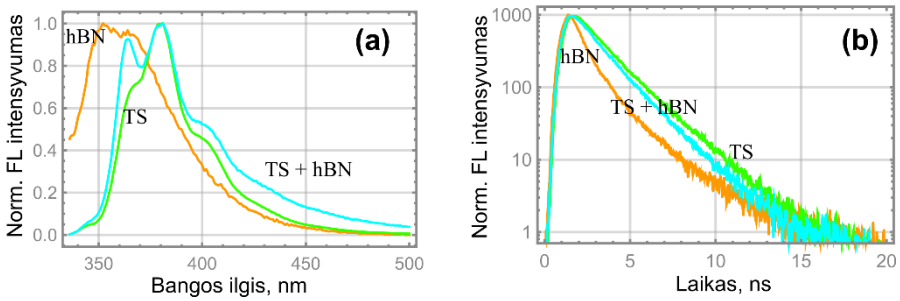
7.6 pav. d dalyje pateikti tiek eksperimentiniai, tiek apskaičiuoti (išsamiau žr. **[*Paper A3*]**) TS, hBN ir TS + hBN van der Waals komplekso Ramano spektrai. Tiek eksperimentiniai duomenys, tiek skaičiavimų

rezultatai rodo tą pačią tendenciją: TS + hBN komplekse kai kurios TS priskiriamos juostos, palyginti su grynu TS, pasislenka į didesnių dažnių sritį, o hBN priskiriama juosta, palyginti su grynu hBN, pasislenka į mažesnių dažnių sritį. 7.3 lentelėje pateikti eksperimentinių Ramano dažnių pokyčiai, kuriuos lemia vdW sąveika tarp TS ir hBN.

7.3 lentelė. *Dėl sąveikos pasislinkusių eksperimentinių hBN, TS ir TS + hBN komplekso Ramano juostų priskyrimas. Adaptuota pagal* **[*Paper A3*]**. *Autorių teisės 2025 m. „American Chemical Society“.*

Ramano dažnis, cm^{-1}			**Juostos priskyrimas**
TS	**hBN**	**TS + hBN**	
994.5		995.5	Žiedo plokštuminė trigonalinė deformacija
1190.5		1191.0	C– žiedo tempimo virpesiai
	1367.5	1363.5	E_{2g} hBN moda (B–N ryšio tempimo virpesiai)
1590.5		1591.0	Žiedo tempimo virpesiai
1635.5		1636.0	C=C tempimo virpesiai

7.7 pav. a ir b dalyse atitinkamai pateikti TS, hBN ir TS + hBN vdW komplekso stacionariosios fluorescencijos spektrai bei fluorescencijos slopimo kinetikos. TS + hBN komplekse, palyginti su grynu TS, stebimas santykinis ties 365 nm esančios juostos intensyvumo padidėjimas. Mažai tikėtina, kad šį padidėjimą lemia hBN, nes jo fluorescencijos intensyvumas yra gerokai mažesnis nei TS (žr. 7.4 lentelę). Labiausiai tikėtina, kad šis santykinis intensyvumo padidėjimas susijęs su subtiliu TS elektronų debesies persiskirstymu sąveikaujant su hBN. Be to, TS + hBN komplekse, palyginti su grynu TS, stebimas nežymus fluorescencijos gesinimas (žr. 7.4 lentelę). Tikėtina, kad šį pokytį taip pat lemia subtilūs TS elektroninės struktūros pokyčiai, atsirandantys dėl sąveikos su hBN.



7.7 pav. *a) hBN, TS ir TS + hBN vdW komplekso stacionariosios fluorescencijos spektrai; b) tų pačių mėginių fluorescencijos slopimo kinetikos. Visuose matavimuose žadinimo bangos ilgis* λ_{exc} = 300 nm. *Adaptuota pagal* ***[Paper A3]***. *Autorių teisės 2025 m. „American Chemical Society“.*

7.4 lentelė. *hBN, TS ir TS + hBN junginių stacionariosios fluorescencijos ir fluorescencijos gesimo kinetikos charakteristikos. Adaptuota pagal* ***[Paper A3]***. *Autorių teisės 2025 m. „American Chemical Society“.*

	hBN			**TS**			**TS + hBN kompleksas**		
Stacionarioji FL									
FL juostos, nm	352, 364			345, 367, 380, 404			364, 380, 405		
FL intens. ties 365 nm	17920			245700			85950		
Laiko skyros FL									
Juosta, nm	τ_1, ns	τ_2, ns	τ_{av}, ns	τ_1, ns	τ_2, ns	τ_{av}, ns	τ_1, ns	τ_2, ns	τ_{av}, ns
345	0.29 (97%)	2.45 (3%)	0.35	0.63 (84%)	1.67 (16%)	0.80	0.35 (83%)	1.51 (17%)	0.54
352	0.35 (97%)	2.70 (3%)	0.42	0.68 (65%)	1.81 (35%)	1.07	0.41 (73%)	1.90 (27%)	0.82
364	0.33 (94%)	2.31 (6%)	0.44				0.53 (70%)	1.88 (30%)	0.94
367				0.70 (68%)	2.10 (32%)	1.14			
380	0.33 (93%)	2.24 (7%)	0.47	0.70 (70%)	2.23 (30%)	1.18	0.47 (70%)	1.94 (30%)	0.92
405	0.40 (90%)	2.41 (10%)	0.60	0.68 (61%)	2.23 (39%)	1.29	0.44 (72%)	2.09 (28%)	0.90
420	0.42 (88%)	2.83 (12%)	0.70	1.02 (57%)	2.48 (43%)	1.65	0.60 (74%)	2.69 (26%)	1.14

7.4. Išvados

Šioje disertacijoje nagrinėjami optinių spektrų pokyčiai, susiję su skirtingų tipų tarpmolekulinėmis sąveikomis.

Tiek bemetalis, tiek cinko ftalocianinas pasižymi fluorescencijos koncentraciniu gesinimu (KG). Didėjant molekulinei tirpalo koncentracijai, nė vieno junginio stacionariosios fluorescencijos spektruose nepastebima ryškių pokyčių, tačiau fluorescencijos gesimo kinetikos reikšmingai paspartėja, taip pat yra stebimas nuoseklus perėjimas nuo monoeksponentinio gesimo esant mažoms koncentracijoms prie multieksponentinio gesimo esant didesnėms koncentracijoms. Toks elgesys buvo priskirtas fluorescencijos gesinimui, kurį lemia Försterio tipo sužadinimo energijos migracija į nefluorescuojančias arba silpnai fluorescuojančias sužadinimo gaudykles. DFT pagrįsti kvantinės chemijos skaičiavimai taip pat parodė, kad šios gaudyklės yra besiformuojantys H dimerai.

Trans-stilbeno (TS) plonosios plėvelės taip pat pasižymi KG esant santykinai mažoms koncentracijoms (nuo 0,5 % iki 20 % TS). Tačiau, priešingai nei ftalocianinų tirpaluose, jų fluorescencijos gesimo kinetikos monoeksponentinės. Labiausiai tikėtina, kad šis gesinimas kyla dėl silpnai fluorescuojančių TS agregatų susidarymo, kurie plėvelėse tampa pagrindinėmis emituojančiomis rūšimis. Toks elgesys skiriasi nuo ftalocianinų atvejo, kai net ir esant didžiausioms koncentracijoms stebima emisija kilo iš monomerinių rūšių.

Apskritai, didėjant molekulinei koncentracijai, TS plonosios plėvelės pasižymi sudėtingesniu elgesiu. Esant santykinai mažoms koncentracijoms stebimą KG dar padidinus koncentraciją pakeičia lėtesnės bieksponentinės fluorescencijos gesimo kinetikos. Didėjant plėvelės storiui, fluorescencijos gesimas lėtėja, o storiausioje plėvelėje (80 % TS, 670 nm) stebimas lėtas monoeksponentinis gesimos, kurio gyvavimo trukmė yra 1,60 ns. Stacionariosios fluorescencijos spektrai, didėjant molekulinei koncentracijai, kinta tolygiai. Toks elgesys aiškinamas struktūriniais pokyčiais TS plonosiose plėvelėse, kurie buvo stebėti taikant CARS mikroskopiją ir AFM. Apskritai nustatytos trys struktūrinės formos: atskiros TS molekulės, netvarkingi TS agregatai ir TS monokristalai. Santykinį kiekvienos TS struktūrinės formos kiekį galima kontroliuoti keičiant molekulinę koncentraciją, o TS agregatų ir kristalų dydį – keičiant plėvelės storį. Visos trys TS struktūrinės formos pasižymi skirtingomis stacionariosios ir laikinės skyros fluorescencijos savybėmis. Todėl tiksliai kontroliuojant mėginių paruošimo sąlygas galima tiksliai valdyti fluorescencines savybes, o tiek stacionarioji fluorescencija,

tiek fluorescencijos gesimo kinetikos yra tinkami ir veiksmingi metodai tokiems nuo morfologijos priklausomiems reiškiniams analizuoti.

Fluorescencijos gesinimas taip pat stebimas TS molekulių ir dvimačio (2D) heksagoninio boro nitrido (hBN) van der Waalso komplekse, palyginti su gryno TS tablete. Šis gesinimas gali būti siejamas su subtilia, sąveikos sukelta TS kristalinės struktūros deformacija sąveikaujant su hBN. Stacionariosios fluorescencijos spektruose taip pat stebimas vienos juostos santykinis intensyvumo padidėjimas, kuris, tikėtina, turi tą pačią kilmę kaip ir fluorescencijos gesinimas.

Apskritai van der Waalso (vdW) sąveika tarp nepolinio TS ir hBN pasireiškia THz, infraraudonojoje ir regimojoje spektro srityse, todėl TS + hBN kompleksas yra tinkama modelinė sistema vdW sąveikos tarp organinių junginių ir dvimatės nepolinės medžiagos ypatybėms tirti. Tokiu atveju Ramano spektruose stebimi su adsorbcija susiję poslinkiai, todėl Ramano spektroskopija yra veiksmingiausias metodas tokio tipo sąveikoms aptikti ir apibūdinti.

Apibendrinant, gauti rezultatai atskleidžia aiškius skirtingų tipų tarpmolekulinių sąveikų spektroskopinius požymius, įskaitant H agregatų susidarymą, nuo morfologijos priklausomą molekulinę organizaciją ir van der Waalso sąveiką tarp dviejų nepolinių junginių. Nors fluorescencijos gesinimas stebimas visose tirtose sistemose, jo kilmė skiriasi priklausomai nuo tarpmolekulinių sąveikų pobūdžio ir molekulinės organizacijos, atspindėdama pagrindinės ir sužadintosios būsenų procesų, lemiančių tirtų sistemų fotofizikinį atsaką, skirtumus.

7.5. Publikacijos

7.5.1. Straipsniai

Disertacija yra pagrįsta trimis publikuotais recenzuotais moksliniais straipsniais:

[A1] **I. Halimski**, S. Streckaite, D. Likandrovas, A. Gelzinis, L. Valkunas, J. Chmeliov, Fluorescence concentration quenching in phthalocyanine solutions: experimental observation and theoretical insights, J. Chem. Phys. 164 (2026) 184304. https://doi.org/10.1063/5.0323795

[A2] **I. Halimski**, R. Karpicz, A. Dementjev, M. Jankunec, J. Chmeliov, M. Macernis, D. Abramavicius, L. Valkunas, *trans*-Stilbene aggregates and crystallites in polystyrene films: microscopy and spectroscopy studies, Phys. Chem. Chem. Phys. 26 (2024) 23692–23702. https://doi.org/10.1039/D4CP02291B

[A3] **I. Halimski**, D. Pashnev, M. Talaikis, A. Dementjev, R. Karpicz, J. Chmeliov, I. Kašalynas, A. Urbanovič, P. Lamberti, M. Shundalau, Spectroscopic manifestation of a weak van der Waals interaction

between *trans*-stilbene and hexagonal boron nitride surface, Langmuir 41 (2025) 7364–7375. https://doi.org/10.1021/acs.langmuir.4c04717

7.5.2. Pranešimai konferencijose

1. Šioje disertacijoje pateikti rezultatai buvo pristatyti šiose konferencijose:

- **Žodiniai pranešimai:**

[C1] **I. Halimski**, S. Streckaitė, J. Chmeliov, A. Gelzinis, L. Valkunas. Fluoerescence concentration quenching in solutions of Zinc- and Free Base phthalocyanines. FizTeCh conference, October 2024, Vilnius, Lithuania.

[C2] **I. Halimski**, S. Streckaitė, R. Karpicz, J. Chmeliov, A. Gelzinis, D. Abramavicius, L. Valkunas. Concentration quenching of fluorescence in different molecular systems: similarities and differences. 68th International Open Readings conference for students of Physics and Natural Science, May 2025, Vilnius, Lithuania.

[C3] **I. Halimski**, M. Talaikis, A. Dementjev, R. Karpicz, J. Chmeliov, I. Kasalynas, P. Lamberti, M. Shundalau. Spectroscopic and theoretical insights into van der Waals interaction between organic compounds and hexagonal boron nitride. 19th Nanotechnology based innovation for the environment, energy and health, September 2025, Salerno, Italy.

[C4] **I. Halimski**, P. Rindzevičius, J. Fedotova, S. Streckaitė, M. Talaikis, A. Dementjev, A. Gelzinis, B. Robert, P. Lamberti, D. Abramavičius, L. Valkunas, M. Shundalau, R. Karpicz, J. Chmeliov. Is fluorescence decay kinetics an effective tool to analyze the origin of fluorescence quecnhing and the manifestation of van der Waals interaction? 46th Lithuanian National Physical Conference (LNFK), October 2025, Kaunas, Lithuania.

[C5] **I. Halimski**, A. Dementjev, J. Chmeliov, M. Mačernis, D. Abramavicius, L. Valkūnas, R. Karpicz. Optical properties of trans-stilbene in different phases: monomers, aggregates and crystallites. FizTeCh conference, October 2025, Vilnius, Lithuania.

[C6] **I. Halimski**, P. Rindzevičius, D. Pashnev, A. Dementjev, M. Talaikis, I. Kašalynas, P. Lamberti, D. Abramavicius, L. Valkunas, M. Macernis, M. Shundalau, R. Karpicz, J. Chmeliov. Optical properties of trans-stilbene under various conditions. 6th EuroCC Vilnius Workshop on using HPC, January 2026, Vilnius, Lithuania.

- **Stendiniai pranešimai:**

[C7] **I. Halimski**, S. Streckaitė, J. Chmeliov, A. Gelzinis. Fluoerescence concentration quenching in (Zinc)-Phthalocyanine solutions. FizTeCh conference, September 2023, Vilnius, Lithuania.

[C8] **I. Halimski**, G. Kareivaitė, R. Karpicz, A. Dementjev, M. Mačernis, D. Abramavičius, L. Valkunas. Trans-stilbene spectral properties

changes induced by aggregates formation in a polystyrene matrix. Lithuanian National Physical Conference (LNFK), October 2023, Vilnius, Lithuania.

[C9] **I. Halimski**, R. Karpicz, A. Dementjev, M. Jankunec, J. Chmeliov, M. Macernis, D. Abramavicius, L. Valkunas. Characterization of trans-stilbene nanocrystals in polystyrene films by CARS and AFM microscopy and optical spectroscopy. 67th International Open Readings conference for students of Physics and Natural Science, April 2024, Vilnius, Lithuania.

[C10] **I. Halimski**, R. Karpicz, A. Dementjev, M. Jankunec, J. Chmeliov, M. Macernis, D. Abramavicius, L. Valkunas. Trans-stilbene aggregates and crystallites in polystyrene films: microscopy and spectroscopy. 8th International Workshop on Advanced Spectroscopy and Optical Materials. July 2024, Gdansk, Poland.

[C11] **I. Halimski**, S. Streckaitė, J. Chmeliov, A. Gelzinis, L. Valkunas. Fluoerescence concentration quenching in Zinc-containing as well as non-containing phthalocyanines. 9th International Workshop Nanocarbon Photonics and Optoelectronics. August 2024, Kuopio, Finland.

[C12] **I. Halimski**, D. Pashnev, M. Talaikis, A. Dementjev, R. Karpicz, J. Chmeliov, I. Kašalynas, A. Urbanovič, Y. Padrez, M. Tutkus, P. Lamberti, M. Shundalau. Interaction of organic molecules and nanomaterials: Spectroscopic and theoretical insights into a weak-bound complex of hexagonal boron nitride and trans-stilbene. Advanced Properties and Processes in Optoelectronic Materials and Systems 'APROPOS 19', October 2024, Vilnius, Lithuania.

[C13] **I. Halimski**, S. Streckaitė, J. Chmeliov, A. Gelzinis, L. Valkunas. Fluorescence concentration quenching in solutions of Zinc-containing and non-containing phthalocyanines. Advanced Properties and Processes in Optoelectronic Materials and Systems 'APROPOS 19', October 2024, Vilnius, Lithuania.

[C14] **I. Halimski**, S. Streckaitė, M. Talaikis, A. Dementjev, A. Gelzinis, B. Robert, P. Lamberti, D. Abramavicius, L. Valkunas, R. Karpicz, M. Shundalau, J. Chmeliov. Probing spectroscopic manifestation of van der Waals interaction and fluorescence quenching with time-resolved fluorescence spectroscopy. Thematic School MECAREACT 2025: Vibrational and electronic spectroscopies applied to the study of reaction mechanisms, June 2025, Paris, France.

[C15] **I. Halimski**, R. Karpicz, A. Dementjev, M. Jankunec, J. Chmeliov, M. Macernis, D. Abramavicius, L. Valkunas. Spectroscopic characterization of different phases of trans-stilbene: monomers, aggregates, mono- and polycrystals. 19th Nanotechnology based innovation for the environment, energy and health, September 2025, Salerno, Italy.

- **Bendraautorių pranešimai konferencijose:**

[C16] **I. Halimski**, D. Pashnev, M. Talaikis, A. Dementjev, R. Karpicz, I. Kašalynas, A. Urbanovič, P. Lamberti, **M. Shundalau**. THz, Raman, and fluorescence characterization of a weak-bound complex of hBN and trans-stilbene. 9th International Workshop Nanocarbon Photonics and Optoelectronics. August 2024, Kuopio, Finland.

[C17] **I. Halimski**, D. Pashnev, M. Talaikis, A. Dementjev, R. Karpicz, J. Chmeliov, I. Kašalynas, A. Urbanovič, B. Robert, P. Lamberti, **M. Shundalau**. Spectroscopy of van der Waals interaction between organic molecules and hexagonal boron nitride. International Conference Celebrating the 220th Anniversary of the First Theory of Electrolysis by Theodor von Grotthuss, June 2025, Vilnius, Lithuania.

2. Konferencijų pranešimai, tiesiogiai nesusiję su disertacijos moksliniu pagrindu:

[C18] **I. Halimski**, V. Jašinskas, A. Aukauloo, R. Karpicz, J. Chmeliov. V. Gulbinas. Time-resolved spectroscopic characterization of the porphyrin-containing molecular dimers. 66th International Open Readings conference for students of Physics and Natural Science, April 2023, Vilnius, Lithuania.

[C19] **I. Halimski**, J. Fedotova, D. Pashnev, M. Talaikis, A. Dementjev, R. Karpicz, J. Chmeliov, I. Kašalynas, A. Urbanovič, B. Robert, P. Lamberti, M. Shundalau. Spectroscopic study of Tetraphenylporphyrin and 2D hexagonal boron nitride van der Waals complex. International Conference Celebrating the 220th Anniversary of the First Theory of Electrolysis by Theodor von Grotthuss, June 2025, Vilnius, Lithuania.

[C20] **J. Fedotova**, **I. Halimski**, M. Talaikis, R. Karpicz, J. Chmeliov, P. Lamberti, M. Shundalau. Spectroscopic study of free-base meso-tetraphenylporphyrin and hexagonal boron nitride van der Waals complex. 68th International Open Readings conference for students of Physics and Natural Science, May 2025, Vilnius, Lithuania.

[C21] **P. Rindzevičius**, **I. Halimski**. Spectroscopic insights into van der Waals interaction between resveratrol and hexagonal boron nitride. LMT 2025 student's summer practice conference, August 2025, Vilnius r, Lithuania.

[C22] A. Dementjev, **I. Halimski**, P. Rindzevičius, S. Malykhin, L. Valkunas, **R. Karpicz**. Application of CARS microscopy to chemical structural imaging of micro- and nanocrystals. 19th Nanotechnology based innovation for the environment, energy and health, September 2025, Salerno, Italy.

[C23] **P. Rindzevičius**, M. Talaikis, A. Dementjev, P. Lamberti, J. Chmeliov, M. Shundalau, **I. Halimski**, R. Karpicz. Spectroscopic investigation of van der Waals interaction between resveratrol and hexagonal boron nitride. 46th Lithuanian National Physical

Conference (LNFK), October 2025, Kaunas, Lithuania.

[C24] **J. Fedotova**, M. Talaikis, P. Lamberti, J. Chmeliov, M. Shundalau. R. Karpicz, **I. Halimski**. Investigation of spectroscopic properties of free-base tetraphenylporphyrin and hexagonal boron nitride van der Waals complex. FizTeCh conference, October 2025, Vilnius, Lithuania

7.6. Autoriaus indėlis

Disertacijos autorius paruošė visus mėginius visiems matavimams. Jis atliko visus stacionariosios sugerties matavimus, taip pat stacionariosios fluorescencijos, fluorescencijos sužadinimo ir fluorescencijos slopimo kinetikos matavimus. Jis apdorojo, analizavo ir interpretavo gautus duomenis, dalyvavo analizuojant papildomų eksperimentų rezultatus, prisidėjo prie visų straipsnių rengimo, įskaitant tiek pirminio rankraščio parengimą, tiek peržiūros ir redagavimo etapus, taip pat prie atsakymų į recenzentų pastabas rengimo.

Žemiau nurodomas šiame darbe panaudotas bendraautorių indėlis:

Paper A1: Darius Likandrovas ir dr. Andrius Gelzinis atliko kvantinės chemijos skaičiavimus, kurie pagrindžia disertacijos išvadas.

Paper A2: Dr. Marija Jankunec atliko AFM mikroskopijos tyrimus, o dr. Andrej Dementjev atliko CARS mikrospektroskopijos eksperimentus. Dr. Mindaugas Mačernis atliko kvantinius cheminius skaičiavimus. Stacionariosios fluorescencijos spektrų ir fluorescencijos slopimo kinetikų globalią analizę, taikant neneigiamos matricos faktorizacijos metodą, disertacijos autorius atliko kartu su savo moksliniu vadovu dr. Jevgenij Chmeliov. Visos minėtos įžvalgos buvo būtinos formuluojant šiuo straipsniu pagrįstas išvadas.

Paper A3: Dr. Martynas Talaikis atliko Ramano sklaidos matavimus. Dr. Daniil Pashnev kartu su dr. Maksim Shundalau, dr. Andžej Urbanovič ir dr. Irmantas Kašalynas atliko THz spektroskopijos matavimus. Be to, dr. Maksim Shundalau atliko kvantinius cheminius skaičiavimus. Visi šie rezultatai buvo panaudoti formuluojant disertacijos išvadas.

7.7. Pareiškimas apie dirbtinio intelekto naudojimą

Disertacijos autorius deklaruoja, kad rengiant šią disertaciją buvo naudojamas generatyvinis dirbtinis intelektas. *GPT-5.6 Sol* modelis (ChatGPT, OpenAI) buvo naudojamas anglų kalbos gramatikai taisyti ir teksto skaitomumui gerinti, taip pat padėti verčiant disertacijos santrauką į lietuvių kalbą. Moksliniam turiniui kurti dirbtinio intelekto priemonės nebuvo naudojamos. Visus mokslinius teiginius, interpretacijas ir išvadas suformulavo disertacijos autorius.

8. BIBLIOGRAPHY

[1] Robert E. Blankenship, Molecular Mechanisms of Photosynthesis, 4th ed., Wiley-VCH, 2026.

[2] S. Fukuzumi, Artificial Photosynthesis, Royal Society of Chemistry, 2025. https://doi.org/10.1039/9781837678853.

[3] R. Gutzler, M. Garg, C.R. Ast, K. Kuhnke, K. Kern, Light–matter interaction at atomic scales, Nat. Rev. Phys. 3 (2021) 441–453. https://doi.org/10.1038/s42254-021-00306-5.

[4] G.D. Scholes, G.R. Fleming, What is quantum biology?, Proc. Natl. Acad. Sci. U. S. A. 123 (2026) e2531134123. https://doi.org/10.1073/pnas.2531134123.

[5] T.W. Ebbesen, A. Rubio, G.D. Scholes, Introduction: Polaritonic Chemistry, Chem. Rev. 123 (2023) 12037–12038. https://doi.org/10.1021/acs.chemrev.3c00637.

[6] H. Altug, S. Oh, S.A. Maier, J. Homola, Advances and applications of nanophotonic biosensors, Nat. Nanotechnol. 17 (2022) pages5–16. https://doi.org/10.1038/s41565-021-01045-5.

[7] N.T. Shaked, S.A. Boppart, L. V Wang, J. Popp, Label-free biomedical optical imaging, Nat. Photonics 17 (2023) 1031–1041. https://doi.org/10.1038/s41566-023-01299-6.

[8] X. Li, J.F. Lovell, J. Yoon, X. Chen, Clinical development and potential of photothermal and photodynamic therapies for cancer, Nat. Rev. Clin. Oncol. 17 (2020) 657–674. https://doi.org/10.1038/s41571-020-0410-2.

[9] L. Valkunas, D. Abramavicius, T. Mančal, Molecular Excitation Dynamics and Relaxation, Wiley-VCH, Weinheim, 2013. https://doi.org/10.1002/9783527653652.

[10] V. V Korolkov, S.A. Svatek, A. Summerfield, J. Kerfoot, L. Yang, T. Taniguchi, K. Watanabe, N.R. Champness, N.A. Besley, P.H. Beton, van der Waals-Induced Chromatic Shifts in Hydrogen-Bonded Two-Dimensional Porphyrin Arrays on Boron Nitride, ACS Nano 9 (2015) 10347–10355. https://doi.org/10.1021/acsnano.5b04443.

[11] J. Mei, N.L.C. Leung, R.T.K. Kwok, J.W.Y. Lam, B.Z. Tang, Aggregation-Induced Emission: Together We Shine, United We Soar!, Chem. Rev. 115 (2015) 11718−11940. https://doi.org/10.1021/acs.chemrev.5b00263.

[12] S. Barysaitė, J. Chmeliov, L. Valkunas, A. Gelzinis, Concentration Quenching of Fluorescence Decay Kinetics of Molecular Systems, J. Phys. Chem. B 128 (2024) 4887−4897. https://doi.org/10.1021/acs.jpcb.3c08254.

[13] R. Karpicz, G. Kareivaite, M. Macernis, D. Abramavicius, L. Valkunas, Two phases of trans-stilbene in a polystyrene matrix, Phys. Chem. Chem. Phys. 25 (2023) 21183–21190. https://doi.org/10.1039/d3cp03015f.

[14] S. Rafique, H. Irshad, S. Majeed, Khadija, R. Rubab, M. Imran, A.M. Khan, S.A. Shahzad, AIEE active stilbene based fluorescent sensor with red-shifted emission for vapor phase detection of nitrobenzene and moisture sensing, J. Photochem. Photobiol. A Chem. 437 (2023) 114459. https://doi.org/10.1016/j.jphotochem.2022.114459.

[15] S.M. Menke, R.J. Holmes, Exciton diffusion in organic photovoltaic cells, Energy Environ. Sci. 7 (2014) 499–512. https://doi.org/10.1039/c3ee42444h.

[16] G.J. Hedley, A. Ruseckas, I.D.W. Samuel, Light Harvesting for Organic Photovoltaics, Chem. Rev. 117 (2017) 796–837. https://doi.org/10.1021/acs.chemrev.6b00215.

[17] D.H. Ahn, S.W. Kim, H. Lee, I.J. Ko, D. Karthik, J.Y. Lee, J.H. Kwon, Highly efficient blue thermally activated delayed fluorescence emitters based on symmetrical and rigid oxygen-bridged boron acceptors, Nat. Photonics 13 (2019) 540–546. https://doi.org/10.1038/s41566-019-0415-5.

[18] J. Tamošiūnaitė, S. Streckaitė, J. Chmeliov, L. Valkunas, A. Gelzinis, Concentration quenching of fluorescence in thin films of zinc-phthalocyanine, Chem. Phys. 572 (2023) 111949. https://doi.org/10.1016/j.chemphys.2023.111949.

[19] M. Aarabi, D. Aranda, S. Gholami, S.K. Meena, F. Lerouge, Y. Bretonniere, I. Gürol, P. Baldeck, S. Parola, F. Dumoulin, J. Cerezo, M. Garavelli, F. Santoro, I. Rivalta, Quantum-Classical Protocol for Efficient Characterization of Absorption Lineshape and Fluorescence Quenching upon Aggregation: The Case of Zinc Phthalocyanine Dyes, J. Chem. Theory Comput. 19 (2023) 5938–5957. https://doi.org/10.1021/acs.jctc.3c00446.

[20] S. Dhami, A.J.D. Mello, G. Rumbles, S.M. Bishop, D. Phillips, A. Beeby, Phthalocyanine Fluorescence At High Concentration: Dimers or Reabsorption Effect?, Photochem. Photobiol. 61 (1995) 341–346. https://doi.org/10.1111/j.1751-1097.1995.tb08619.x.

[21] A.C. Nellissen, E. Fron, J.B.F. Vandenwijngaerden, S. De Feyter, S.F.L. Mertens, M. Van der Auweraer, Spectroscopic Characterization of Thiacarbocyanine Dye Molecules Adsorbed on Hexagonal Boron Nitride: a Time-Resolved Study, ACS Omega 8 (2023) 35638–35652. https://doi.org/10.1021/acsomega.3c02020.

[22] A. Nellissen, Y. Xia, T. Hu, J.B.F. Vandenwijngaerden, E. Fron, S. De Feyter, K. Watanabe, T. Taniguchi, S.F.L. Mertens, M. Van Der Auweraer, Concentration dependence of the adsorption of metalfree tetra (4-carboxyphenyl) porphyrin (TCPP) on hexagonal boron nitride, Dye. Pigment. 237 (2025) 112695. https://doi.org/10.1016/j.dyepig.2025.112695.

[23] K. Sano, M. Oshima, Y. Hirade, T. Ishida, T. Shimada, S. Takagi, Dependence of the molecular adsorption orientation and photo-absorption behavior of porphyrins on the surface property of inorganic

nanosheets, Langmuir 41 (2025) 17584−17589. https://doi.org/10.1021/acs.langmuir.5c01177.
[24] V. Gulbinas, Šviesos sukelti molekuliniai vyksmai ir jų lazerinė spektroskopija, TEV, Vilnius, 2008.
[25] J.M. Hollas, Modern Spectroscopy, Wiley-VCH, 2013.
[26] B. Valeur, M.N. Berberan-Santos, Molecular Fluorescence: Principles and Applications, Wiley-VCH, 2012. https://doi.org/10.1002/9783527650002.
[27] S. Kakade, R. Ghosh, D.K. Palit, Excited state dynamics of zinc-phthalocyanine nanoaggregates in strong hydrogen bonding solvents, J. Phys. Chem. C 116 (2012) 15155–15166. https://doi.org/10.1021/jp304369r.
[28] Y. Dong, H. Cha, J. Zhang, E. Pastor, P.S. Tuladhar, I. McCulloch, J.R. Durrant, A.A. Bakulin, The binding energy and dynamics of charge-transfer states in organic photovoltaics with low driving force for charge separation, J. Chem. Phys. 150 (2019) 104704. https://doi.org/10.1063/1.5079285.
[29] P.P. Roy, S. Kundu, J. Valdiviezo, G. Bullard, J.T. Fletcher, R. Liu, S.-J. Yang, P. Zhang, D.N. Beratan, M.J. Therien, N. Makri, G.R. Fleming, Synthetic Control of Exciton Dynamics in Bioinspired Cofacial Porphyrin Dimers, J. Am. Chem. Soc. 144 (2022) 6298−6310. https://doi.org/10.1021/jacs.1c12889.
[30] P. Baltaševičiūtė, R. Gegevičius, V. Pakštas, A. Naujokaitis, V. Gulbinas, M. Franckevičius, Impact of Argon, Nitrogen, and Oxygen Exposure on the Structural and Optoelectrical Properties of Mixed Tin–Lead Halide Perovskites, ACS Omega 10 (2025) 25538−25545. https://doi.org/10.1021/acsomega.5c00956.
[31] M. Kasha, Characterization of electronic transitions in complex molecules, Discuss. Faraday Soc. 9 (1950) 14–19. https://doi.org/10.1039/DF9500900014.
[32] T. Itoh, Fluorescence and Phosphorescence from Higher Excited States of Organic Molecules, Chem. Rev. 112 (2012) 4541−4568. https://doi.org/10.1021/cr200166m.
[33] A.P. Demchenko, V.I. Tomin, P.-T. Chou, Breaking the Kasha Rule for More Efficient Photochemistry, Chem. Rev. 117 (2017) 13353–13381. https://doi.org/10.1021/acs.chemrev.7b00110.
[34] J.R. Lakowicz, Principles of fluorescence spectroscopy, 3rd ed., Springer, New York, 2006. https://doi.org/10.1007/978-0-387-46312-4.
[35] M. Taniguchi, J.S. Lindsey, D.F. Bocian, D. Holten, Comprehensive review of photophysical parameters (ε, Φf, τs) of tetraphenylporphyrin (H2TPP) and zinc tetraphenylporphyrin (ZnTPP) – Critical benchmark molecules in photochemistry and photosynthesis, J. Photochem. Photobiol. C Photochem. Rev. 46 (2021) 100401. https://doi.org/10.1016/j.jphotochemrev.2020.100401.

[36] R. Karpicz, N. Ostapenko, Y. Ostapenko, Y. Polupan, I. Lazarev, N. Galunov, M. Macernis, D. Abramavicius, L. Valkunas, Unusual temperature dependence of the fluorescence decay in heterostructured stilbene, Phys. Chem. Chem. Phys. 23 (2021) 3447–3454. https://doi.org/10.1039/d0cp05436d.

[37] P.P. Roy, S. Kundu, N. Makri, G.R. Fleming, Interference between Franck-Condon and Herzberg-Teller Terms in the Condensed-Phase Molecular Spectra of Metal-Based Tetrapyrrole Derivatives, J. Phys. Chem. Lett. 13 (2022) 7413–7419. https://doi.org/10.1021/acs.jpclett.2c01963.

[38] D. Wu, A.C. Sedgwick, T. Gunnlaugsson, E.U. Akkaya, J. Yoon, T.D. James, Fluorescent chemosensors: the past, present and future, Chem. Soc. Rev. 46 (2017) 7105--7123. https://doi.org/10.1039/c7cs00240h.

[39] T. Terai, T. Nagano, Fluorescent probes for bioimaging applications, Curr. Opin. Chem. Biol. 12 (2008) 515–521. https://doi.org/10.1016/j.cbpa.2008.08.007.

[40] J. Chan, S.C. Dodani, C.J. Chang, Reaction-based small-molecule fluorescent probes for chemoselective bioimaging, Nat. Chem. 4 (2012) 973–984. https://doi.org/10.1038/nchem.1500.

[41] L. Golubewa, Y. Padrez, M. Franckevičius, P. Zemaityte, S. Streckaitė, J. Chmeliov, L. Valkunas, B. Robert, C. Büchel, A. Gelzinis, Mapping the Energy Transfer Network in the Diatom Cyclotella meneghiniana by Picosecond Time-Resolved Fluorescence Spectroscopy down to Cryogenic Temperatures, J. Phys. Chem. Lett. 17 (2026) 10191–10198. https://doi.org/10.1021/acs.jpclett.6c02173.

[42] S. Tretiakov, A. Nigam, R. Pollice, Studying Noncovalent Interactions in Molecular Systems with Machine Learning, Chem. Rev. 125 (2025) 5776–5829. https://doi.org/10.1021/acs.chemrev.4c00893.

[43] J. Ángyán, J. Dobson, G. Jansen, T. Gould, London Dispersion Forces in Molecules, Solids and Nano-structures: An Introduction to Physical Models and Computational Methods, Royal Society of Chemistry, 2020. https://doi.org/10.1039/9781782623861.

[44] A.M. Reilly, A. Tkatchenko, van der Waals dispersion interactions in molecular materials: beyond pairwise additivity, Chem. Sci. 6 (2015) 3289–3301. https://doi.org/10.1039/c5sc00410a.

[45] S. Grimme, A. Hansen, J.G. Brandenburg, C. Bannwarth, Dispersion-Corrected Mean-Field Electronic Structure Methods, Chem. Rev. 116 (2016) 5105–5154. https://doi.org/10.1021/acs.chemrev.5b00533.

[46] G. Frenking, S. Shaik, The Chemical Bond: Chemical Bonding Across the Periodic Table, Wiley-VCH, Weinheim, 2014.

[47] L. Rummel, P.R. Schreiner, Advances and Prospects in Understanding London Dispersion Interactions in Molecular Chemistry, Angew. Chemie Int. Ed. 63 (2024) e202316364. https://doi.org/10.1002/anie.202316364.

[48] T. Förster, K. Kasper, Ein Konzentrationsumschlag der Fluoreszenz,

Z. Phys. Chem. (Muenchen, Ger.) 1 (1954) 275–277. https://doi.org/10.1524/zpch.1954.1.5_6.275.
[49] J. Luo, Z. Xie, J.W.Y. Lam, L. Cheng, H. Chen, C. Qui, H.S. Kwok, X. Zhan, Y. Liu, D. Zhu, B.Z. Tang, Aggregation-induced emission of 1-methyl-1,2,3,4,5-pentaphenylsilole, Chem. Commun. 37 (2001) 1740–1741. https://doi.org/10.1039/b105159h.
[50] M. Kasha, Relation between Exciton Bands and Conduction Bands in Molecular Lamellar Systems, Rev. Mod. Phys. 31 (1959) 162–169. https://doi.org/10.1103/RevModPhys.31.162.
[51] M. Kasha, Energy Transfer Mechanisms and the Molecular Exciton Model for Molecular Aggregates, Radiat. Res. 20 (1963) 55–70. https://doi.org/10.2307/3571331.
[52] M. Kasha, H.R. Rawls, M.A. El-Bayoumi, The exciton model in molecular spectroscopy, Pure Appl. Chem. 11 (1965) 371–392. https://doi.org/10.1351/pac196511030371.
[53] N.J. Hestand, F.C. Spano, Expanded Theory of H- and J-Molecular Aggregates: The Effects of Vibronic Coupling and Intermolecular Charge Transfer, Chem. Rev. 118 (2018) 7069–7163. https://doi.org/10.1021/acs.chemrev.7b00581.
[54] Electronic Energy Migration, in: IUPAC Compend. Chem. Terminol., 2025. https://doi.org/10.1351/goldbook.E01997.
[55] S. Saini, G. Srinivas, B. Bagchi, Distance and Orientation Dependence of Excitation Energy Transfer: From Molecular Systems to Metal Nanoparticles, J. Phys. Chem. B 113 (2009) 1817–1832. https://doi.org/10.1021/jp806536w.
[56] O. Kühn, V. May, Charge and Energy Transfer Dynamics in Molecular Systems, Wiley-VCH, 2023. https://doi.org/10.1002/9783527696277.
[57] Radiative Energy Transfer, in: IUPAC Compend. Chem. Terminol., 2025. https://doi.org/10.1351/goldbook.R05063.
[58] Y. Ishida, T. Shimada, D. Masui, H. Tachibana, H. Inoue, S. Takagi, Efficient Excited Energy Transfer Reaction in Clay/Porphyrin Complex toward an Artificial Light-Harvesting System, J. Am. Chem. Soc. 133 (2011) 14280–14286. https://doi.org/10.1021/ja204425u.
[59] M. Maiuri, J.J. Snellenburg, I.H.M. Van Stokkum, S. Pillai, K. WongCarter, D. Gust, T.A. Moore, A.L. Moore, R. Van Grondelle, G. Cerullo, D. Polli, Ultrafast energy transfer and excitonic coupling in an artificial photosynthetic antenna, J. Phys. Chem. B 117 (2013) 14183–14190. https://doi.org/10.1021/jp401073w.
[60] M.R. Melechalil, T. Sawasaki, T. Shimada, T. Ishida, S. Takagi, Design of Efficient Artificial Light-Harvesting Systems Using Cationic Porphyrin−Titania Nanosheet Assemblies: Insights into Excitation Energy Transfer and Deactivation Pathways, J. Phys. Chem. C 129 (2025) 11487−11496. https://doi.org/10.1021/acs.jpcc.5c02536.
[61] R. Dutta, D.G.A. Cabral, N. Lyu, N.P. Vu, Y. Wang, B. Allen, X. Dan, R.G. Cortinas, P. Khazaei, M. Schafer, A.C.C. Albornoz, S.E. Smart,

S. Nie, M.H. Devoret, D.A. Mazziotti, P. Narang, C. Wang, J.D. Whitfield, A.K. Wilson, H.P. Hendrickson, D.A. Lidar, P.-B. Francisco, L.F. Santos, S. Kais, E. Geva, V.S. Batista, Simulating Chemistry on Bosonic Quantum Devices, J. Chem. Theory Comput. 20 (2024) 6426–6441. https://doi.org/10.1021/acs.jctc.4c00544.

[62] L.J.S. Allen, An Introduction to Stochastic Processes with Applications to Biology, 2nd ed., CRC Press, 2010.

[63] J.D. Schultz, J.L. Yuly, E.A. Arsenault, K. Parker, S.N. Chowdhury, R. Dani, S. Kundu, H. Nuomin, Z. Zhang, J. Valdiviezo, P. Zhang, K. Orcutt, S.J. Jang, G.R. Fleming, N. Makri, J.P. Ogilvie, M.J. Therien, M.R. Wasielewski, D.N. Beratan, Coherence in Chemistry: Foundations and Frontiers, Chem. Rev. 124 (2024) 11641−11766. https://doi.org/10.1021/acs.chemrev.3c00643.

[64] Dexter Excitation Transfer, in: IUPAC Compend. Chem. Terminol., 2025. https://doi.org/10.1351/goldbook.D01654.

[65] T. Förster, Zwischenmolekulare Energiewanderung und Fluoreszenz, Ann. Phys. 437 (1948) 55–75. https://doi.org/10.1002/andp.19484370105.

[66] F. Eckart, H. Löhmannsröben, N. Hildebrandt, Theodor Förster: Life and FRET from 1933 to 1951. A Viewpoint from the Archives, Angew. Chemie Int. Ed. 64 (2025) e202416843. https://doi.org/10.1002/anie.202416843.

[67] Förster excitation transfer, in: IUPAC Compend. Chem. Terminol., 2025. https://doi.org/10.1351/goldbook.F02488.

[68] W.-J. Shi, J. Barber, Y. Zhao, Role of formation of statistical aggregates in chlorophyll fluorescence concentration quenching, J. Phys. Chem. B 117 (2013) 3976–3982. https://doi.org/10.1021/jp311821t.

[69] S. Bourne-Worster, O. Feighan, F.R. Manby, Charge transfer as a mechanism for chlorophyll fluorescence concentration quenching, Proc. Natl. Acad. Sci. U. S. A. 120 (2023) No. e2210811120. https://doi.org/10.1073/pnas.2210811120.

[70] M. Hauser, U.K.A. Klein, U. Gösele, Extension of Förster's Theory of Long-Range Energy Transfer to Donor-Acceptor Pairs in Systems of Molecular Dimensions, Zeitschrift Für Phys. Chemie Neue Folge 101 (1976) 255–266. https://doi.org/10.1524/zpch.1976.101.1-6.255.

[71] A.I. Burshteĭn, Concentration quenching of noncoherent excitation in solutions, Sov. Phys. Uspekhi 27 (1984) 579–606. https://doi.org/10.1070/PU1984v027n08ABEH004062.

[72] L.M. Herz, C. Silva, A.C. Grimsdale, K. Müllen, R.T. Phillips, Time-dependent energy transfer rates in a conjugated polymer guest-host system, Phys. Rev. B 70 (2004) 165207. https://doi.org/10.1103/PhysRevB.70.165207.

[73] A.J. Ward, A. Ruseckas, I.D.W. Samuel, A Shift from Diffusion Assisted to Energy Transfer Controlled Fluorescence Quenching in

Polymer−Fullerene Photovoltaic Blends, J. Phys. Chem. C 116 (2012) 23931–23937. https://doi.org/10.1021/jp307538y.
[74] F. Montilla, A. Ruseckas, I.D.W. Samuel, Exciton−Polaron Interactions in Polyfluorene Films with β-Phase, J. Phys. Chem. C 122 (2018) 9766–9772. https://doi.org/10.1021/acs.jpcc.8b01300.
[75] W.F. Watson, R. Livingston, Self-quenching and sensitization of fluorescence of chlorophyll solutions, J. Chem. Phys. 18 (1950) 802–809. https://doi.org/10.1063/1.1747779.
[76] G.S. Beddard, G. Porter, Concentration quenching in chlorophyll, Nature 260 (1976) 366–367. https://doi.org/10.1038/260366a0.
[77] B. Zhang, H. Soleimaninejad, D.J. Jones, J.M. White, K.P. Ghiggino, T.A. Smith, W.W.H. Wong, Highly fluorescent molecularly insulated perylene diimides: Effect of concentration on photophysical properties, Chem. Mater. 29 (2017) 8395–8403. https://doi.org/10.1021/acs.chemmater.7b02968.
[78] H. Yue, Y. Tian, S. Huang, H. Su, H. Shao, Q. Zhang, R. Guo, L. Wang, Enhancing the stereo structure via bulky peripheral groups to improve resistance to concentration quenching in OLEDs, J. Mater. Chem. C 13 (2025) 4069–4077. https://doi.org/10.1039/d4tc04656k.
[79] S. Nakamoto, Y. Ishida, Y. Ohtani, T. Shimada, S. Takagi, Long-Range Excitation Energy Migration in a Cationic BODIPY/Clay Nanosheet Light-Harvesting Antenna, Artif. Photosynth. (2026). https://doi.org/10.1021/aps.6c00022.
[80] V. Šlachtová, D. Bím, K. Németh, E. Barańska, S. Bellová, M. Dračínský, R. Dzijak, P. Kele, T. Slanina, M. Vrabel, Fluorescence Quenching Properties and Bioimaging Applications of Readily Accessible Blue to Far-Red Fluorogenic Triazinium Salts, J. Am. Chem. Soc. 148 (2026) 1183–1196. https://doi.org/10.1021/jacs.5c17428.
[81] X. Hu, J. Zhang, Z. Yu, Y. Xie, H. He, J. Qi, X. Dong, Y. Lu, W. Zhao, W. Wu, Environment-responsive aza-BODIPY dyes quenching in water as potential probes to visualize the in vivo fate of lipid-based nanocarriers, Nanomedicine Nanotechnology, Biol. Med. 11 (2015) 1939–1948. https://doi.org/10.1016/j.nano.2015.06.013.
[82] S. Sommer, T. Raidt, B.M. Fischer, F. Katzenberg, J.C. Tiller, M. Koch, THz-Spectroscopy on High Density Polyethylene with Different Crystallinity, J. Infrared, Millimeter, Terahertz Waves 37 (2016) 189–197. https://doi.org/10.1007/s10762-015-0219-8.
[83] N. Kobayashi, H. Ogata, N. Nonaka, E.A. Luk'yanets, Effect of Peripheral Substitution on the Electronic Absorption and Fluorescence Spectra of Metal-Free and Zinc Phthalocyanines, Chem. A-European J. 9 (2003) 5123–5134. https://doi.org/10.1002/chem.200304834.
[84] The pandas development team., Pandas, (2026). https://doi.org/10.5281/zenodo.20127038.
[85] C.R. Harris, K.J. Millman, S.J. van der Walt, R. Gommers, P. Virtanen,

D. Cournapeau, E. Wieser, J. Taylor, S. Berg, N.J. Smith, R. Kern, M. Picus, S. Hoyer, M.H. Van Kerkwijk, M. Brett, A. Haldane, J. Fernández del Río, M. Wiebe, P. Peterson, P. Gérard-Marchant, K. Sheppard, T. Reddy, W. Weckesser, H. Abbasi, C. Gohlke, T.E. Oliphant, Array programming with NumPy, Nature 585 (2020) 357–362. https://doi.org/10.1038/s41586-020-2649-2.

[86] P. Virtanen, R. Gommers, T.E. Oliphant, M. Haberland, T. Reddy, D. Cournapeau, E. Burovski, P. Peterson, W. Weckesser, J. Bright, S.J. van der Walt, M. Brett, J. Wilson, K.J. Millman, N. Mayorov, A. Nelson, E. Jones, R. Kern, E. Larson, C.J. Carey, İ. Polat, Y. Feng, E.W. Moore, J. VanderPlas, D. Laxalde, J. Perktold, R. Cimrman, I. Henriksen, E.A. Quintero, C.R. Harris, A.M. Archibald, A.H. Ribeiro, F. Pedregosa, P. van Mulbregt, Et.al., SciPy 1.0: fundamental algorithms for scientific computing in Python, Nat. Methods 17 (2020) 261–272. https://doi.org/10.1038/s41592-019-0686-2.

[87] M. Newville, R. Otten, A. Nelson, T. Stensitzki, A. Ingargiola, D. Allan, A. Fox, F. Carter, M. Rawlik, LMFIT: Non-Linear Least-Squares Minimization and Curve-Fitting for Python, (2025). https://doi.org/10.5281/zenodo.16175987.

[88] K.V. Price, R.M. Storn, J. Lampinen, Differential Evolution. A Practical Approach to Global Optimization, Springer, 2005. https://doi.org/10.1007/3-540-31306-0.

[89] I.H.M. Van Stokkum, D.S. Larsen, R. van Grondelle, Global and target analysis of time-resolved spectra, Biochim. Biophys. Acta 1657 (2004) 82–104. https://doi.org/10.1016/j.bbabio.2004.04.011.

[90] W.H. Lawton, E.A. Sylvestre, Self Modeling Curve Resolution, Technometrics 13 (1971) 617–633. https://doi.org/10.2307/1267173.

[91] D.D. Lee, H.S. Seung, Learning the parts of objects by non-negative matrix factorization, Nature 401 (1999) 788–791. https://doi.org/10.1038/44565.

[92] Y. Braver, A. Gelzinis, J. Chmeliov, L. Valkunas, Application of decay- and evolution-associated spectra for molecular systems with spectral shifts or inherent inhomogeneities, Chem. Phys. 525 (2019) 110403. https://doi.org/10.1016/j.chemphys.2019.110403.

[93] V. Mascoli, A. Gelzinis, J. Chmeliov, L. Valkunas, R. Croce, Light-harvesting complexes access analogue emissive states in different environments, Chem. Sci. 11 (2020) 5697–5709. https://doi.org/10.1039/d0sc00781a.

[94] J. Chmeliov, A. Gelzinis, E. Songaila, R. Augulis, C.D.P. Duffy, A. V Ruban, L. Valkunas, The nature of self-regulation in photosynthetic light-harvesting antenna, Nat. Plants (2016) 16045. https://doi.org/10.1038/nplants.2016.45.

[95] A. Gelzinis, J. Chmeliov, M. Tutkus, E. Vitulskienė, M. Franckevičius, C. Büchel, B. Robert, L. Valkunas, Fluorescence quenching in aggregates of fucoxanthin–chlorophyll protein complexes: Interplay of

fluorescing and dark states, Biochim. Biophys. Acta - Bioenerg. 1865 (2024) 149030. https://doi.org/10.1016/j.bbabio.2023.149030.
[96] M.W. Berry, M. Browne, A.N. Langville, V.P. Pauca, R.J. Plemmons, Algorithms and applications for approximate nonnegative matrix factorization, Comput. Stat. Data Anal. 52 (2007) 155–173. https://doi.org/10.1016/j.csda.2006.11.006.
[97] A. Dementjev, G. Mordas, V. Ulevičius, V. Gulbinas, Investigation of microstructured chitosans by coherent anti-Stokes Raman microscopy, J. Microsc. 257 (2015) 217–225. https://doi.org/10.1111/jmi.12204.
[98] R. Berera, C. Herrero, I.H.M. Van Stokkum, M. Vengris, G. Kodis, R.E. Palacios, H. Van Amerongen, R. Van Grondelle, D. Gust, T.A. Moore, A.L. Moore, J.T.M. Kennis, A simple artificial light-harvesting dyad as a model for excess energy dissipation in oxygenic photosynthesis, Proc. Natl. Acad. Sci. U. S. A. 103 (2006) 5343–5348. https://doi.org/10.1073/pnas.0508530103.
[99] M. Kloz, S. Pillai, G. Kodis, D. Gust, T.A. Moore, A.L. Moore, R. Van Grondelle, J.T.M. Kennis, Carotenoid photoprotection in artificial photosynthetic antennas, J. Am. Chem. Soc. 133 (2011) 7007–7015. https://doi.org/10.1021/ja1103553.
[100] M.E. El-Khouly, Energy transfer between two light harvesting phthalocyanine derivatives as model for artificial photosynthetic antenna: Laser photolysis studies, Spectrochim. Acta - Part A Mol. Biomol. Spectrosc. 205 (2018) 508–513. https://doi.org/10.1016/j.saa.2018.07.064.
[101] B.P. Rand, D. Cheyns, K. Vasseur, N.C. Giebink, S. Mothy, Y. Yi, V. Coropceanu, D. Beljonne, J. Cornil, J.L. Brédas, J. Genoe, The impact of molecular orientation on the photovoltaic properties of a phthalocyanine/fullerene heterojunction, Adv. Funct. Mater. 22 (2012) 2987–2995. https://doi.org/10.1002/adfm.201200512.
[102] M. Alkhamisi, V. V. Korolkov, A.S. Nizovtsev, J. Kerfoot, T. Taniguchi, K. Watanabe, N.A. Besley, E. Besley, P.H. Beton, The growth and fluorescence of phthalocyanine monolayers, thin films and multilayers on hexagonal boron nitride, Chem. Commun. 54 (2018) 12021–12024. https://doi.org/10.1039/c8cc06304d.
[103] T. James, J. Bradford, J. Kerfoot, V. V Korolkov, M. Alkhamisi, T. Taniguchi, K. Watanabe, A.S. Nizovtsev, E. Antolín, E. Besley, S.A. Svatek, P.H. Beton, Electroluminescence from a phthalocyanine monolayer encapsulated in a van der Waals tunnel diode, Mol. Phys. 121 (2023) e2197081. https://doi.org/10.1080/00268976.2023.2197081.
[104] L. Liu, T. Dienel, C.A. Pignedoli, R. Widmer, X. Song, Y. Wang, O. Gröning, Two-Level Electronic Switching in Individual Manganese-Phthalocyanine Molecules with Jahn-Teller Distortion, ACS Nano 18 (2024) 31967–31973. https://doi.org/10.1021/acsnano.4c09815.
[105] M.S. Ebied, S. Elnobi, A.A. Abuelwafa, Structural and optical

properties of spin coated ZnTTBPc thin films for optoelectronics via DFT and experiments, Sci. Rep. 15 (2025) No. 36301. https://doi.org/10.1038/s41598-025-21726-8.
[106] T. Fujimura, K. Okada, M. Nishiguchi, Y. Araki, T. Ikeue, R. Sasai, Effect of excited state self-quenching on singlet oxygen photogeneration using nanosheet surface assembled zinc phthalocyanine, Phys. Chem. Chem. Phys. 27 (2025) 4328–4334. https://doi.org/10.1039/d4cp04126g.
[107] X. Li, B.-D. Zheng, X.-H. Peng, S.-Z. Li, J.-W. Ying, Y. Zhao, Phthalocyanines as medicinal photosensitizers : Developments in the last five years, Coord. Chem. Rev. 379 (2019) 147–160. https://doi.org/10.1016/j.ccr.2017.08.003.
[108] L. Naimovičius, M. Miroshnichenko, E. Opar, H. Hölzel, M. Morikawa, N. Kimizuka, M. Dapkevičius, J. Lekavičius, E. Radiunas, K. Kazlauskas, V. Cilleros-Mañé, F. Riefolo, C. Matera, K. Harmandar, M. Taniguchi, F. Dumoulin, J.S. Lindsey, P. Bharmoria, P. Gorostiza, K. Moth-Poulsen, Noninvasive cardiac modulation via triplet-sensitized photoswitching in the phototherapeutic window, Nat. Commun. 16 (2025) 6377. https://doi.org/10.1038/s41467-025-61301-3.
[109] A.G. Martynov, J. Mack, A.K. May, T. Nyokong, Y.G. Gorbunova, A.Y. Tsivadze, Methodological Survey of Simplified TD-DFT Methods for Fast and Accurate Interpretation of UV-Vis-NIR Spectra of Phthalocyanines, ACS Omega 4 (2019) 7265–7284. https://doi.org/10.1021/acsomega.8b03500.
[110] V. Gulbinas, M. Chachisvilis, L. Valkunas, V. Sundstrom, Excited state dynamics of phthalocyanine films, J. Phys. Chem. 100 (1996) 2213–2219. https://doi.org/10.1021/jp951910j.
[111] L. Schraut-May, S. Hammer, L.N. Philipp, K. Radacki, G. Tauscher, H. Hollstein, K. Strauß, M. Kamp, H. Schwoerer, H. Braunschweig, R. Mitric, J. Pflaum, Competing excitonic couplings as origin of mimicked phase transitions in zinc-phthalocyanine single crystals, 2025. https://doi.org/10.48550/arXiv.2512.02639.
[112] E.R. Windle, D.G. MacKay, D. Graczyk, C.C. Rennie, P. Malakar, S.J. Quinn, R.M. Edkins, Femto- to Microsecond excited-state dynamics of aggregated and monomeric regiopure zinc and copper phthalocyanines, Phys. Chem. Chem. Phys. (2026). https://doi.org/10.1039/d6cp02573k.
[113] C.G. Claessens, U. Hahn, T. Torres, Phthalocyanines: From outstanding electronic properties to emerging applications, Chem. Rec. 8 (2008) 75–97. https://doi.org/10.1002/tcr.20139.
[114] V.J. Balevičius, A. Gelzinis, D. Abramavicius, L. Valkunas, Excitation Energy Transfer and Quenching in a Heterodimer: Applications to the Carotenoid − Phthalocyanine Dyads, J. Phys. Chem. B 117 (2013) 11031−11041. https://doi.org/10.1021/jp3118083.

[115] A.Y. Tolbin, B.N. Tarasevich, M.K. Beklemishev, V.K. Brel, V.E. Pushkarev, Clamshell-type Bis-phthalocyanine with Tetrachlorocyclotriphosphazene Intramolecular Bridge: Synthesis and Structural Evaluation by DFT, NMR and Optical Spectroscopy, Chem. Sel. 7 (2022) e202201065. https://doi.org/10.1002/slct.202201065.
[116] J.B. Birks, D.J. Dyson, I.H. Munro, "Excimer" Fluorescence . II . Lifetime Studies of Pyrene Solutions, Proc. R. Soc. A 275 (1963) 575–588. https://doi.org/10.1098/rspa.1963.0187.
[117] U. Gösele, M. Hauser, U.K.. Klein, R. Frey, Diffusion and long-range energy transfer, Chem. Phys. Lett. 34 (1975) 519–522.
[118] D.H. Waldeck, Photoisomerization dynamics of stilbenes in polar solvents, J. Mol. Liq. 57 (1993) 127–148. https://doi.org/10.1016/0167-7322(93)80051-V.
[119] G. Likhtenshtein, Stilbenes: Applications in Chemistry, Life Sciences and Materials Science, Wiley-VCH, 2009.
[120] T. Teka, L. Zhang, X. Ge, Y. Li, L. Han, X. Yan, Stilbenes: Source plants, chemistry, biosynthesis, pharmacology, application and problems related to their clinical Application-A comprehensive review, Phytochemistry 197 (2022) 113128. https://doi.org/10.1016/j.phytochem.2022.113128.
[121] C. Wang, M.D.J. Waters, P. Zhang, J. Suchan, V. Svoboda, T.T. Luu, C. Perry, Z. Yin, P. Slavíček, H.J. Wörner, Different timescales during ultrafast stilbene isomerization in the gas and liquid phases revealed using time-resolved photoelectron spectroscopy, Nat. Chem. 14 (2022). https://doi.org/10.1038/s41557-022-01012-0.
[122] M.R. Ams, D. Ajami, S.L. Craig, J.-S. Yang, J.J. Rebek, Control of stilbene conformation and fluorescence in self-assembled capsules, Beilstein J. Org. Chem. 5 (2009) 79. https://doi.org/10.3762/bjoc.5.79.
[123] G.F. Knoll, Radiation Detection and Measurement (4th Edition), 2010.
[124] N. Zaitseva, L. Carman, A. Glenn, J. Newby, M. Faust, S. Hamel, N. Cherepy, S. Payne, Application of solution techniques for rapid growth of organic crystals, J. Cryst. Growth 314 (2011) 163–170. https://doi.org/10.1016/j.jcrysgro.2010.10.139.
[125] S.K. Lee, Y.H. Cho, B.H. Kang, W.G. Lee, J.K. Kim, G.D. Kim, N.Z. Galunov, Y.K. Kim, Scintillation Properties of Composite Stilbene Crystal for Neutron Detection, Prog. Nucl. Sci. Technol. 1 (2011) 292–295. https://doi.org/10.15669/pnst.1.292.
[126] L. Carman, N. Zaitseva, H.P. Martinez, B. Rupert, I. Pawelczak, A. Glenn, H. Mulcahy, R. Leif, K. Lewis, S. Payne, The effect of material purity on the optical and scintillation properties of solution-grown trans-stilbene crystals, J. Cryst. Growth 368 (2013) 56–61. https://doi.org/10.1016/j.jcrysgro.2013.01.019.
[127] H. Klapper, N. Zaitseva, L. Carman, X-ray topographic study of growth defects of trans-stilbene crystals grown from solutions, J. Cryst. Growth 429 (2015) 74–81.

https://doi.org/10.1016/j.jcrysgro.2015.07.012.
[128] J.F. Arenas, I.L. Tocon, J.C. Otero, J.I. Marcos, A Priori Scaled Quantum Mechanical Vibrational Spectra of trans- and & -Stilbene, J. Phys. Chem. 99 (1995) 11392–11398. https://doi.org/10.1021/j100029a015.
[129] G. Baranovic, Z. Meic, A.H. Maulitz, Vibrational analysis of stilbene and its isotopomers on the ground state potential energy surface, Spectrochim. Acta Part A Mol. Biomol. Spectrosc. 54 (1998) 1017–1039. https://doi.org/10.1016/S1386-1425(98)00010-9.
[130] M. Agati, S. Fanetti, R. Bini, Pressure induced modification of the electronic properties of stilbene by two-photon spectroscopy, J. Chem. Phys. 158 (2023) 034505. https://doi.org/10.1063/5.0133610.
[131] R. Dobužinskas, R. Maldžius, M. Solovjovaitė, M. Viliūnas, A. Poškus, S. Urnikaitė, M. Grigalavičius, Structural and dielectric properties of trans-stilbene–TPD-type molecular composites, Lith. J. Phys. 66 (2026) 125–135. https://doi.org/10.3952/physics.2026.66.2.7.
[132] B.C. Chen, S.H. Lim, Three-dimensional imaging of director field orientations in liquid crystals by polarized four-wave mixing microscopy, Appl. Phys. Lett. 94 (2009). https://doi.org/10.1063/1.3127535.
[133] S. Grimme, S. Ehrlich, L. Goerigk, Effect of the Damping Function in Dispersion Corrected Density Functional Theory, J. Comput. Chem. 32 (2011) 1456–1465. https://doi.org/10.1002/jcc.21759.
[134] Y. Lin, J.W. Connell, Advances in 2D boron nitride nanostructures: nanosheets, nanoribbons, nanomeshes, and hybrids with graphene, Nanoscale 4 (2012) 6908–6939. https://doi.org/10.1039/c2nr32201c.
[135] L.H. Li, Y. Chen, Atomically Thin Boron Nitride: Unique Properties and Applications, Adv. Funct. Mater. 26 (2016) 2594–2608. https://doi.org/10.1002/adfm.201504606.
[136] L. Stagi, J. Ren, P. Innocenzi, From 2-D to 0-D Boron Nitride Materials, The Next Challenge, Materials (Basel). 12 (2019) 3905. https://doi.org/10.3390/ma12233905.
[137] J.D. Caldwell, I. Aharonovich, G. Cassabois, J.H. Edgar, B. Gil, D.N. Basov, Photonics with hexagonal boron nitride, Nat. Rev. Mater. 4 (2019) 552–567. https://doi.org/10.1038/s41578-019-0124-1.
[138] L. Lin, Y. Xu, S. Zhang, I.M. Ross, A.C.M. Ong, D.A. Allwood, Fabrication and Luminescence of Monolayered Boron Nitride Quantum Dots, Small 10 (2014) 60–65. https://doi.org/10.1002/smll.201301001.
[139] Y. Ding, P. He, S. Li, B. Chang, S. Zhang, Z. Wang, J. Chen, J. Yu, S. Wu, H. Zeng, L. Tao, Efficient Full-Color Boron Nitride Quantum Dots for Thermostable Flexible Displays, ACS Nano 15 (2021) 14610–14617. https://doi.org/10.1021/acsnano.1c04321.
[140] X. Zhang, L. An, C. Bai, L. Chen, Y. Yu, Hexagonal boron nitride

quantum dots : Properties , preparation and applications, Mater. Today Chem. 20 (2021) 100425. https://doi.org/10.1016/j.mtchem.2021.100425.
[141] V. Kumar, N. Kumar, P. Roy, D. Lahiri, I. Lahiri, Emergence of fluorescence in boron nitride nanoflakes and its application in bioimaging, RSC Adv. 6 (2016) 48025–48032. https://doi.org/10.1039/c6ra05288f.
[142] A. Kavčič, R. Podlipec, A. Krišelj, A. Jelen, D. Vella, M. Humar, Intracellular biocompatible hexagonal boron nitride quantum emitters as single-photon sources and barcodes, Nanoscale 16 (2024) 4691–4702. https://doi.org/10.1039/d3nr05305a.
[143] Q. Weng, B. Wang, X. Wang, N. Hanagata, X. Li, D. Liu, X. Wang, X. Jiang, Y. Bando, D. Golberg, Highly Water-Soluble, Porous, and Biocompatible Boron Nitrides for Anticancer Drug Delivery, ACS Nano 8 (2014) 6123–6130. https://doi.org/10.1021/nn5014808.
[144] O. Gnatyuk, G. Dovbeshko, A. Dementjev, K. Chernyakova, O. Posudievsky, I. Kupchak, D. Kolesnyk, G. Solyanik, R. Karpicz, Spectroscopic and microscopic evidence of 2D boron nitride nanoflake interaction with doxorubicin, Opt. Mater. X 22 (2024) 100323. https://doi.org/10.1016/j.omx.2024.100323.
[145] W. Zhao, J. Xiao, Z. Ma, L. Ma, G. Tian, Adsorption of magnesium porphyrin on Au (111)-supported graphene and hexagonal boron nitride monolayers : A first-principles study, Phys. Rev. B 110 (2024) 205410. https://doi.org/10.1103/PhysRevB.110.205410.
[146] J. Zhang, Y. Jing, M. Wan, J. Xue, J. Liu, J. Li, Y. Du, Investigation into polymorphism within ethenzamide-ethylmalonic acid cocrystal using Raman and terahertz vibrational spectroscopy, Spectrochim. Acta Part A Mol. Biomol. Spectrosc. 305 (2024) 123478. https://doi.org/10.1016/j.saa.2023.123478.
[147] M. Ge, Y. Wang, F. Zhang, Z. Wang, H. Li, D. Xu, J. Yao, Study of low-frequency spectroscopic characteristics of γ -aminobutyric acid with THz and low-wavenumber Raman spectroscopy, Spectrochim. Acta Part A Mol. Biomol. Spectrosc. 305 (2024) 123550. https://doi.org/10.1016/j.saa.2023.123550.
[148] Y. Duan, Q. Liu, M. Wang, Y. Zhu, Q. Zhang, X. Duan, H. Deng, L. Shang, Insights into temperature-induced phase transition mechanism of CL-20 using terahertz spectroscopy, Spectrochim. Acta Part A Mol. Biomol. Spectrosc. 307 (2024) 123640. https://doi.org/10.1016/j.saa.2023.123640.
[149] T. Chen, X. Liao, L. Gao, Hydrogen bonding and Hirshfeld surface analysis of gallic acid and its monohydrate based on terahertz spectroscopy, Chem. Phys. 578 (2024) 112159. https://doi.org/10.1016/j.chemphys.2023.112159.
[150] A.J. Gatesman, R.H. Giles, J. Waldman, Submillimeter optical properties of hexagonal boron nitride, J. Appl. Phys. 73 (1993) 3962–

3966. https://doi.org/10.1063/1.352860.
[151] T. Sainsbury, A. Satti, P. May, Z. Wang, I. Mcgovern, Y.K. Gun'ko, J. Coleman, Oxygen Radical Functionalization of Boron Nitride Nanosheets, J. Am. Chem. Soc. 134 (2012) 18758–18771. https://doi.org/10.1021/ja3080665.
[152] S. Angizi, F. Shayeganfar, M.H. Azar, A. Simchi, Surface/edge functionalized boron nitride quantum dots : Spectroscopic fingerprint of bandgap modification by chemical functionalization, Ceram. Int. 46 (2020) 978–985. https://doi.org/10.1016/j.ceramint.2019.09.061.
[153] L. Museur, E. Feldbach, A. Kanaev, Defect-related photoluminescence of hexagonal boron nitride, Phys. Rev. B 78 (2008) 155204. https://doi.org/10.1103/PhysRevB.78.155204.
[154] P. Innocenzi, L. Stagi, From Defects to Photoluminescence in h-BN 2D and 0D Nanostructures, Accounts Mater. Res. 5 (2024) 413–425. https://doi.org/10.1021/accountsmr.3c00242.
[155] B. De Filippis, A. Ammazzalorso, M. Fantacuzzi, L. Giampietro, C. Maccallini, R. Amoroso, Anticancer Activity of Stilbene-Based Derivatives, ChemMedChem 12 (2017) 558–570. https://doi.org/10.1002/cmdc.201700045.
[156] G.D. Scholes, G.R. Fleming, A. Olaya-Castro, R. Van Grondelle, Lessons from nature about solar light harvesting, Nat. Chem. 3 (2011) 763–774. https://doi.org/10.1038/nchem.1145.

About Author (In English)

Ivan Halimski was born in Minsk, Belarus. In 2017, he graduated from Gymnasium No. 30 (Minsk) and enrolled at the Faculty of Physics of Belarusian State University. During his studies, he carried out his final thesis research at the Department of Energy Physics. In 2022, he completed the Specialist degree programme in Physics and obtained the qualification of the Physicist-Researcher. In the same year, he began his doctoral studies at the Department of Molecular Compound Physics of the Center for Physical Sciences and Technology (FTMC) in Vilnius. His main research interests include aggregation-induced phenomena and excitation energy transfer dynamics in molecular systems.

Apie autorių (lietuvių kalba)

Ivan Halimski gimė Minske, Baltarusijoje. 2017 m. baigė Minsko 30-ąją gimnaziją ir įstojo į Baltarusijos valstybinio universiteto Fizikos fakultetą. Studijų metu baigiamąjį darbą rengė Energetinės fizikos katedroje, o 2022 m. baigė fizikos specialisto studijas ir įgijo fiziko tyrėjo kvalifikaciją. Tais pačiais metais pradėjo doktorantūros studijas Fizinių ir technologijos mokslų centro (FTMC) Molekulinių darinių fizikos skyriuje Vilniuje. Pagrindinės jo mokslinių tyrimų kryptys – agregacijos sukelti reiškiniai ir sužadinimo energijos pernašos dinamika molekulinėse sistemose.

Vilniaus universiteto leidykla
Saulėtekio al. 9, III rūmai, LT-10222 Vilnius
El. p. info@leidykla.vu.lt, www.leidykla.vu.lt
bookshop.vu.lt, journals.vu.lt
Tiražas 40 egz.

NUO / SINCE 1579



Fragmentas iš Vilniaus universiteto auklėtinio Alberto Diblinskio (1601–1665) vieno geriausių XVII a. astronomijos veikalų *Centuria astronomica* (Vilnius, 1639), kuriame pateikta astronomijos pasiekimų apžvalga, remiantis stebėjimais teleskopu, atliktais kartu su kitu VU mokslininku, matematiku ir astronomu Osvaldu Krygeriu (apie 1598–1655).

VU biblioteka, BAV 47.10.21

Fragment from *Centuria astronomica* (Vilnius, 1639), one of the most well-known works on astronomy from the 17th c., written by Vilnius University graduate Albertas Diblinskis (1601–1665). It presents an overview of achievements in the field of astronomy, based on observations using a telescope together with another VU scientist, mathematician, and astronomer Osvaldas Krygeris (c. 1598–1655).

VU Library, BAV 47.10.21

bookshop.vu.lt journals.vu.lt

https://doi.org/10.15388/vu.thesis.1015